Wetting Hydraulic Functions and Infiltration Characteristics of Bentonites: Influence of Plasticity and Compaction Density

Thesis
submitted in partial fulfilment of the requirements
for the degree of

DOCTOR OF PHILOSOPHY

by

Yagom Gapak

(Roll No. 136104023)

Department of Civil Engineering
Indian Institute of Technology Guwahati
Guwahati – 781039, India

July 2018

CERTIFICATE

This is to certify that the thesis entitled **"Wetting Hydraulic Functions and Infiltration Characteristics of Bentonites: Influence of Plasticity and Compaction Density"** submitted by **Yagom Gapak** to the Indian Institute of Technology Guwahati, for the award of the degree of Doctor of Philosophy in Civil Engineering is a record of bonafide research work carried out by her under my supervision and guidance. The thesis work, in my opinion, has reached the requisite standard fulfilling the requirement for the degree of Doctor of Philosophy.

The results contained in this thesis have not been submitted in part or full to any other University or Institute for award of any degree or diploma.

(Dr. T.V Bharat)
Associate Professor
Department of Civil Engineering
Indian Institute of Technology Guwahati
Guwahati 781039
India

Date:
IIT Guwahati

STATEMENT

I do hereby declare that the matter embodied in this thesis is the result of investigations carried out by me in the Department of Civil Engineering, Indian Institute of Technology Guwahati, Guwahati, Assam, India.

In keeping with the general practice of reporting scientific observations, due acknowledgements have been made wherever the work described is based on the findings of other investigators.

(Yagom Gapak)

IIT Guwahati

Date

ACKNOWLEDGEMENTS

With my deep gratitude and reverence, I would like to express sincere thanks to my supervisor **Dr. T.V Bharat** for his skillful guidance, precious time and continuous support which ensured the successful completion of this work. His passion towards research and his vast knowledge and expertise in unsaturated soils exceptionally inspired and enriched my growth as a researcher. I would also like to acknowledge the financial support received by my supervisor from the Department of Science and Technology (DST), Government of India through INSPIRE FACULTY AWARD, IFA12-ENG- 41 which was instrumental for completion of my PhD research.

I am sincerely thankful to the members of my doctoral progress committee: Professor Gautam Barua, Dr. Anil Kumar Mishra and Late Dr. Narayan Reddy for reviewing my work and providing their valuable suggestions that helped in improving my thesis. I am also thankful to Civil engineering department, Centre for Environment and Department of Physics, IIT Guwahati for providing laboratory facilities which helped in smooth completion of the project work. I thank Dr. Sukanya Sharma and Mr. Pankaj Singh of HSS Department, IIT Guwahati; for the valuable discussion on identifying the clay minerals by different XRD forms. I am grateful to Sophisticated Analytical Instrument Facility (SAIF) center, Gauhati University for conducting the XRF test of the materials used in this research work. I would like to express deep sense of gratitude towards Central workshop, IITG, for their gracious help in fabricating apparatus required for conducting laboratory experiments.

Heartfelt thanks to my colleagues and juniors associated with my work who cooperated in completing my work. They are Uday, Bharat Solanki, Ashish, Ankit, Dhanesh,

Seema, Geetanjali, Praisy, Subrat Mallik, Puneet, Lakshay and Rohit. I appreciate their help with my research work. I am thankful to my friends – Jumrik, Kimjolly, Amrita, Geotech Research scholar friends, Subansiri prayer group sisters and my 2011 batch Mtech friends, who stood through thick and thin during my stay here. I am grateful to my colleagues of NIT Nagaland for rendering their support whenever I needed leave to come to Guwahati for my thesis work. I am indebted to my parents and siblings for showering their love, support and blessings throughout my life. I would like to thank my husband, Mr Supong Sashi, IFS for his constant support and encouragement during my PhD tenure.

Finally, I am thankful to the Almighty for blessing me in every stage of my life.

Yagom Gapak

TABLE OF CONTENTS

ABSTRACT

Knowledge of water movement through unsaturated bentonite clays is important in numerous geotechnical engineering applications such as landfills, mine tailings, buffer and backfill material in high–level nuclear waste (HLNW) repositories. Theoretical infiltration analysis in these studies requires an estimation of hydraulic functions of the compacted bentonites viz. soil water characteristic curve (SWCC) and hydraulic conductivity function (HCF). Available studies on the estimation of hydraulic functions of compacted bentonites are scarce due to difficulties associated in controlling/measuring the suction over a wide range of saturation. Lack of independently estimated hydraulic functions of the compacted bentonites, further, limits the validation of existing infiltration models. Therefore, the main objective of this research work is to study the influence of soil plasticity and compaction density on the SWCC, HCFs, and infiltration characteristics of compacted Indian bentonites under the volume-restrained conditions.

Four commercially available bentonites of different quality (i.e., plasticity) were used in the present study. Drying SWCC behavior of initially slurried bentonites under zero applied stress and wetting SWCC behavior of compacted bentonites in volume-restrained conditions were experimentally investigated by independent methods viz. osmotic technique, vapor equilibrium technique, and chilled-mirror dew-point potentiometer (i.e., WP4). The measured drying SWCC data, in terms of gravimetric water content versus matric suction (SWCCw), were combined with the volumetric shrinkage data to establish SWCC in terms of volumetric water content versus matric suction (SWCC□) and degree of saturation versus matric suction (SWCCSR). The influence of measurement errors in

the volumetric shrinkage data by different procedures was investigated based on the estimated SWCCSR data. A theoretical procedure based on the hysteretic model was proposed for the estimation of wetting SWCC of compacted bentonites from the drying SWCC data and validated with the independently obtained data over a wide suction range. In addition to that, the application of rectangular hyperbola method was verified for linearizing the kinetic hydration data in vapor equilibrium technique for estimating SWCC data in the high suction range. The HCFs predicted from the SWCC data using statistical model were used in the Richards' infiltration model for theoretically studying the transient water infiltration profiles. The infiltration model was validated with the experimental observations of spatial and temporal moisture content distribution in compacted bentonites. Several controlled experiments were carried out by considering the influence of water density, hydraulic head, and specimen size in the infiltration tests for investigating the measured deviation of water movement from the theory.

Keywords: Unsaturated bentonite clays, Soil water characteristics curve, Hydraulic conductivity function, Compaction density, Plasticity, Volumetric Shrinkage, Infiltration studies.

List of Figures

List of Tables

Nomenclature

w	Gravimetric water content
w_s	Saturated gravimetric water content
w_r	Residual gravimetric water content
α, m, n	van Genutchen fitting parameters
ψ	Suction
S_r	Degree of saturation
θ	Volumetric water content
θ_s	Saturated volumetric water content
θ_r	Residual volumetric water content
e	Void ratio
e_{min}	Minimum void ratio
β ,m_2	Fitting parameters of Kim et al. (1992) model
G_s	Specific gravity of soil solids
a_{sh}, b_{sh}, c_{sh}	Fitting parameters of Fredlund (2002)model
λ_s	Slopes of the linear asymptote on $S_r - \psi$ plane
λ_e	Slopes of the linear asymptote on $S_r - e$ plane
C_d	Constant of integration
β_{td}	Exponent of the power function which relates the slope of the generic and main drying curves
S_u , w_u, θ_u	Degree of saturation/ gravimetric/ volumetric water content at zero soil suction on the main drying/wetting curves
b, c, d	Curve fitting parameters of Feng and Fredlund (1999) model
ψ_{1w}, ψ_{2w}, w_1, w_2	Position of additional points on the main wetting curve
b_d, d_d	Best fit parameters of the main drying curve
b_w, d_w	Best fit parameters of the main wetting curve
b_{id}, c_{id}, and d_{id}	Curve-fitting parameters of the initial drying data
S_{1w}	Degree of saturation corresponding to suction value at the first additional point

S_{2w}	Degree of saturation corresponding to suction value at the second additional point
k	Unsaturated hydraulic conductivity
k_s	Saturated hydraulic conductivity
k_r	Relative hydraulic conductivity
Θ	Dimensionless water content
w_{LL}	Liquid limit water content
w_{PL}	Plastic limit water content
w_{SL}	Shrinkage limit
R	Universal Gas constant
T	Absolute temperature
v_o	Specific volume of water
ω_r	Molecular mass of water vapour
p	Partial vapor pressure of the air
p_0	Saturated vapor pressure
ρ_{wax}	Density of wax
ρ_d	Dry density of soil
w_{AEV}	Water content corresponding to air entry suction
R^2	Coefficient of determination
$d\theta/d\psi$	Specific moisture capacity
M_s	Mass of solids
M_w	Mass of water
X, Y	Variables of hyperbolic model
c	Intercept of hyperbolic model
m	Slope of the linear portion of hyperbolic model
t	Time
w_{eq}	Equilibrium water content
w_p	Predicted water content
w_m	Measured water content
D_h	Average degree of hysteresis
w_{di}	Gravimetric water content at point i on drying curve
w_{wi}	Gravimetric water content at point i on wetting curve
V	Total volume of the specimen

ρ_w	Density of water
ρ_b	Bulk density
ψ_{AEV}	Suction corresponding to air entry value
x	Spatial variable
H	Hydraulic head

Abbreviation

AEV	Air entry value
B1	Bentonite 1
B2	Bentonite 2
B3	Bentonite 3
B4	Bentonite 4
CEC	Cation exchange capacity
DDL	Diffuse double layer
DVM	Direct Volume Measurement
EGME	Ethylene glycol mono-ethyl ether
ESP	Exchangeable sodium percentage
HAE	High air-entry
HCF	Hydraulic conductivity function
HLNW	High level nuclear waste
HMS	Hot mix asphalts
MWCO	Molecular weight cut-off
PEG	Polyethylene glycol
PVAc	Polyvinyl acetate
RH	Relative humidity
SSA	Specific surface area
SWCC	Soil-water characteristic curve
SWCC*w*	Gravimetric water content based SWCC
$SWCC_{\theta}$	Volumetric water content based SWCC
$SWCC_{SR}$	Degree of saturation based SWCC
S_r	Degree of saturation
VET	Vapor equilibrium technique
vG	van Genutchen
vGM	van Genutchen- Mualem
VSC	Volumetric shrinkage curve
WC	Wax coated
WP-4	Chilled-mirror hygrometer
WRC	Water retention curve

XRD	X-ray diffraction
XRF	X-ray fluorescence

Chapter 1

Introduction

1.1 General

India's dependency on nuclear energy is increased tremendously for meeting the power demand in recent years. Management of harmful radioactive waste, generated from the nuclear fuel cycle activity, is a crucial aspect in the radioactive waste management for safeguarding the environment and human beings. Mining, nuclear fuel manufacturing industry, defence, medicine, and scientific research produce nuclear waste of different levels. Radioactive waste management received global concern after recent earthquake in Japan and waste leakage at the waste isolation pilot plant in New Mexico, USA. Deep geologic disposal of high-level nuclear waste (HLNW) is widely studied using laboratory tests, exploratory boreholes, and underground pilot tests (IAEA, 2001). The proposed deep geological disposal of high-level nuclear waste (HLNW) is widely accepted as an effective solution for the isolation of water from the biosphere (Pusch et al., 1985; Pusch, 1992; ENRESA, 2000; Pusch, 2006). The proposed final disposal facilities are situated between 50 m – 1000 m below the ground surface in a suitable rock mass (Pusch, 1982; Pusch, 1992). Vertical deposition holes are drilled in the horizontal tunnels to place the waste containers and buffer material is used to fill the space between container and the rock. Compacted bentonite clays are widely considered as the candidate buffer material in deep geological disposal (Pusch et al., 1985; Pusch, 1992; Ogata et al., 1999; ENRESA, 2000; Pusch, 2006). The choice of bentonite clay as sealing and buffer material in most disposal concepts is due to its low permeability, swelling capacity, self-healing ability, and retention capability of nuclides (Pusch, 1992, 1994; Bharat et al., 2009; Bharat et al., 2013). The presence of high percentage of montmorillonite content in bentonite clays provides useful features for these clays such as high swelling capacity,

low hydraulic conductivity, and high sorption capacity. Therefore, bentonite clays are also increasingly used as liner for containing the municipal solid waste and in the final cover to restrict the rainfall infiltration rates into the landfills due to low hydraulic conductivities and high sorption capacity (Daniel, 1984; Rowe et al., 1995; Qian et al., 2002; Bharat et al., 2012, 2015). Different types of liner systems viz. single liner, single composite, and double composite are often used where the compacted bentonite is directly placed at a given compaction density or mechanically held by geotextiles and/or geomembranes. The constitutive parameters such as diffusion coefficient and sorption coefficient control the placement thickness and compaction density of the bentonites in single liners. The quality of the bentonites used in manufactured geosynthetic clay liners (GCLs) for the application as composite liners, on the other hand, governs the design considerations.

Knowledge of water movement in unsaturated, compacted bentonite clays is important in the aforementioned applications. Bentonite clays in HLNW repositories are subjected to continuous cycles of wetting and drying conditions due to water ingression from the surrounding saturated host rock (Pusch, 1992; Pusch et al., 2015). The hydro-mechanical stability of and long-term performance of the bentonite clays (Fujita et al., 1990, 1996; Yong et al., 1997; Lee et al., 2011; Kim, 2017), therefore, requires the estimation of transient water infiltration rates in the coupled analysis. Similarly, the bentonite liners in landfills are subjected to wetting process due to infiltration of different leachates. The design of cover systems of landfills and mine tailings require an accurate determination of flow characteristics to predict the evaporation rates from the cover surface by considering the soil-weather interactions in the coupled analysis. The time rate of geosynthetic clay liner hydration from the underlying foundation soils requires the knowledge of water migration rates in compacted bentonites. Such studies are also used

for the determination of depth and degree of wetting in active zone for accurate heave prediction in the design of foundations on expansive soils and in the rainfall induced slope stability analysis.

Soil hydraulic functions viz., soil-water characteristic curve (SWCC) and hydraulic conductivity function (HCF) are required for studying the unsaturated flow behavior (Huang et al., 2011) in various applications discussed earlier. Soil-water characteristic curve is an important constitutive relationship, which represents the variation in soil water content (w, θ, or S_r) with suction (ψ) (Mbonimpa et al., 2006; Tripathy et al., 2014). The SWCC data of expansive soils exhibits significant hysteresis due to which the soil water content is higher along the drying path compared to wetting path at the same suction value. Most of the available SWCC data of bentonites are in volume unrestrained condition and for drying case from an initially slurry state (Tadza, 2011; Zhang et al., 2014). The measured SWCC data is required to be combined with volumetric shrinkage (VSC) data to account for the volume changes in drying process (Fredlund, 2002; Fredlund and Houston, 2013; Wijaya et al., 2015). A precise estimation of VSC data is, therefore, important for accurate determination of the unsaturated soil characteristics (Wijaya et al., 2015). The wetting SWCC data of compacted bentonites over a wide suction range are very limited (Seiphoori et al., 2014), but important in all the geoenvironmental applications. The nonavailability of the wetting data is mainly due to the requirement of long-testing time (ranging from few days to several months) and complexity of the testing (Hong et al., 2016). The estimation of HCF is also important in the theoretical study of unsaturated flow behavior. Hydraulic conductivity function represents the variation in hydraulic conductivity with suction (or water content). Direct estimation of HCF of the bentonites clays is not possible. Statistical methods are successfully utilized to indirectly estimate the HCF data from SWCCs. The SWCC

estimation for compacted bentonites is, therefore, very crucial for accurately predicting the HCF and for theoretically studying the infiltration characteristics for various applications.

1.2 Motivation for the study

A precise estimation of hydraulic functions of the compacted bentonites is utmost important for several geotechnical applications. However, the limitations and difficulties associated with the laboratory measurement techniques restricted the availability of soil hydraulic data of compacted bentonite clays for the geotechnical field applications. The available drying SWCC data of an initially slurried data may be related to the compacted wetting SWCC data by hysteretic models for establishing the wetting SWCC data from the existing drying data of many bentonites. Further, limited studies are available on the measurement of VSC data of bentonites. The hydraulic behavior of the bentonites in volume restrained condition at different initial compaction density is important for various applications.

1.3 Organization of the thesis

The thesis consists of nine chapters including five contributing chapters. **Chapter 1** presents the introduction to the problem, motivation behind this research work, and the importance of the outcome. A detailed review of the available literature pertaining to the soil hydraulic studies and their application were presented in **Chapter 2**. The critical appraisal of the existing related work leading to the objectives of the present study was also presented in this chapter. A detailed characterization of the studied bentonites in this work using X-ray diffraction (XRD) in different forms, X-ray fluorescence (XRF), etc. was provided in **Chapter 3** for physical, geotechnical, and mineralogical properties.

This chapter presents different laboratory measurement methodologies for establishing SWCC data of the studied bentonites along the drying and wetting paths. The adopted procedure for the one-dimensional infiltration tests was also discussed in this chapter. Results and discussion from the study are presented in chapters 4 - 8. **Chapter 4** presents the drying SWCC data of the bentonites in volume unrestrained condition. The influence of wax coating method, clod test, balloon method, and direct measurement techniques on the measured volumetric shrinkage data of the studied bentonites was presented. The limitations associated with the shrinkage tests were discussed. Theoretical models were presented to fit the measured data for analyzing different shrinkage characteristics. The influence of measurement errors in VSC tests on the estimated SWCC data was discussed on two of the studied bentonites. **Chapter 5** presents wetting SWCC data of the bentonites in volume restrained conditions. Linearization approach of the vapor sorption data for the studied bentonites at different compaction states was also discussed in this chapter for estimating the equilibrium water contents at a given relative humidity using the vapor equilibrium technique. The SWCC hysteretic behaviour of the bentonites was presented in **Chapter 6.** The proposed theoretical model for predicting the boundary wetting SWCC from the initial drying SWCC data using two additional data points along the wetting path was discussed. The estimated HCFs from the measured SWCCs using statistical approach were presented in **Chapter 7**. The influence of compaction density and bentonite plasticity on the estimated HCFs was discussed. The measured transient moisture profiles in the compacted bentonites were presented using one-dimensional water infiltration studies in **Chapter 8**. The influence of bentonite plasticity and compaction density on the water distribution in bentonites was studied. The independently estimated soil hydraulic functions in the previous chapters for the compacted bentonites were inputted in Richards' model for estimating the theoretical

transient water infiltration profiles. The comparison between the theoretical trends with the observed infiltration data was presented. Important conclusions were drawn in **Chapter 9** based on the detailed investigation of the results and gaps in the present work were presented as a scope for future work.

Chapter 2

Literature Review

2.1 General

The literature review is covered in five sections. The first section presents the available research studies in establishing drying and wetting SWCC data using different methodologies. The next section deals with literature studies on volumetric shrinkage curve of soils using different methodologies. Further, the studies on hysteretic SWCC data were presented in third section. The literature related to unsaturated permeability functions of the bentonites were given in the fourth section. The last section focuses on one-dimensional infiltration studies. A critical appraisal of the available work was presented by highlighting the gaps in the research findings. The scope of the present research and the research objectives were presented at the end of this chapter.

2.2 Soil water characteristic curve of bentonites

Water retention curve (WRC) or soil water characteristic curve representing the variation of gravimetric water content with matric suction is an important constitutive relationship for analyzing the hydro-mechanical behavior of the bentonites (Leong and Rahardjo, 2002; Mbonimpa et al., 2006; Tripathy et al., 2014). The SWCC depend on pore size distribution, compaction density, and mineralogy of the soils (Tinjum et al., 1997; Vanapalli et al., 1999; Lu and Likos, 2004; Yang et al., 2004; Thu et al., 2007; Ye et al., 2009).

Laboratory methods such as osmotic technique (Delage et al., 1998), chilled mirror hygrometer (Leong et al., 2003), vapor equilibrium technique (Delage et al., 1998; Tang and Cui, 2005, 2007; Sun et al., 2014; Tripathy et al., 2014), axis-translation (Tripathy et

al., 2014), relative humidity (RH) sensors (Agus and Schanz, 2005), tensiometer (Take and Bolton, 2003), and fixed-matrix porous ceramic discs (Tripathy et al., 2016) are widely used either to control or measure the suction in soil. Most of the available SWCC data on bentonites are in volume unrestrained condition where powder specimens are utilized (Tadza, 2011; Tripathy et al., 2014; Zhang et al., 2014). Only limited techniques viz., tensiometer, RH sensors, and fixed-matrix porous ceramic discs are feasible for the estimation of suction in volume restrained condition and for reading continuous data when the water content changes. However, these techniques are highly time-consuming to establish hydraulic equilibrium between soil specimen and the sensor; the continuous evaluation of transient suction data by fixed-matrix porous ceramic discs is erroneous (Tripathy et al., 2016). The required equilibrium time for the measurement of wetting SWCC data was, moreover, significantly higher compared to drying data (Tinjum et al., 1997; Yaldo, 1999; Fredlund, 2006; Fredlund et al., 2011; Hong et al., 2016). The measurement of SWCC data of bentonites over a wide range of suctions by single technique, further, poses several limitations (Agus and Schanz, 2005; Bulut and Leong, 2008; Nam et al., 2010; Pan et al., 2010). Therefore, limited data are available on bentonites using independent laboratory techniques for establishing SWCC over a wide range of suctions. The SWCC data of compacted bentonites over a wide suction range is very scarce (Ye at al., 2009, 2016), but important for accurate study of unsaturated flow characteristics of buffer material.

Several equations have been proposed for defining SWCC. Some of the most common models are Gardner (1958) equation, Brooks and Corey (1964) equation, van Genuchten (1980) equation, Mualem (1976) equation and Fredlund and Xing (1994) equation.

The van Genuchten (vG) model is often represented in terms of different state variables such as gravimetric water content (w), degree of saturation (S_r) and volumetric water

content (θ) based on the adopted measurement technique. The SWCC in terms of *w* is given by (Vereecken et al.,1989; Fredlund et al., 2002).

$$w=w_r+\frac{(w_s-w_r)}{\left(1+(\alpha\psi)^n\right)^m} \tag{2.1}$$

where w_s is saturated water content and w_r is residual water content. However, the identification of residual water content and air-entry value in this representation is not feasible for plastic clays due to the variation in the water content from saturated to residual state (Fredlund and Houston, 2013).

The following representation of van Genuchten model is given by (Zhou and Yu, 2004; Hosseini et al., 2011)

$$S_r=\frac{1}{\left(1+(\alpha\psi)^n\right)^m} \tag{2.2}$$

where α, *m*, and *n* are the model parameters.

Huang et al. (2011) represented vG (1980) model in terms of volumetric water content to fit wide range of soils.

$$\theta=\theta_r+\frac{(\theta_s-\theta_r)}{\left(1+(\alpha\psi)^n\right)^m} \tag{2.3}$$

where, θ is water content (cm^3/cm^3); θ_s is saturated water content; θ_r is residual water content; ψ is matric suction (kPa); α, *n* and *m* are empirical soil parameters. The parameter α is related to the air entry value of the soil (kPa^{-1}), *n* controls the slope at the inflection point in the soil water characteristic curve, and *m* is related to residual water content of the soil.

2.3 Volumetric Shrinkage Characteristics

The hydro- mechanical behavior of the expansive soils is required to be estimated in terms of degree of saturation versus suction as the balance equations are based on either volumetric water content or degree of saturation (Lu and Likos, 2006; Lu et al., 2010; Jacinto et al., 2012; Baille et al., 2014). The estimation of S_r from the $SWCC_w$ requires the estimation of volumetric shrinkage behavior of soils which is a relationship between the specimen volume and the corresponding water content, represented by volumetric shrinkage curve (VSC) (Fredlund, 2002; Fredlund and Houston, 2013; Wijaya et al., 2015). Determination of volumetric shrinkage behaviour is important for the analysis of flow, compressibility, and shear strength behaviour of unsaturated bentonite clays. The study of volumetric shrinkage behavior is also important in the design of impoundments for mine tailings (Saleh-Mbemba, 2010) and to address the problem of subsidence caused due to volumetric shrinkage (Nelson and Miller, 1992; Tariq and Durnford, 1993a). Further, the shrinkage behavior is important in GCLs and clay liners due to waste generated heat as the generated heat causes loss of moisture from the bentonite (Doll, 1997; Cripps and Parmar, 2001; Tay et al., 2001; Southen and Rowe, 2005; Azad et al., 2012). A precise estimation of VSC data is, therefore, important for accurate determination of the unsaturated soil characteristics (Wijaya et al., 2015). Laboratory determination of gravimetric water content of a soil specimen is straightforward and the water content is estimated using well-established techniques such as oven drying method (ASTM D2216-10, 2010). However, an accurate measurement of volume of the specimen at different saturated states of the soil specimen is challenging.

The soil bulk volume is measured in the laboratory using standard methods such as mercury displacement (IS: 2720 Part 6 1972; BS 1377: Part2 1990; ASTM D427-04, 1998) or wax method (ASTM D7263, 2009). Pertaining to serious health hazards with

the mercury to the skin and prolonged inhalation of mercury vapors, mercury displacement technique is withdrawn from the standards in some countries (ASTM C493-98, 2002). The wax method is, therefore, widely used in engineering practice as an alternative technique to measure the bulk volume of the soil specimen (Lauritzen and Stewart, 1941; Braudeau et al., 1999). Alternative techniques are surfaced to minimize possible errors in wax method due to the requirement of volume measurement on duplicate soil specimens. Non-wetting fluids such as Kerdane oils are used to estimate the volume of the specimen from weights taken after the inhibition and apparent weight while immersed in non-wetting fluid (Fleureau et al., 1993). Encasement techniques using water-repellent solutions such as MEK Saran (Nelson and Miller, 1992; Crescimanno and Provenzano, 1999), waterproof polyvinyl acetate (PVAc) based adhesives (Krosley et al., 2003), automotive varnish (de Almeida et al., 2009) are widely used to estimate the volume of the specimen for establishing the VSC for different clay soils (Baille et al., 2014; Tripathy et al., 2014). Direct measurement techniques are used for measuring the specimen volume with the help of a caliper (Peron et al., 2009) or analyzing the images (Puppala et al., 2004; Tang et al., 2011; Stewart et al., 2012) for low-plastic tailings (Saleh-Mbemba et al., 2016) and clays soils (Por et al., 2015). Balloon method (Tariq and Durnford, 1993a) is used in few studies (Cornelis et al., 2006a, 2006b) for quasi-continuous measurement of both soil volume and water content on the same specimen. Comparative studies (Cornelis et al., 2006; Tripathy et al., 2014) for establishing shrinkage data on VSC by different volume measurement techniques are scarce. Moreover, the available studies only focus on the difference in the estimated model parameters from different volume measurement techniques (Cornelis et al., 2006). The significance of these model parameters on the estimated S_r is not known.

While a saturated soil specimen left for thermodynamic equilibrium with the surrounding environment in the laboratory, the specimen attains a thermodynamic potential of the environment by reducing its water content. The loss of moisture from the expansive clay specimen during the drying process causes rearrangement of particles and aggregates; results in decrease of its bulk volume. The change in the magnitude of the volume of the specimen with reduction in the water content is described by VSC. The VSC data is expressed in terms of specific volume versus water content (w), void ratio (e) versus water content (w), or void ratio versus moisture ratio (Groenevelt and Grant, 2002; Saleh-Mbemba et al., 2016). A typical illustration of volumetric shrinkage curve was shown in Fig. 2.1. Volumetric shrinkage curve consists of four distinguished phases such as structural, normal, residual, and zero shrinkage phases (Bensallam et al., 2012). The structural shrinkage signifies that the reduction in volume of the soil is smaller than the amount of extracted water from the soil. The reduction in volume in this phase is governed by the free water extracted from the soil. However, this phase is absent in clayey soils (Chertkov, 2003). The rate of volume reduction and the amount of water extracted is same during normal shrinkage phase (McGarry and Malafant, 1987; Tariq and Durnford, 1993a). Normal shrinkage phase plays a major role in the VSC as it represents about 30 - 80% of the total water loss and a decrease of about 64 - 94% of the total volume in many soils (Peng and Horn, 2005). Tripathy et al. (2002) also reported that more than 80% of volume change occurs in this zone. The volume of the soil specimen is not influenced by change in water content in zero shrinkage phase. The air-entry water content is the point on the volumetric shrinkage curve where the rate of volume reduction deviates from the normal shrinkage trend and the shrinkage limit is the water content at which the volume of the specimen remains constant (Wijaya et al., 2015).

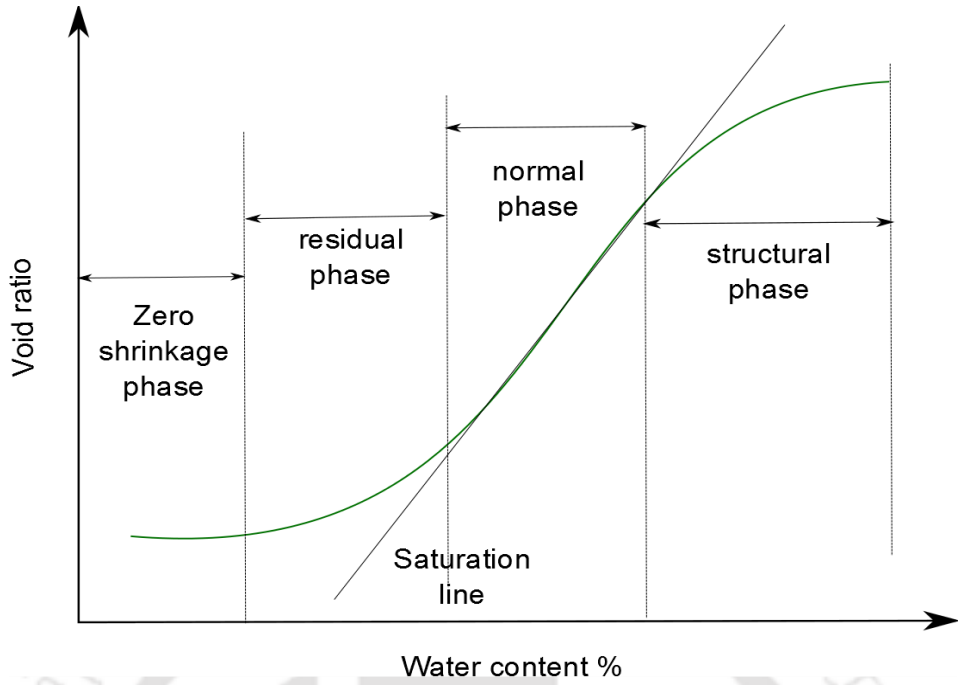

Fig. 2.1 Volumetric Shrinkage Curve (after Bensallam et al., 2012)

The VSC data is described by several theoretical models (Kim et al., 1992; Tariq and Durnford, 1993b; Braudeau et al., 1999; Fredlund et al., 2002; Chertkov, 2003; Cornelis et al., 2006). The number of fitting parameters varies from two to seven in these models. Some models require air-entry value (AEV) and minimum void ratio as the input parameters.

Kim et al. (1992) presented a theoretical model in terms of void ratio as

$$e = e_{\min} \times \exp(-\beta w) + m_2 w \qquad (2.4)$$

where β is the slope parameter which depends on AEV, m_2 is slope of the saturation line of VSC, w is the water content. The zero and residual zones are expressed by the inverse exponential function, in this model, that gradually advances to a certain denominator value with decrease in water content or moisture ratio.

The mechanical changes to the soil specimens due to several drying-wetting cycles were directly corroborated with the model parameters of Kim et al. (1992).

Fredlund et al. (2002) proposed a three-parameter model which is given by

$$e(w) = a_{sh}\left[\frac{w^{c_{sh}}}{b_{sh}^{c_{sh}}} + 1\right]^{\left(\frac{1}{c_{sh}}\right)} \tag{2.5}$$

and

$$\frac{a_{sh}}{b_{sh}} = \frac{G_S}{S_r} = \text{constant} \tag{2.6}$$

where G_s is the specific gravity of soil and S_r is degree of saturation. Parameter a_{sh} is related to the minimum void ratio (e_{min}) and b_{sh} parameter is the slope of the line of tangency. The curvature of the VSC at desaturation region is controlled by the c_{sh} parameter. The Fredlund et al. (2002) model is used for the prediction of field settlement which involves the use of limiting lower void ratio after drying, e_{min} (Bardanis and Kavvadas, 2006). It has application to study the unsaturated soil behavior as far as the evolution of limiting lower void ratio with initial void ratio and physical properties of soils is concerned. Further, the model is used to study the drying behavior of oil sand tailings (Vardon et al., 2014); volume change behavior of environmentally stabilized soils (Gould et al., 2011).

2.4 Hysteretic water retention behaviour of bentonites

The drying and wetting SWCCs of sands and loams (Pham, 2001) are obtained by pressure plate apparatus which limits the maximum measurable suction range to 500 – 1500 kPa, depending on the capacity of the high air entry (HAE) ceramic disc. Yang et al. (2004) utilized Tempe pressure cell and hanging column to determine the drying and wetting hysteresis cycles of sands. Ebrahimi-Birang et al. (2007) studied the hysteresis behaviour of clayey silt and low plastic clay (liquid limit varied between 20–81%) only in the high suction range. Ng and Leung (2012) utilized tensiometers and theta-probe to measure suction and volumetric water content, respectively, for the compacted silty clays. Similar studies are carried out by Mijares and Khire (2010) to determine cyclic drying–wetting SWCCs of silty clay by utilizing instantaneous profile method using potential sensors. Most of the cyclic drying – wetting tests are limited to non-plastic to low plastic soils due to the requirement of large hydraulic equilibrium time between the soil specimen and the sensors. The equilibrium time to estimate single data point for plastic clays may vary over months (Tripathy et al., 2016). The SWCC studies on highly expansive clays such as bentonites over a wide suction range, therefore, utilize multiple techniques (Tadza, 2011; Tripathy et al., 2014; Zhang et al., 2014). In these studies, different suction controlled techniques are used in different suction ranges on independent specimens. Osmotic technique using semi-permeable membrane is used to control the suction in lower – intermediate suction range. The cellulose acetate membranes, however, are susceptible to microbial attacks and the membrane degrades with aging (Tripathy et al., 2011). Only single data point on the SWCC curve is, therefore, obtained by these techniques. Very limited studies are, therefore, available on drying – wetting behaviour of clay soils (Fleureau et al., 1993; Sharma, 1998; Romero and Vaunat, 2000; Fleureau et al., 2002) due to the requirement of multiple techniques to

control the soil suction in different suction ranges. Lin and Cerato (2012) investigated the hysteretic soil water characteristics curve of two compacted expansive soils (liquid limit 84% and 100%) using combination of pressure plate apparatus and chilled mirror hygrometer in a limited suction range. Few researchers (Jayanth et al., 2012; Akin and Likos, 2016) ascertained wetting–drying SWCCs of powdered clay soils using isotherm generator in the high suction range, but the volume changes in the specimen are not available. Fleureau et al. (1993, 2002) presented the hysteretic SWCC data of low – medium plastic clay soils using multiple techniques to either control or measure the suction. Sharma (1998) conducted wetting and drying tests on mixtures of Speswhite kaolin and Wyoming sodium bentonite in compacted state. The wetting and drying paths of SWCC are achieved by controlling the matric suction in the extended triaxial test set-up in isotropic stress conditions.

The hysteretic behavior is, therefore, often predicted by theoretical models due to limitations associated with the suction control/measurement in clay soils (Fredlund et al., 2003; Pham et al., 2003, 2005). The existing theoretical models are, however, validated only on the non-plastic and low plastic soils due to the requirement of entire hysteretic data (initial drying and main SWCCs). Moreover, the predictive models for estimating boundary wetting curve from the initial drying curve are not available. The availability of both initial drying and main hysteresis data of bentonites is also very scarce (Seiphoori et al., 2014) for validation of the models and understanding the influence of plasticity on the degree of hysteresis.

A typical illustration of hysteretic SWCC was shown in Fig. 2.2. When a saturated soil is allowed to dry until the residual saturation stage, water content decreases significantly with increase in the suction. This desorption curve of the soil from the initial saturation state to the residual saturation stage is called the initial drying curve. The SWCC curve

initiating from the residual water content on the drying path to saturated state due to wetting is termed as boundary (main) wetting curve. The soil specimen follows boundary (main) drying curve when the soil specimen is further dried from its saturated state on the main wetting curve, which follows a different path from the initial drying curve. The boundary drying and wetting curves form the main hysteresis loop. Infinite number of such curves exists within the hysteresis loop termed as scanning curves. Measurement of the whole hysteretic behaviour of a given soil is time consuming and difficulties associated with the suction measurement as stated earlier. The hysteresis data of clays over a wide suction range are, therefore, very scarce. Therefore, various theoretical models are used to estimate the hysteretic behaviour from the measured data of the hysteretic curves.

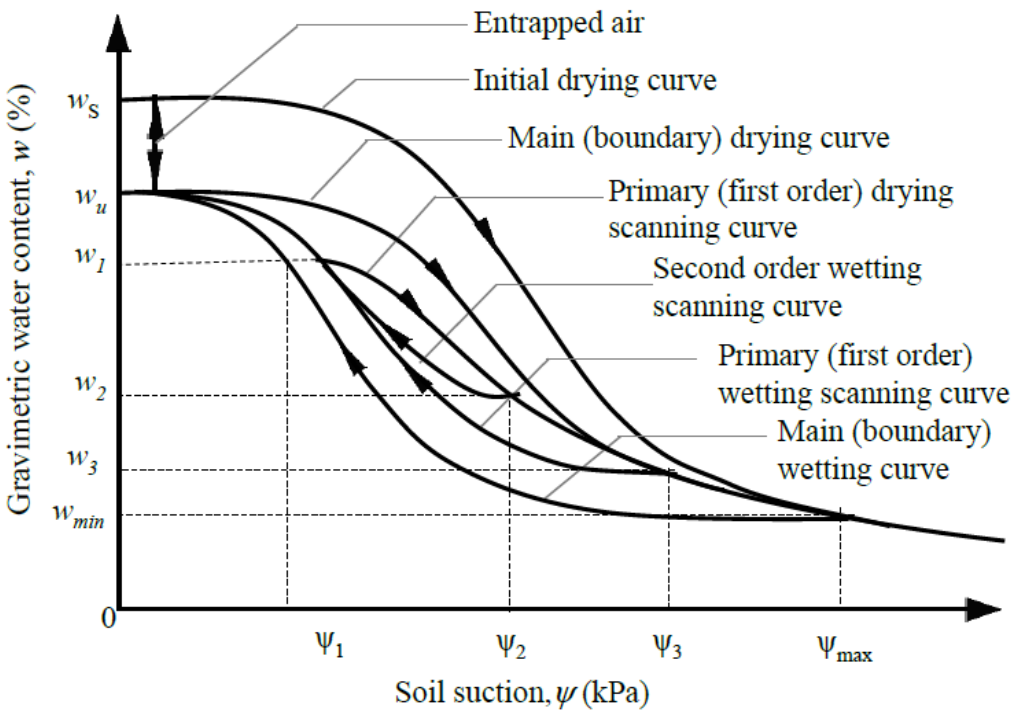

Fig. 2.2. Hysteretic soil water characteristic curve (after Pham et al., 2005)

Several domain models (Philip, 1964; Poulovassilis, 1962; Poulovassilis and Childs, 1971; Mualem, 1973; Liu et al., 1995) are available based on Néel (1942) diagram to describe wetting and drying behavior of soils. The water distribution data, $f(\psi_d, \psi_w)$, at any pair of soil suctions on the wetting and drying curves (ψ_d, ψ_w) and additional scanning curve data are required for calibration of the domain models. Gallipoli et al. (2015) proposed a bounding surface hysteretic water retention model for expansive soils based on the water retention surface in $S - \psi - e$ space by representing the air-entry suction parameter of van Genuchten (1980) equation as a function of void ratio (Gallipoli, 2003)

$$S = \left[1 + \left(\psi \frac{e^{\lambda_{ei}/\lambda_{si}}}{\omega_i}\right)^{\lambda_{si}/m_i}\right]^{-m_i} \tag{2.7}$$

where S is the degree of saturation; ψ is suction; e is the void ratio; m and ω are the fitting parameters; and λ_s and λ_e are the slopes of the linear asymptote on $S - \psi$ and $S - e$ planes, respectively. The subscript 'i' is equal to 'id', 'd', or 'w' depending on whether the equation refers to initial drying, boundary drying, or boundary wetting, respectively. The parameter λ_e is set equal to one to control the theoretical expression in high suction range based on the experimental observations. Equation (2.7) is further modified to account for the generic (initial) drying curve as

$$S = \left[1 + \left(\frac{\left(\psi e^{1/\lambda_{sid}}\right)^{\beta_d} + C_d}{\omega_{id}^{\beta_{id}}}\right)^{\lambda_{sid}/\beta_{id} m_{id}}\right]^{-m_{id}} \tag{2.8}$$

where C_d is the constant of integration (≥ 0) and β_d is exponent of the power function which relates the slope of the generic and main drying curves which is fitted using the initial drying data. The parameter C_d is obtained by matching the initial soil state. Complete data of initial drying and boundary curves are, therefore, required for

representation of hysteretic data theoretically. Due to difficulties associated with the measured data on the main drying, boundary drying, and scanning paths, empirical models (Jaynes, 1984; Nimmo, 1992; Feng and Fredlund, 1999; Pham et al., 2003; Wheeler et al., 2003) are widely used. The boundary drying and boundary wetting SWCCs are represented by (Feng and Fredlund, 1999)

$$S(\psi) = \frac{S_u b_i + c_i \psi^{d_i}}{b_i + \psi^{d_i}} \tag{2.9}$$

where S_u is the degree of saturation at zero soil suction on the main drying/wetting curves; b, c, and d are the curve fitting parameters. The parameter c represents water content at relatively high soil suction and, therefore, is considered to be constant for all the hysteresis curves. The fitting parameter d represents the slope at the inflection point of the curve; parameters b and d control the air-entry suction value. Equation (2.9) is used for predicting the entire boundary wetting curve from the boundary drying curve with additional two measured data points on the wetting curve. Pham et al. (2003) provided recommendations for locations of the two points on the boundary wetting curve for the prediction of boundary wetting curve from boundary drying curve. The first point is estimated using

$$\psi_{1w} = \left(\frac{b_d}{10}\right)^{\frac{1}{d_d}} \tag{2.10}$$

where ψ_{1w} is the soil suction at the first additional point on the main-wetting curve; b_d and d_d are the best fit parameters of the main drying curve. The location of the second additional point (ψ_{2w}) on the main-wetting curve is estimated by

$$\psi_{2w} = \psi_{1w} - 2\left\{\left[\frac{b_d (S_u - S_1)}{S_{1w} - c}\right]^{\frac{1}{d_d}} - b_d^{\frac{1}{d_d}}\right\} \tag{2.11}$$

where S_{1w} is the degree of saturation corresponding to suction value at the first additional point (Eq. 2.10). The two data points S_{1w} and S_{2w} are used for estimating two unknown fitting parameters d_w and b_w of the main wetting curve by

$$d_w = \frac{\log\left[\frac{(S_{1w}-c)(S_u-S_{2w})}{(S_u-S_{1w})(S_{2w}-c)}\right]}{\log\left(\frac{\psi_{2w}}{\psi_{1w}}\right)} \tag{2.12}$$

$$b_w = \frac{(S_{1w}-c)\psi_{1w}^{\,d_w}}{S_u - S_{1w}} \tag{2.13}$$

where c is considered to be constant for both drying/wetting curves. The fitting parameters (b_w, d_w, c) are thus used to predict the boundary wetting curve using Eq. (2.9). Several studies (Pham et al., 2005; Zhang et al., 2014) also showed that the predicted boundary wetting curve from boundary drying curve by Pham et al. (2003) is more accurate than the existing models after a thorough review of several domain and empirical models. Pham et al. (2005) replaced the variable S_u in Eq. (2.9) with S_s for theoretically representing the initial drying curve. Further, Pham et al. (2005) proposed a scaling method to estimate boundary wetting curve from the initial drying data in two stages. The method uses a relationship between water content at zero soil suction on the boundary hysteresis curve and water content at zero suction on the initial drying curve (i.e., $S_u = 0.9S_s$) for estimating the boundary drying curve from the initial drying data in the first stage. The boundary wetting curve is then estimated using the scaling parameters such as distance and slope ratios between the boundary curves. The major limitation of this approach is that the nature of the boundary curves is required for obtaining the scaling parameters. The extended constitutive model based on Pham et al. (2005) for studying the drying – wetting behavior of soils under isotropic loading – unloading conditions (Pham and Fredlund, 2011) also requires these scaling parameters to represent

the hysteresis. In summary, physical-based (domain) models require the measured data along the boundary and scanning curves for calibration. The recent hysteretic models for deformable soils (Gallipoli et al., 2012, 2015; Pham and Fredlund, 2011) are useful for continuous representation of hysteretic data as the models require the measured data of all the initial drying and boundary drying curves. Models for predicting boundary wetting curve directly from the initial drying data are useful in plastic clays due to limitation on the measurements, but such models are not available.

2.5 Hydraulic conductivity functions (HCFs) of expansive clays

Hydraulic conductivity function (HCF) or coefficient of unsaturated permeability (k), which is used to evaluate the infiltration rate of water in the soil, is a function of matric suction and water content/degree of saturation. Statistical models such as Childs and Collis-George (1950), Burdine (1953), and Mualem (1976a) are used for the estimation of HCF from the SWCC. Mualem (1976a) provided a useful statistical model and widely used model to relate relative hydraulic conductivity (k/k_s) and suction using the model parameters obtained by fitting van Genuchten model on the measured SWCC data. The relative hydraulic conductivity is given by

$$k_r(\theta) = \sqrt{\Theta}\left[\int_0^{\Theta} \frac{dx}{\psi(x)} \Big/ \int_0^{1} \frac{dx}{\psi(x)}\right]^2 \qquad (2.14)$$

where Θ is a dimensionless water content represented by $\Theta = \left(\theta - \theta_r / \theta_s - \theta_r\right)$ and substituting the functional relationship, $\psi(\Theta)$, from Eq. (2.3.) provides the following analytical solution.

$$k_r(\psi) = \frac{\left\{1-(\alpha\psi)^{n-1}\left[1+(\alpha\psi)^n\right]^{-m}\right\}^2}{\left[1+(\alpha\psi)^n\right]^{\frac{m}{2}}} \quad (2.15)$$

where the model parameters are obtained by optimization techniques

Direct measurement of HCFs of bentonites using multistep outflow method and other laboratory methods is possible only in a limited suction range due to the limitations associated with the air-entry value of a high air-entry (HAE) porous discs (Take and Bolton, 2003). However, the air-entry suction of bentonites in volume unrestrained condition, where volume of the specimen during the wetting is allowed to change, is generally more than 10,000 kPa (Tripathy et al., 2014). The air-entry value in volume restrained condition is, therefore, expected to be much higher when compared to unrestrained condition. Several indirect methods such as infiltration method and instantaneous profile method are used for the prediction of hydraulic characteristics of non-plastic soils (Šimůnek and van Genuchten, 1996; Šimůnek et al., 1998). These techniques utilize tensiometers for the measurement of suction at two ends of a soil column. However, the measurement range of tensiometers is limited and the suctions at dry side of SWCC can't be obtained (Schindler et al., 2010). HCFs are, therefore, commonly estimated from soil water characteristic curve (SWCC) using statistical methods (Fredlund et al., 1994; Meerdink et al., 1996). The wetting HCFs of bentonites at different compaction densities are also useful for understanding the capillary barrier effect between dissimilar soil layers in landfill liners, slope stability, and other applications (Zornberg et al., 2010). Ye et al. (2009, 2016) studied the water retention and hydraulic behavior of compacted GMZ bentonite using instantaneous profile method by measuring the relative humidity (RH) at a given depth in the specimen with time. The transient suction data, obtained from psychrometers, were utilized for estimating the

hydraulic conductivity data at different suctions by assuming the validity of Darcy's law. Moreover, the changes in SWCC and HCF with plasticity and compaction density are not available by these studies.

2.6 Infiltration studies

Knowledge of water movement/distribution in unsaturated bentonite clays is important in many geotechnical applications. For example, the design of cover systems of landfills and mine tailings (Huang et al., 2015; Knidiri et al., 2016) require an accurate determination of flow characteristics to predict the evaporation rates from the cover surface by considering the soil-weather interactions in the coupled analysis (Or et al., 2013). The time rate of geosynthetic clay liner hydration from the underlying foundation soils requires the knowledge of water migration rates in compacted bentonites (Rayhani et al., 2008; Siemens et al., 2012). Accurate determination of water movement is also important in the bentonite buffer and backfill material for the assessment of hydro-mechanical stability of high–level nuclear waste repositories (HLNWRs) and long-term performance of the bentonite clays (Fujita et al., 1990, 1996; Yong et al., 1997; Lee et al., 2011; Kim, 2017). Similarly, transient water migration analysis is important in the determination of depth and degree of wetting in active zone for accurate heave prediction in the design of foundations on expansive soils (Siemens and Baltz, 2008; Chao et al., 2014; Nelson et al., 2015) and in the rainfall induced slope stability analysis (Qi and Vanapalli, 2015).

Green-Ampt model (1911) is a simple infiltration model, for flow through homogeneous soils, which assumes the presence of a sharp wetting front in the soil profile. Further, the total infiltration displacement for a unit cross sectional area at any time is assumed to be equal to the product of the change in water content relative to the initial condition and

the distance (Lu and Likos, 2004). The wetting front separates the soil profile into an upper saturated zone and a lower unsaturated zone. This model is commonly used for infiltration studies in coarse-grained soils (Chen and Yong, 2006; Ma et al., 2010; Siemens et al., 2013) due to the assumptions in the model. Ye et al. (2009) combined total infiltration displacement assumption of Green–Ampt's model with the Darcy's law to estimate the hydraulic conductivity variation with water content. The hydraulic conductivity is estimated to be nearly invariant with water content (or suction) and estimated to be slightly increasing with decrease in water content in the tightly adsorbed regime – where the water flow is negligible. The abnormal behaviour in the hydraulic conductivity variation with water content is due to the absence of mass conservation equation in the model. Richards' (1931) equation received a wide attention for infiltration studies in different soils as the equation satisfies mass conservation principle (Haverkamp et al., 1997). Validation of Richards' equation for predicting the infiltration characteristics of several textured soils is well reported (Pachepsky et al., 2003; Kargas and Kerkides, 2011). However, the applicability of this equation for flow behaviour in compacted bentonites is not received any attention, albeit widely applied for the theoretical estimation of moisture distribution in hydro-mechanical analysis for HLNWRs projects. In such projects, the diffusivity function is estimated from the laboratory 1D studies (Nielsen et al., 1962; Cassel et al., 1968) by Philip's (1957) model which uses Boltzmann transformation of the Richards' equation (Klute and Dirksen, 1986; Guerrini and Swartzendruber, 1992) and is used as input in Richards' equation for hydro-mechanical analysis in prototype experiments (Fujita et al., 1990, 1996; Lee et al., 2011). However, the applicability of the model for infiltration studies is not verified using independent estimation of hydraulic functions except using the Richards' model as an empirical model (Lee et al., 2011). The two hydraulic functions – soil water

characteristic curve, SWCC, and hydraulic conductivity function, HCF, – are required for the theoretical estimation of water distribution in soils using Richards' equation. The lack of independently measured or estimated data of hydraulic functions for the compacted bentonites over a wide suction range (Seiphoori et al., 2014) limits the validation of flow models.

2.7 Critical appraisal of reviewed literature

The reviewed literature revealed that the hydraulic behavior of compacted clays under restrain and under the wetting-drying cycles is of great interest for the performance assessment of HLNW repositories. However, the hydraulic characteristics of unsaturated bentonites under the restrain condition (i.e. no volume change during the saturation) have been scarcely studied. Earlier studies in water resources discipline focus on the indirect techniques for predicting the soil hydraulic characteristics by utilizing the tensiometer measurements (Simunek and van Genuchten, 1996; Simunek et al., 1998, 2008). However, the chosen soils are non-expansive thus relatively insensitive to the compaction densities and the measurement range of these procedures is limited on the wet of SWCC due to the inability of pressure transducers to accurately measure the suctions at nearly dry side of SWCCs (Schindler et al., 2010). The effect of compaction density on the SWCC representation in different state variables was not clearly understood. Establishing unsaturated HCFs of compacted bentonites are not feasible in the laboratory, therefore HCFs were obtained from correct SWCC representation using statistical model. Studies related to the influence of compaction density and bentonite plasticity on the estimated HCFs are scarce. The predicted hydraulic characteristics were also not validated from the independent measurements.

It was also observed limited research work was done on the shrinkage behavior of clays. The methods adopted to obtain shrinkage curve data lack reliability as a comparative study of the methods is not made in many cases. The objective of this work aims at establishing and comparing the VSC from different methods.

2.8 Objective and scope of the proposed research work:

Based on the critical review of the literature, the objectives of the research work are defined as:

1. Establishing wetting SWCC of four bentonites of varying plasticity and at different compaction densities over a wide suction range using different measurement techniques. Comparison of restrained and unrestrained SWCCs for understanding the flow behavior in compacted clays.
2. Establishing drying SWCC over a wide suction range where bentonites varied from slurry state to the residual saturation state. Study of theoretical models to relate wetting SWCC of compacted bentonites with the measured drying SWCC data by hysteresis models.
3. Establishing and comparing VSCs of studied clays by different laboratory methods. Studying the effect of established VSC on the estimated $SWCC_{SR}$ data.
4. Prediction of HCFs of bentonites at different compaction densities from SWCC data using statistical model. The influence of compaction density on $SWCC_{\theta}$ and $SWCC_{SR}$; HCF will be evaluated.
5. Infiltration characteristics of compacted bentonites in terms of moisture diffusion profiles will be studied. The influence of plasticity and compacted bentonites on the water movement will be explored. Theoretical analysis of water movement through compacted bentonites using independently estimated soil hydraulic

functions (SWCC and HCF) will be explored for validation with the measurements.

Chapter 3
Materials and Methods

3.1 General

The experimental investigations carried out for fulfilling the objective of this research work were discussed in detail in this chapter. The evaluation of various physical and geotechnical characterization of the soils used in this study were included. The methodologies adopted for establishing volumetric shrinkage curve and soil hydraulic functions were also presented here.

3.2 Bentonites

Four commercially available bentonites designated as B1, B2, B3, and B4 were used in this study. The bentonites were procured from Barmer district of Rajasthan and Kutch region of Gujarat, India. The clay soils were dominated by the percentage of clay content with a clay size fraction varying between 60-80% for different soils (Table 3.1). The particle size analyses of all the clays were determined using the standard test methods (ASTM D 422-63, 2007) and summarized in Table 3.1. Specific gravity of the soils (G_s) was determined by density bottle method as per the ASTM D 854-92 (1994). The Atterberg's limits of the soils were determined (ASTM D4318, 2010; IS: 2720 Part 6 1972).

The XRD phase identification was performed in normal, glycoled (Mosser-Ruck et al., 2005), and calcined (Grim, 1968) forms. In the glycoled form the bentonite samples were solvated in Ethylene Glycole vapors at elevated temperatures i.e., 60^0 C in an incubator nearly for 72 hours (Olsson, 1991); in the calcined form the samples were heated to 600^0 C in muffle furnace and then cooled at the room temperature before carrying out the XRD. The XRD data were presented in Fig. 3.1. The *d* spacing and corresponding

mineral was presented against the peak intensities. The XRD data of the studied bentonites showed the presence of montmorillonite mineral with multiple peaks. The XRD data in glycoled and calcined forms improved the phase identification with the presence of sharp and clear peaks for montmorillonite. Other important minerals such as kaolinite, illite, quartz, etc. were present in all the bentonites as presented in Fig. 3.1. However, the peaks corresponding to kaolinite were absent in the calcined form which is also reported by Grim (1968) as the heating to 600^0C causes kaolinite to lose its crystalline character.

Table 3.1 Basic properties of the studied bentonites

Property	B1	B2	B3	B4
Particle size distribution (%)				
Fine sand (0.425-0.075 mm)	2.35	3.79	1.39	1.53
Silt size (0.075-0.002 mm)	35.33	27.48	20.18	14.71
Clay size (<0.002 mm)	62.32	68.73	78.43	83.75
Consistency limits (%)				
Liquid limit, w_{LL}	175	296	393	597
Plastic limit, w_{PL}	27	46	50	51
Shrinkage limit, w_{SL}	12	14	18	23
Specific Gravity, G_s	2.76	2.76	2.77	2.77
SSA (m^2/g)	402	376	495	445
Total CEC (meq/100g)	31.35	50.8	65	107.4
Na^+ (%)	45	67	53	86
Ca^{2+} (%)	50	24	45	14
K^+ (%)	5	10	2	0
Montmorillonite content* (%)	37	41	54	61

*based on the regression method (Chittoori, 2008; Ashraf, 2008)

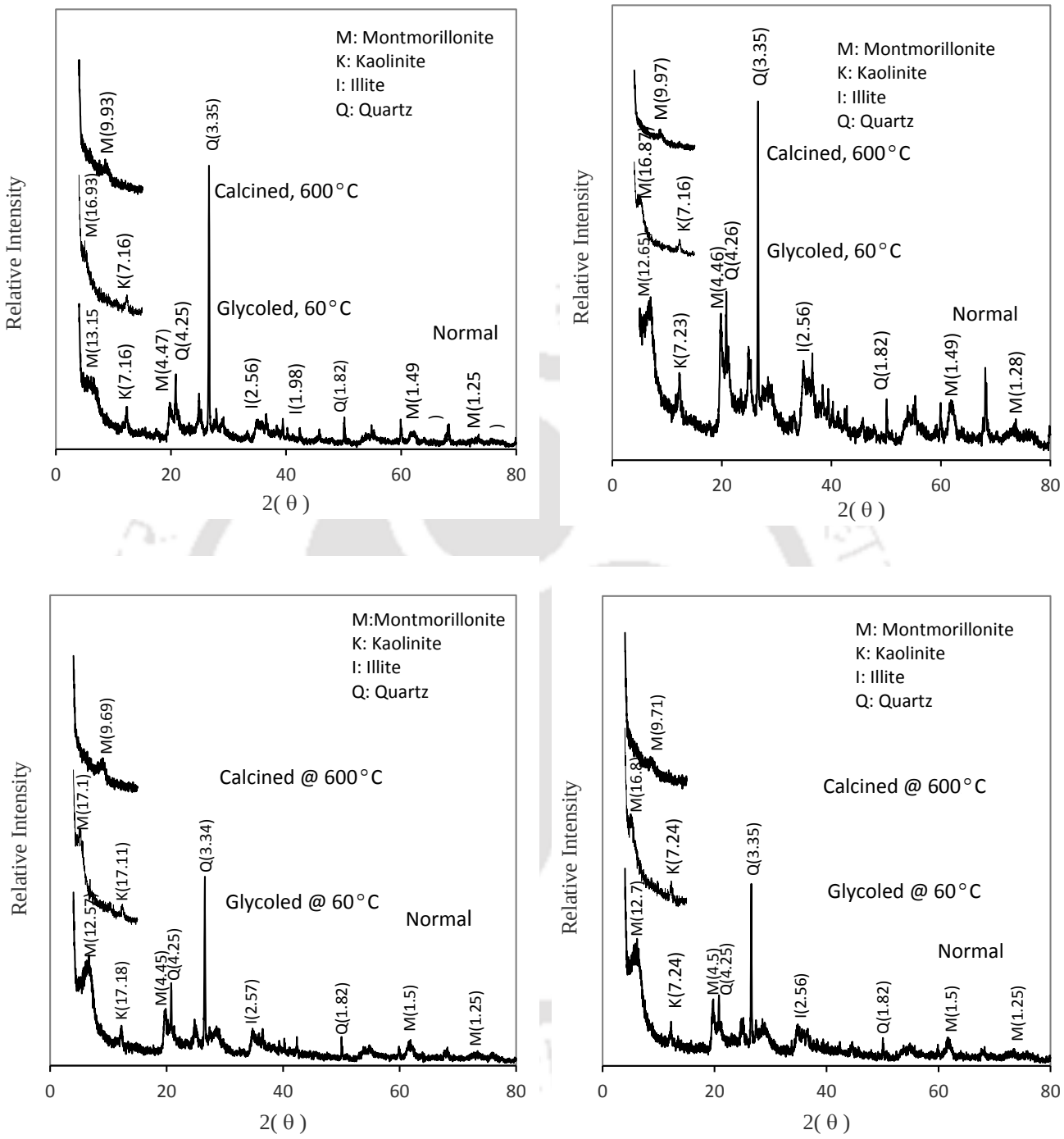

Fig. 3.1 XRD pattern of B4 in normal, glycoled, and calcined forms

The chemical composition of the studied bentonites was determined using X-ray fluorescence (XRF) and presented in Table 3.2. The oxide elemental composition was similar to the data for the standard MX80 bentonite (Karnland, 2010). Specific surface

areas (SSA) of the soil specimens passing through 425-μm sieve were determined using ethylene glycol mono-ethyl ether (EGME) retention procedure (Cerato and Lutenegger, 2002) on four duplicate samples for each bentonite. The average values were reported in Table 3.1. The cation exchange capacity (CEC) was determined using a predetermined amount (i.e., 25 g) of oven dried samples by washing thoroughly with 250 mL of 1 M ammonium acetate solution at pH 7.0 (Chapman, 1965) in an orbital shaker for four hours and allowing to stand for overnight (Muurinen, 2011). The supernatant solution was extracted by centrifugation at 1000 rpm for 3-4 minutes for the determination of exchangeable cation concentration. The concentrations of individual major cations (i.e., Na^+, Ca^{2+}, and K^+) in the extracted solution were determined using the flame photometer. The total CEC was determined using the procedure given by Ross (1995) while the nitrogen determination was carried out using Kjeldahl method (IS 14684, 1999). The average data obtained from three trials is reported in Table 3.1. The percentage of exchangeable sodium varied between 45% - 86% and the percentage of exchangeable calcium varied between 14% - 50% for different bentonites. The exchangeable calcium percentage was very high in both B1 and B3. Therefore, the liquid limit water contents of B1 and B3 were smaller than B2 and B4 while the average SSA values of B1 and B3 were higher than B2 and B4, respectively. The total CEC of B1 was smallest, possibly, due to the lowest clay size content (i.e., 62%). An approximate percentage of montmorillonite mineral content was estimated using the regression technique (Chittoori, 2008; Ashraf, 2008) and reported in Table 3.1. The montmorillonite content varied from 37% to 61% for different studied bentonites.

Table 3.2 Chemical composition of the bulk materials expressed as weight percent of major element oxides

Sample	SiO_2	Al_2O_3	Fe_2O_3(T)	MnO	MgO	CaO	Na_2O	K_2O	TiO_2	P_2O_5
B1	59.72	23.21	4.72	0.124	1.57	1.09	2.83	1.54	3.54	0.45
B2	57.10	24.88	5.29	0.151	1.57	0.61	3.12	1.04	3.81	0.42
B3	59.55	22.53	4.47	0.154	1.97	1.11	2.97	1.66	3.60	0.48
B4	53.97	20.45	8.71	0.101	1.92	1.15	4.34	1.60	3.25	0.26

3.3. Methodology

3.3.1 Saturated hydraulic conductivities of bentonites

Saturated hydraulic conductivities (k_s) of the bentonites at different compaction densities were determined by falling head method (IS 2720 part (XVII), 1986) in specially fabricated fixed-wall permeameters. Small-size permeameters of size 20 mm (internal diameter) × 10 mm (thickness) were used to reduce the time required for saturation and hydraulic conductivity estimation under restrained condition (Fig. 3.2b). The air-dry specimens (hygroscopic water content varied between 9.6 to 12% for different bentonites, see Table 3.1) were statically compacted to different densities in permeameters and the permeameter set-up was immersed in water reservoir for hydration (ASTM D 5084-03, 2003). The set-up was weighted at frequent intervals and the equilibrium value was noted to ensure full saturation. Four different compaction densities were used for each bentonite for hydraulic conductivity estimation. One additional density, 0.5 g/cm^3, was considered for all the bentonites to represent the HCF of an unrestrained condition (loosest state) by loosely placing the specimen in

permeameters without significant compaction energy to represent the hydraulic conductivity in unrestrained condition. The saturation time varied between 15 – 20 days. A total head of about 2 m was applied by connecting to a burette (Fig. 3.2a) and the time required for water to drop from upper level to lower level was noted to determine the saturated permeability. The drop of head at different time intervals was noted in independent trials and permeability was estimated. The measured permeability from different trials was consistent which indicated that the specimens were fully saturated.

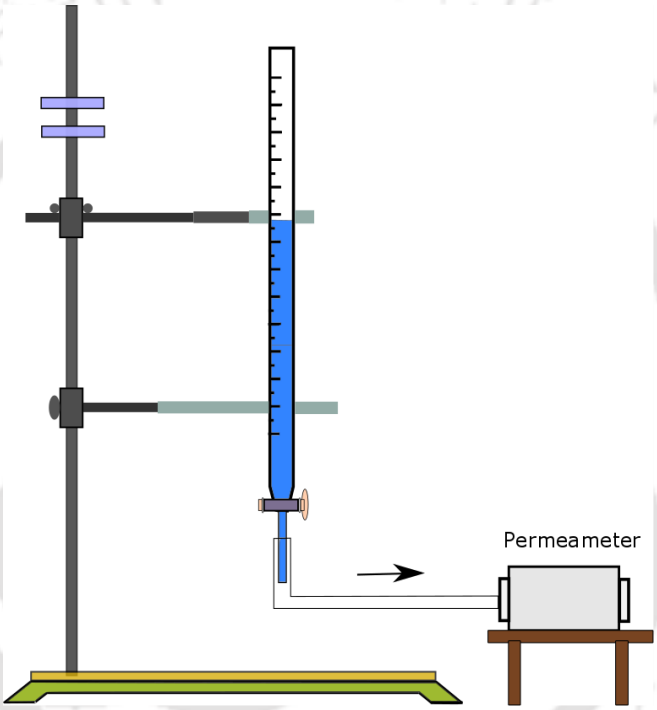

Fig. 3.2a Saturated permeability measurement set up

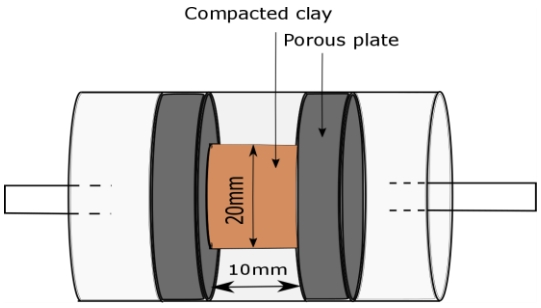

Fig. 3.2b Laboratory permeameter set-up

The estimated conductivities for different bentonites and at different initial compaction densities were reported in Table 3.3.

Table 3.3 Hydraulic properties of bentonites compacted at different densities

Soil	Dry density (g/cm^3)	0.5	1.0	1.4	1.6	1.8
B1	k_s (m/s) #	2.97×10^{-10}	5.11×10^{-11}	3.99×10^{-12}	4.04×10^{-13}	2.61×10^{-13}
	k_s (m/s) *	-	-	1.27×10^{-12}	4.87×10^{-13}	2.97×10^{-13}
	w_s (%)	175.69	67.91	44.95	32.02	27.80
B2	k_s (m/s) #	1.83×10^{-10}	3.57×10^{-11}	3.76×10^{-12}	2.81×10^{-13}	1.99×10^{-13}
	k_s (m/s) *	-	-	1.24×10^{-12}	4.08×10^{-13}	2.50×10^{-13}
	w_s (%)	186.67	78.69	48.13	37.68	31.20
B3	k_s (m/s) #	7.22×10^{-10}	2.29×10^{-11}	1.08×10^{-12}	2.25×10^{-13}	1.21×10^{-13}
	k_s (m/s) *	-	-	1.20×10^{-12}	3.20×10^{-13}	2.29×10^{-13}
	w_s (%)	188.64	80.89	53.73	38.68	33.72
B4	k_s (m/s) #	6.48×10^{-10}	1.29×10^{-11}	1.17×10^{-12}	2.12×10^{-13}	1.92×10^{-13}
	k_s (m/s) *	-	-	1.15×10^{-12}	2.39×10^{-13}	1.98×10^{-13}
	w_s (%)	192.37	79.33	55.84	40.70	33.80

using falling head test; * using consolidation test

The saturated conductivities of these bentonites at the studied compaction densities were compared against the data obtained from Oedometer tests (Sahu, 2016). In consolidation tests, the clay specimens at water contents equal to 1.2 times liquid limit are placed in oedometer rings and consolidated in saturated state by mechanical loading. The k_s is obtained from the estimated coefficient of consolidation and coefficient of volume compressibility. The measured k_s values in falling head tests were in agreement with the estimated data from oedometer tests. The saturated hydraulic conductivity values varied between 10^{-10} m/s and 10^{-13} m/s for different bentonites at different compaction densities. The saturated hydraulic conductivity of the bentonites was influenced by the compaction

density and plasticity which is in agreement with the earlier observations (Pusch, 1982; Rao and Matthew, 1995; Cho et al., 1999; Dixon et al., 1999). The saturated water contents of the bentonites in compacted state were estimated by extruding the clay plugs from the permeameters after the testing was completed. The saturated water content was represented in gravimetric basis and presented in Table 3.3 for different densities.

3.3.2 Soil water characteristic curve (SWCC) Estimation

The suction of the bentonites at different water contents were estimated by three independent techniques in different suction ranges as the measurement or control of suction over wide range of water content is not possible by a single method for plastic clays (Tripathy et al., 2014). Osmotic technique (Delage et al., 1998; Delage and Cui, 2008) was utilized to control the suction in the range of $20 < \psi < 1600$ kPa. On the other hand, chilled-mirror hygrometer (WP4) was utilized for estimating the suction data from RH and temperature measurement for suction values over 1000 kPa. The suction was controlled using vapour equilibrium technique in the higher suction range ($\psi > 20000$ kPa) using saturated salt vapours. A detailed description of the adopted techniques in unrestrained and restrained conditions was given here.

3.3.2.1 Osmotic technique

Osmotic method is based on maintaining an osmotic suction head across a semipermeable membrane, which separates the soil pore water and a known concentration of the polyethylene glycol (PEG) solution (Zur, 1966; Williams and Shaykewich, 1969; Fleureau et al., 1993). A PEG solution containing PEG molecular size larger than the molecular weight cut-off (MWCO) value of the semipermeable membrane is used for inducing an osmotic head across the membrane (Lagerwerff et al., 1961). The membrane induces osmotic suction head due to restriction of PEG molecule

diffusion, but favoring the osmotic flow of water molecules from PEG solution to the clay specimen. A semipermeable membrane with MWCO value of 14000 was used to separate the powder bentonite specimen and poly ethylene glycol (PEG) 20000 solution in volume unrestrained condition during the wetting tests. The powder clay specimen was wrapped in a membrane and placed in a flask containing PEG solution, after tying the two ends with a thread, as shown in Fig. 3.3. The flask was covered with polythene sheet to avoid any possible evaporation of the PEG solution, which may otherwise alter the concentration. A sufficient space was provided for the clay specimen to swell during the wetting. Different PEG solution concentrations were prepared and used in the flask to induce different targeted osmotic suctions, varied between 20 kPa and 1600 kPa. Osmotic flow of water from PEG solution into clay chamber takes place to equalize the total head across the membrane. PEG solution concentration in the flask was monitored frequently by measuring the brix index. A handheld, brix refractometer was used for measuring the brix index in this work. Graphical relationship between brix index and the PEG 20000 concentration was utilized from the previous work (Delage et al., 1998) to estimate the osmotic suction. The changes in PEG concentration in the flask indicated the osmotic flow across the membrane. The flow continued until the equilibrium. The equilibrium time varied between 5 – 7 days for different bentonites. The moisture content was determined by oven drying the wet specimen after the test.

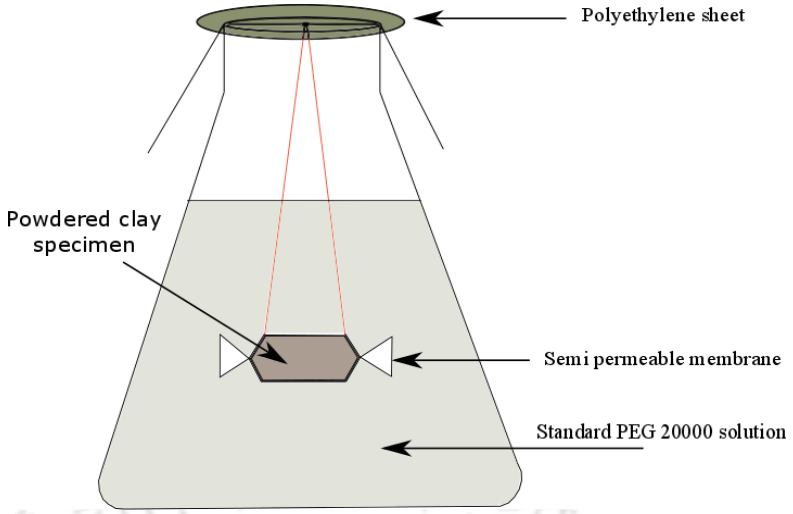

Fig. 3.3 Schematic diagram of osmotic test (unrestrained test)

The suction in the wetting process in volume restrained condition were estimated by conducting the osmotic tests in small perspex cells. A specimen size of 38 mm diameter and 20 mm length was obtained by static compaction technique at air-dry state in Perspex cell (Fig. 3.4b). Four different compaction dry densities viz., 1 g/cm^3, 1.4 g/cm^3, 1.6 g/cm^3 and 1.8 g/cm^3 were used for each bentonite. Two porous stones of 6 mm thick were used either side of the clay specimen. Semipermeable membrane was placed between the specimen and the porous stone to control the osmotic head. The osmotic cell was connected to a burette which contained PEG solution as shown in Fig. 3.4a. Different PEG solution concentrations were maintained to induce osmotic heads similar to the unrestrained condition. The equilibrium time varied between 12 – 14 days for different compaction densities in these tests. The equilibrium water content was obtained from the extruded specimen from the cell after each test. Testing, in both restrained and unrestrained cases, was done cautiously to prevent any intrusion of PEG solution into the clay specimen.

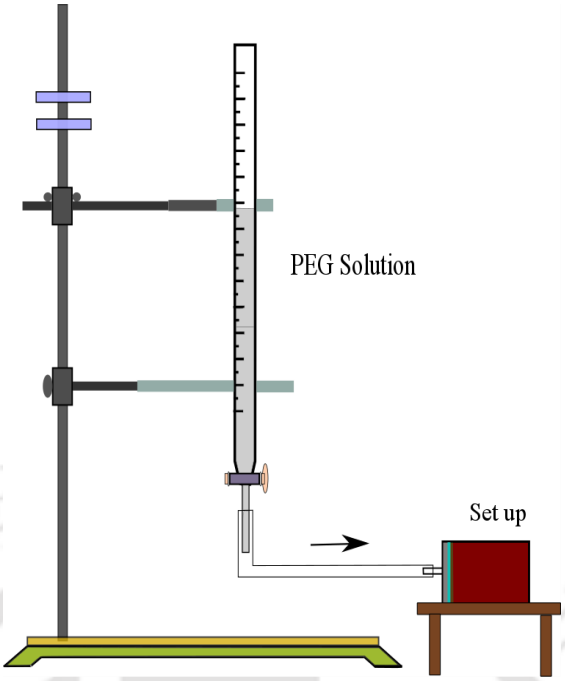

Fig. 3.4a Schematic diagram of SWCC test using osmotic technique for restrained case

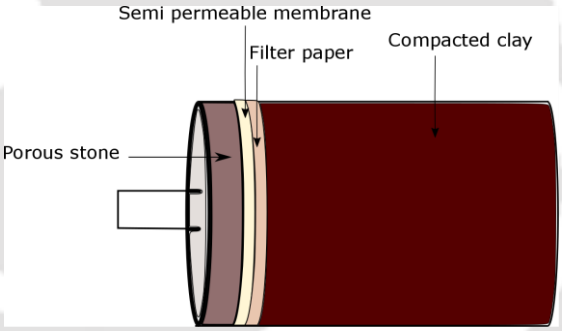

Fig. 3.4b Set up for compacting soil sample

3.3.2.2. Method of Vapor equilibrium

The total suction of the clay specimen is controlled, in this technique, by controlling the vapor pressure and temperature of the ambient environment. The vapor pressure of a closed environment is controlled by different concentrations of the salt solutions (ASTM E104-02, 2012). The clay specimens were brought to equilibrium with the controlled

vapor pressures in the closed environment. The vapor pressure is related to total suction by Kelvin's equation (Hillel, 1980) and is given by

$$\psi = -\frac{RT}{v_o \omega_r} \ln \frac{p}{p_o} = -\frac{RT}{v_o \omega_r} \ln (RH) \qquad (3.1)$$

where R is the universal gas constant (8.31 J/mol.K), T is the absolute temperature of the sample (K), v_o is the specific volume of water (m^3/kg), ω_r is the molecular mass of water vapour (18.016 kg/kmol), p is the partial vapor pressure of the air and p_o is the saturated vapor pressure at sample temperature. The vapor equilibrium method was utilized here for establishing the SWCCs in the "dry-end" state of the bentonites under volume restrained and unrestrained conditions. The tests for the powder specimens were carried out in a glass desiccator. The specimens in small, open containers of size 20 cm^3 were placed on the perforated shelves in the desiccators. Different saturated salt solutions were placed at the bottom of the desiccator and the lid was closed to maintain a specific vapor pressure of the ambient atmosphere as shown in Fig. 3.5a. A 20^0 C ambient temperature was maintained by placing the desiccators in temperature controlled chambers as shown in Fig. 3.5b. The details of the saturated solutions used in this work were given in Table 3.4. The corresponding total suctions at 20^0 C (ASTM E104-02, 2012) were also given in this table. In general, only saturated salt solutions are used as the molar fraction of water in a solution does not change with the exchange of humidity between liquid phase and gaseous phase (Delage et al., 1998; Saiyouri et al., 2000; Tang and Cui, 2005). The application of unsaturated solutions for vapor equilibrium technique is not common as the salt concentration decreases with time and the equilibrium vapor pressure may not be same as the targeted vapor pressure (Tang and Cui, 2005). However, the vapor pressures of the salt solutions were continuously monitored using hygrometer and the equilibrium values were used in establishing the SWCCs. The specimen weight

was frequently monitored and the moisture content was determined by over-drying method at equilibrium. Care was taken to minimize the exposure time for the saturated solutions to the outside atmosphere while weighing the clay specimens. The vapor pressures of the saturated solutions at the end of the testing were measured using chilled mirror hygrometer (Decagon Devices, Pullman, WA) and the corresponding suction was used in establishing the SWCCs. The equilibration time varied between 30 – 90 days for different bentonites.

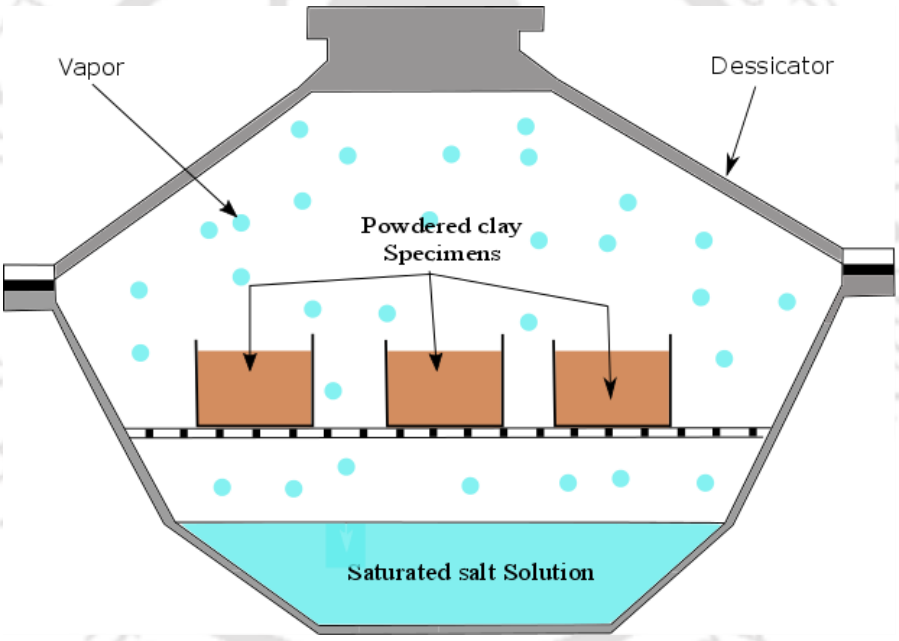

Fig. 3.5a Schematic diagram of Vapor equilibrium test (unrestrained case)

Fig. 3.5b Vapor equilibrium test in temperature controlled chamber in unrestrained condition

Table 3.4. Saturated salt solutions and corresponding suction values at 20°C in vapor equilibrium test

Volume unrestrained specimens			Volume restrained specimens		
Salt solution	RH(%)	Total suction (MPa)	Salt solution	RH(%)	Total suction (MPa)
KCl (4.6M)	85.1	20.5	KCl (0.5M)	98.47	2.15
NaCl (6 M)	75.5	38	NaCl (1.1M)	96.81	5.6
NaBr (8M)	59.1	71.12	KNO_3 (3.1 M)	94.6	7.5
LiCl (8.3M)	53.2	85.31	KCl (4.6M)	85.1	20.5
LiCl(13.3M)	12	286.7	NaCl (6 M)	75.5	38
			LiCl (8.3M)	53.2	85.31

In case of compacted specimens, the vapor equilibrium tests were conducted in aluminum cells similar to the osmotic technique (Fig. 3.4b). In these tests, however, the

two ends of the cells were connected to vapors of the salt solution through pneumatic pump as shown in Fig. 3.6. The compacted specimens hydrated due to circulation of the vapors to equalize vapor pressure of the specimen with the salt solutions. The circulation of salt vapors by the pumps reduced the equilibration time. All the four bentonites were compacted to four different compaction densities similar to the earlier tests. Various saturated and unsaturated salt solutions were used to vary the total suction in the range of 2000 – 85000 kPa in compacted condition at 20°C. The salt concentrations that were utilized in the study and the corresponding total suction values were reported in Table 3.4. The equilibrium time varied between 15– 25 days, depending on the soil type and concentration of the salt solution. The equilibrium time was estimated by monitoring the weight of the soil cell at frequent intervals. The vapor pressure of the salt solution at equilibrium was determined using the chilled mirror hygrometer for estimating the equilibrium value of total suction. The equilibrium water content was estimated by extruding the clay specimen from the cell after the test.

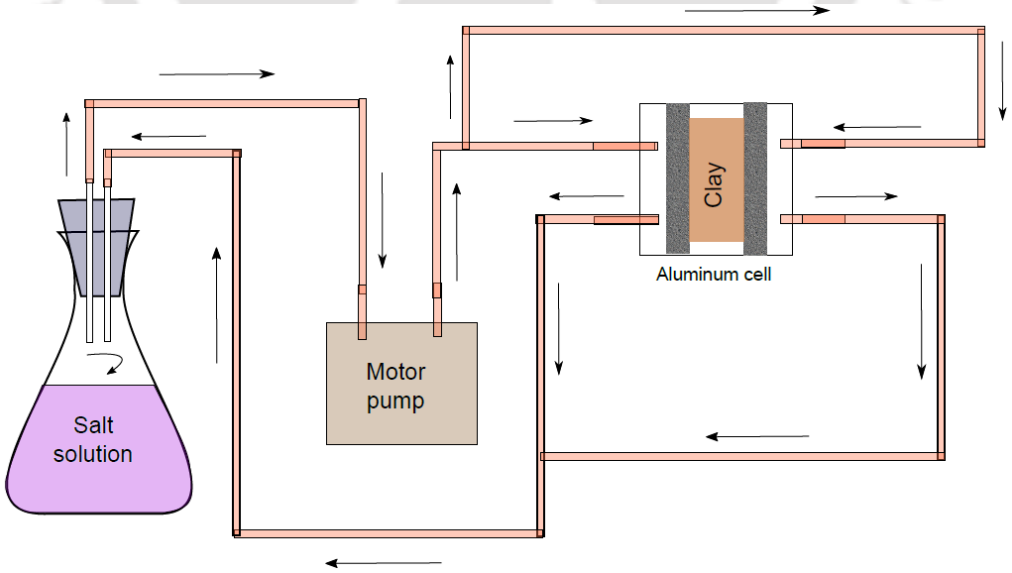

Fig. 3.6. Vapor sorption test set-up for compacted bentonite specimens

3.3.2.3. Transient water sorption method

Transient water sorption technique was used for estimating the water retention data of powder specimens in the higher suction range. This method was similar to vapor sorption analyzer (Decagon Devices, Pullman, WA) used by several researchers recently (Khorshidi and Lu, 2016; Akin and Likos, 2016) for dynamic estimation of water retention data. In the present technique, however, the sorption data were analyzed manually at different time intervals when the clay specimen was exposed to 100% RH environment. Distilled water was used in desiccators instead of salt solutions while the weight of the specimen and vapor pressure of the specimen were monitored regularly. Chilled-mirror hygrometer was used to measure the vapor pressure at meta-stable state of the specimens. The water retention data was obtained in the suction range of 2 – 100 MPa for different bentonites by this technique. SWCC data were also presented in terms of volumetric water content ($SWCC_{\theta}$) and degree of saturation ($SWCC_{SR}$) to understand the influence of compaction density. The data could not be used to establish $SWCC_{\theta}$ and $SWCC_{SR}$ in volume unrestrained condition as it requires the estimation of volumetric swelling behavior of bentonites.

3.3.3. Volumetric shrinkage characteristics

The volumetric shrinkage behavior of clay soils was determined by different laboratory techniques. The initial state of the soil specimen was same in all the techniques. The soil samples were prepared with water content equal to 1.2 times of their liquid limit water contents, w_{LL}. The specimens were transferred to plastic bags and kept in desiccators for uniform moisture distribution for about three days before commencing the volumetric shrinkage tests. The samples in all the tests, except the balloon method, were subjected to natural drying process. The ambient temperature varied between 25-30^0 C and the

relative humidity varied between 75-80% during the testing in the laboratory. A detailed description of the employed techniques was presented here.

3.3.3.1 Wax coated (WC) technique

This method is widely used for determining the bulk specific gravity of hot mix asphalts (HMS) (Bhattacharjee and Mallick, 2002) and for determining the shrinkage limit of soils in engineering (ASTM D7263, 2009). A slight modification to the standard procedure was adopted to obtain the volume of the specimens at different saturation states. In this method, shrinkage dishes of initial volume of 22 cm^3 were lubricated with a thin layer of oil before filling the soil into them to avoid any frictional resistance between the metal surface and soil during the shrinkage process. Shrinkage dish was filled with the soil specimen gradually with continuous tapping to expel any air voids present. The samples were allowed to dry until attaining a considerable strength to handle them for wax coating. The mass of the specimen was recorded and then the melted wax was carefully coated around the sample. Care was taken not to disturb the state of the soil specimen during this process. The mass of the wax-coated specimen was recorded to find out mass and volume of the wax using the density of wax, ρ_{wax} = 0.9 g/cm^3. The submerged mass of the wax-coated specimen was recorded by immersing in water with the help of a wire. The volume of the specimen was estimated knowing the volume of the coated wax around the specimen using Archimedes' principle. The water content of the specimen was measured again after peeling out the coated wax. Duplicate soil specimens were used for measuring the mass and volume of the specimens at different drying time periods to establish the entire shrinkage path.

3.3.3.2 Clod test

Clod test utilizes different encasement materials such as MEK Saran (Nelson and Miller, 1992) or PVAc glue (Krosley et al., 2003) in place of wax. The encasement material in

clod test allows vapor transfer, but restricts the moisture transfer between the specimen and the atmosphere through the encasement. Therefore, a single soil specimen is adequate to establish the entire shrinkage path, which is a major advantage of this technique. The specimens for clod tests were prepared in a shrinkage dish in a similar manner to the WC technique. The clay specimens in this study were coated with commercially available Elmer's glue, which is a variety of unibond waterproof polyvinyl acetate (PVAc). The glue was diluted by preparing the encasement with a ratio of 10 part of glue to 1 part of deionized water as suggested by Tadza (2011) to improve its workability. The clod specimens were suspended with the help of a thread and allowed to dry out at an ambient laboratory temperature. The submerged mass of the glue-coated specimens in water were measured to estimate the volume of the specimen at different saturated states. However, the estimation of initial clod volume was difficult due to requirement of sufficient time for the glue to solidify. It is well known that PVAc glue requires longer drying/setting time (Liebig, 2003). Difficulties are encountered in the initial volume measurement as the clod specimen is immersed in water for the measurement of mass and wet-glue does not act as water-repellent material. Similar observations are also made by Tadza (2011). Therefore, the volume measurement of specimen was obtained by immersing the specimen in mercury until the encasement was dried. However, as the application of mercury is limited pertaining to serious health hazards, non-polar liquids such as kerosene were found to be a good alternative to mercury and provided accurate VSC estimation during the encasement drying process. A constant glue density of 1.05 g/cm^3 was considered in the mass-volume calculations. Extreme care was taken to wipe out the excess water accumulated on the clod specimen after the water immersion. The measurements were taken until no further reduction in the

volume of the clods was noticed. The time required for achieving the residual shrinkage state varied for different clays and with different initial volumes.

3.3.3.3 Balloon Method

Balloon method is often used to encase the soil specimen for establishing the shrinkage curve in the literature. The saturated soil sample was carefully filled into a rubber balloon to lower than its mouth level. A wooden stopper, with inlet and outlet pipes for circulating the ambient air, was fitted to the mouth of the balloon (Fig. 3.7a). These pipes were connected to the valves and to inlet pipe was connected to an air pump to circulate the ambient air to control the shrinkage process (Fig. 3.7b). The entire setup was suspended with the help of a burette stand and a hook support. The individual weights of all the components of balloon the setup were measured before the test was started. The water content of the sample was estimated from the weight of soil specimen at any given time and dry mass of the soil after completion of the test. The volume of the soil specimen was estimated using the Archimedes' principle by measuring the mass of balloon with specimen after in air and immersing in water. The valves were closed and a small vacuum was applied during the volume measurement to ensure a perfect encasement to the soil specimen by the balloon. The volume of the balloon is generally neglected in the specimen volume calculations. Three independent shrinkage volume tests using different balloon sizes (initial specimen volumes) on B2 specimen were conducted to understand the influence of balloon volume on the established VSC data.

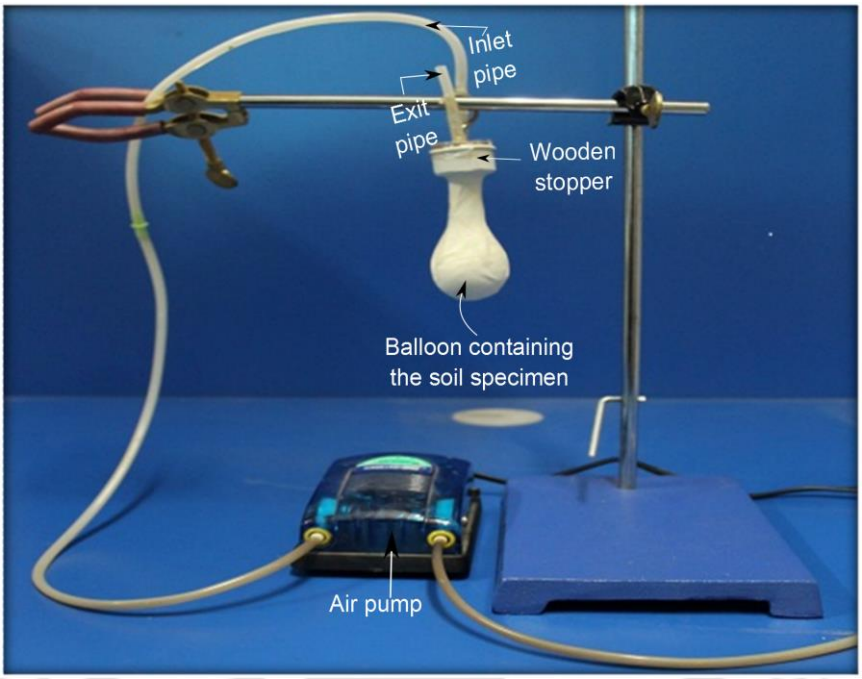

Fig. 3.7a Laboratory set-up for the Balloon method

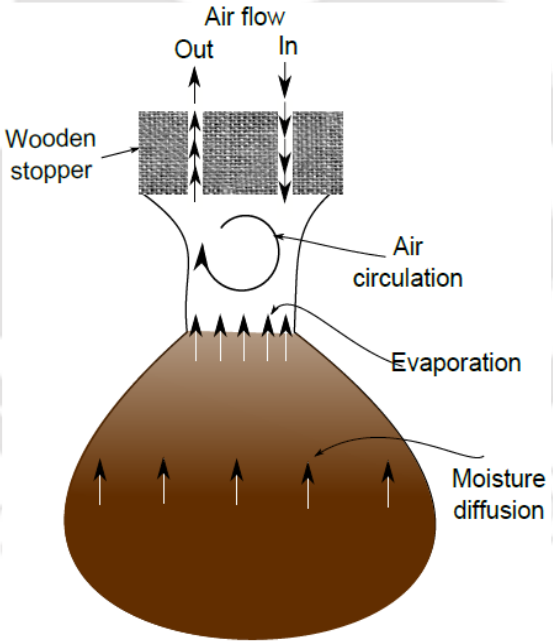

Fig. 3.7b Shrinkage mechanism in Balloon method

3.3.3.4 Direct Volume Measurement (DVM) technique

This method was originally introduced for low plasticity tailings (Peron et al., 2009; Saleh-Mbemba et al., 2016). The testing set-up consisted of a rectangular shrinkage mould of dimension 200 mm x 30 mm x 10 mm made up of a perspex glass plate (Fig. 3.8). The mould height can be adjusted by stacking glass plates on the present one. Two different mould sizes were used to verify the effect of mould height on the test results. The sample was filled in the box in layers with gentle tapping on the side during the placement to remove any entrapped air bubbles. Excess material was removed by trimming the top surface with a spatula. The initial water content was determined for each specimen by carefully weighing the mould with its content on the scale. The initial volume of the sample was equal to the mould volume. The specimen dimensions were measured at frequent time intervals to obtain the volume of the specimen with time. The weight of the specimen was also obtained at the same time to establish volumetric shrinkage behavior of different clay soils.

Fig. 3.8 Shrinkage box (200 x 30 x 10 mm) with specimen at the initial state

3.3.4 Water infiltration tests

Infiltration tests were carried out on bentonites of different quality in Perspex glass columns (Fig. 3.9a). Any volume change during the infiltration was prevented by the glass column which simulates the confined environment in HLNWRs. The bentonite specimens, in air-dry state, were statically compacted in to the columns of 38 mm diameter and 100 mm long at four different compaction densities (ρ_d = 1 g/cm^3, 1.4 g/cm^3, 1.6 g/cm^3, and 1.8 g/cm^3) (Fig. 3.9a). A porous stone of 6 mm thickness was placed at one end of the horizontal column and a filter paper was placed between the porous stone and clay specimen (Fig. 3.9b). The caps were screwed at both ends of the column. One end of the column was connected to a source reservoir and a constant water head of 0.1 m was maintained throughout the test (Fig. 3.9b – 3.9c). The hydraulic head was found to have no influence on the infiltration characteristics of the compacted bentonites as detailed later. The cap of the other end contained an air vent for escaping of air. The specimen was extruded after terminating the experiment at a specified time interval (t = 24, 72, and 120 h) and was cut into 10 mm thick slices with a thin blade. Care was taken to terminate the test before water reached the other boundary of the column to avoid effect of lower boundary on the infiltration characteristics. Water did not reach the other boundary in the specified testing durations in the current study. The clay slices were analyzed for the gravimetric water content by oven-drying technique. All the tests were conducted at room temperature, which varied between 22 – 27°C during the testing.

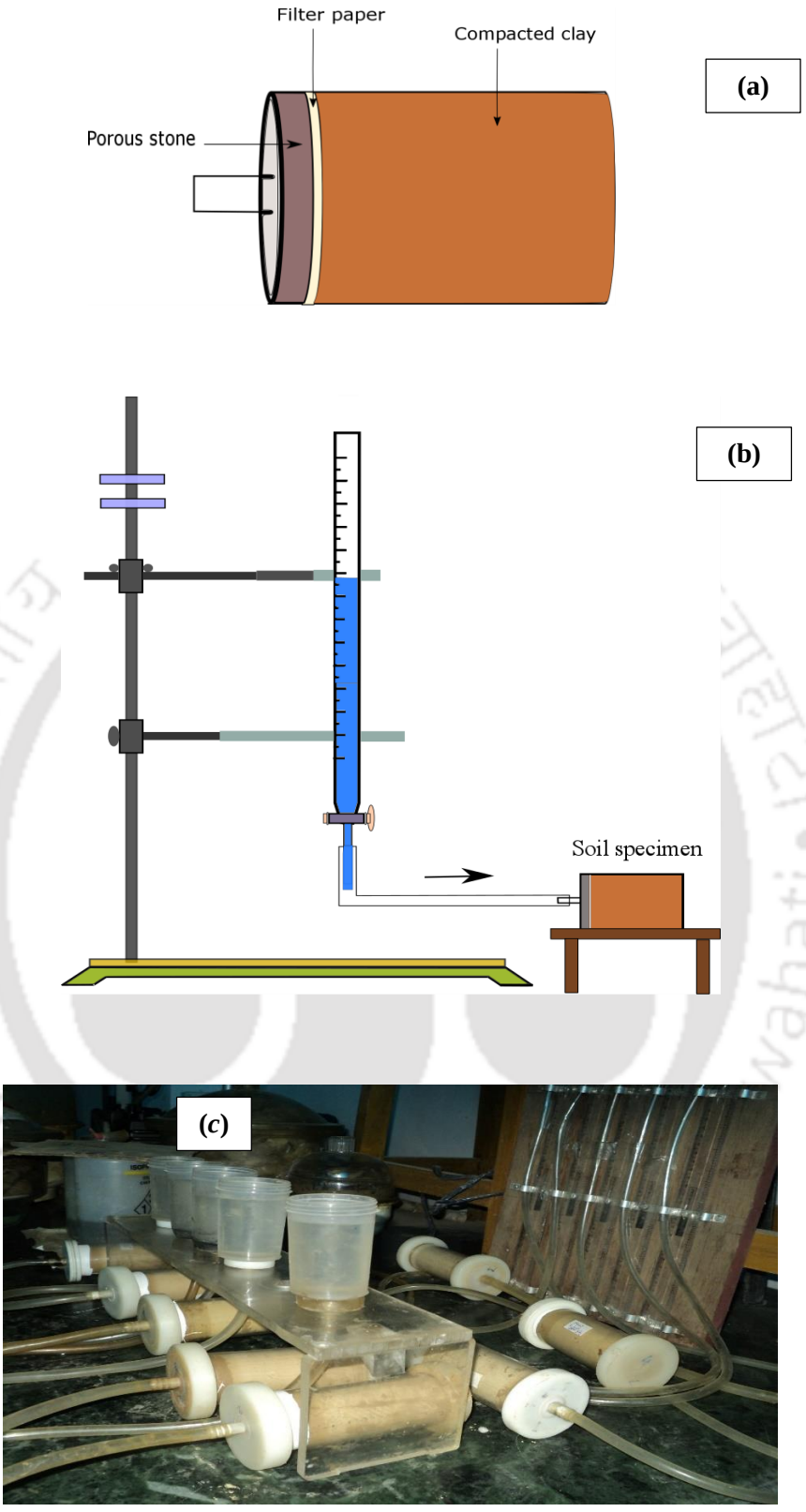

Fig 3.9 Infiltration test set-up (a) schematic diagram of the soil column (b) schematic diagram of the set-up (c) series of laboratory column set-up

Chapter 4

Drying SWCC data in unrestrained condition

4.1 General

In this chapter, the drying $SWCC_w$ of the bentonites was obtained for a wide suction range. However, correct interpretation of hydraulic characteristics like AEV, θ_r is not feasible using $SWCC_w$ for plastic soils. Therefore, VSCs were studied to determine the shrinkage characteristics of the slurried bentonites upon drying. Four different VSC measurement techniques were evaluated and compared. The drying $SWCC_w$ was combined with the VSC data for establishing $SWCC_{SR}$ and $SWCC_{\theta}$. The limitations of the volume measurement techniques were discussed and the best VSC measurement technique was recommended based on accurate estimation of $SWCC_{SR}$ from the measured $SWCC_w$.

4.2 VSC data

The VSC data is often expressed in terms of water content vs. void ratio or moisture ratio vs. void ratio (Fredlund and Rahardjo, 1993). The VSC data of all the four techniques for different bentonites were presented in Fig. 4.1a - 4.1d in the form of void ratio vs. moisture ratio. The slope of the normal shrinkage phase in this representation follows 1:1-line indicating that the decrease in the water content is equal to the decrease in the soil volume ($\Delta w = \Delta e$) or the degree of saturation is unity. A comparison between VSC data obtained from different techniques for B1 was presented in Fig. 4.1a. At any given water content, the void ratio obtained from the Balloon method was highest and the DVM technique was the lowest. The void ratios of the specimen at different time intervals obtained by clod tests were consistently following the results of DVM, but the data from the WC technique were scattered between these two extreme ranges. The void

ratio obtained from the clod test was close to the values obtained by DVM technique, but void ratios by WC method were close to the Balloon method for B1. Similar trend was observed for all the other bentonites (Fig. 4.1b-4.1c). However, the difference in the data by different techniques decreased for B3 and B4. The final water content of all the bentonites at equilibrium was about 10%. The observed scatter in the measured data by clod and DVM techniques was lowest compared to other methods and was more predominant for B1 and B2, that have smaller percentage of clay content compared to the other bentonites. The discrepancy in VSC data by WC method was mainly due to changes to the state of the soil specimen during the contact with the hot wax. A small percentage of water was evaporated during the wax encasement observed from the water content measurements made before and after the encasement. Although the water content of the sample was taken after peeling off the encasement in this study, the volume changes in the specimen due to wax solidification process, which varies with the state of the soil specimen, could not be accounted in establishing the VSC data. Few additional tests were conducted on duplicate specimens of B2 sample to understand the influence of wax solidification process on specimen volume change. A thin layer of wax was coated around a small clay clod and allowed to solidify. The volume of the clod was measured before applying the encasement and after peeling off the solidified wax by mercury displacement method. The volume of the specimen decreased due to the application of the wax and varied between 3-6% at an initial water content of 60-66% for B2. The solidification process of paraffin wax from liquid to solid phase is reported to be inflicting great volume changes (Ukrainczyk et al., 2010). The stresses due to solidification process of the wax decrease the volume of the specimen. However, this volume change behavior is different from the natural shrinkage process. The discrepancy of the volume measurement was, therefore, expected. Moreover, duplicate soil

specimens were used for establishing the shrinkage path which also persuades the errors. Other techniques were superior to WC method in these aspects. However, similar to WC method, the initial VSC data could not be obtained by clod method due to the requirement of coating the specimen with PVAc glue after attaining a sufficient strength to endure encasement process. The advantage of PVAc encasement is that the phase change process does not influence the specimen volume significantly and the entire shrinkage path could be established with a single soil specimen.

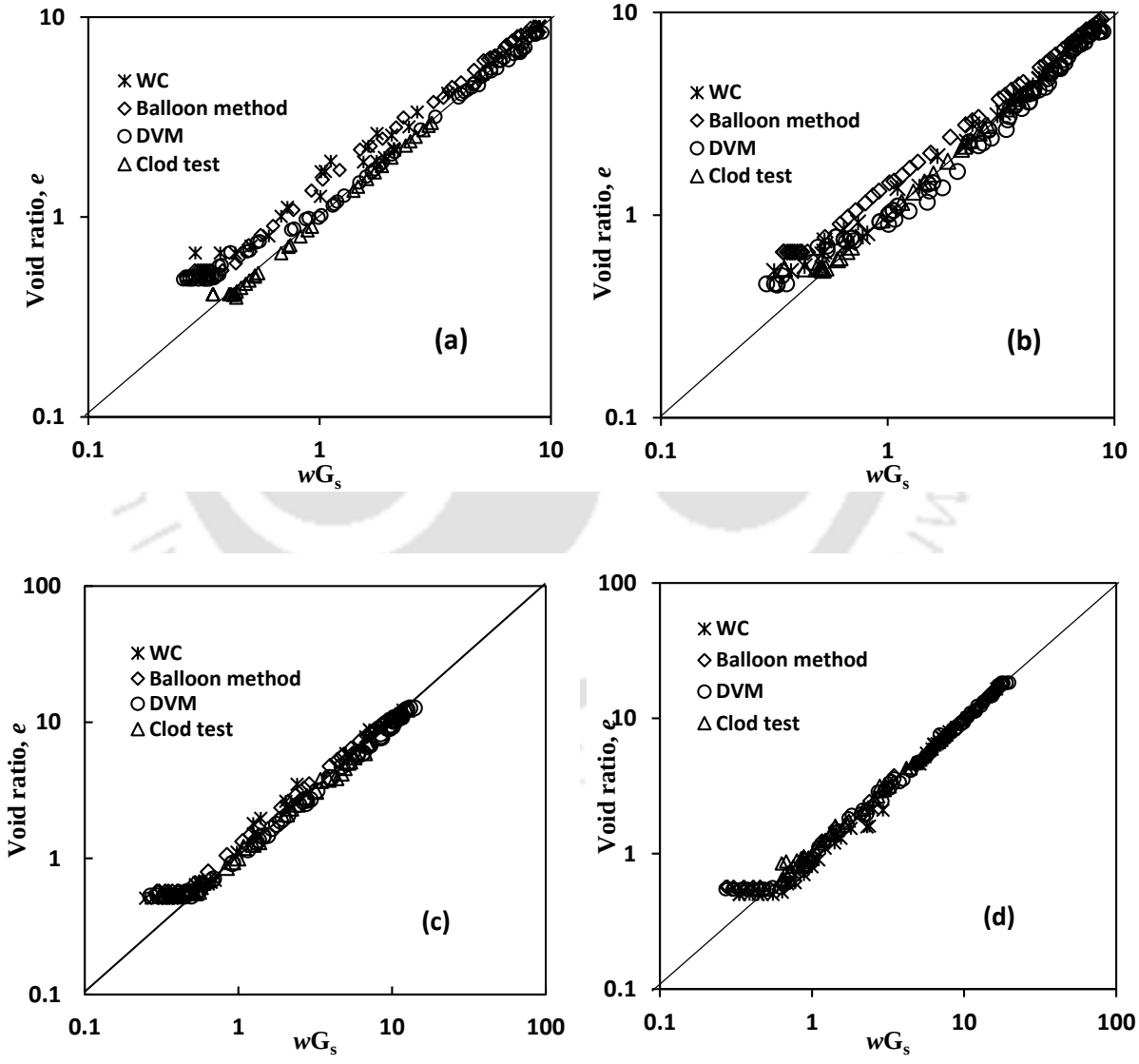

Fig. 4.1 VSC data of bentonites by different tests (a) B1 (b) B2 (c) B3 (d) B4

To understand the influencing parameters in Balloon and DVM techniques few additional tests were conducted. The VSC data of B2 were obtained by Balloon method with three different initial balloon volumes (i.e., sizes). The VSC data in terms of normalized void ratio, which is the ratio of void ratio to the initial void ratio, against water content was presented for different initial balloon volumes in Fig. 4.2a. The initial water content was same in these tests. The balloon volume directly influenced the measured void ratio of the specimen as shown in the figure. The measured void ratio decreased with the size of the initial Balloon volume. The change was significant for gravimetric water content values less than 100% for B2. The error in the measured volume was due to the following reasons: (i) neglecting the volume of the balloon in the specimen volume computations significantly overestimated the void ratio. The volume of balloon along with the specimen was measured on a duplicate B2 specimen by immersing it to a marked level, close to the balloon's mouth, at different saturated states of the specimen. The balloon volume up to the marked level was cut and measured its volume after completion of the test. The percentage error in the estimated void ratio was as high as 30% in the initial stage of saturation. Therefore, the error in the estimated void ratio was more for the balloon with higher initial volume. (ii) New problems were encountered while considering the balloon volume. Volume of the balloon containing the specimen was measured to a marked level at different saturated states during the shrinkage process. However, as the shrinkage reached the residual phase, the specimen volume decreased to a very small value (i.e., 1.7 cm^3). The balloon started floating when submerged in water to the initial marked level due to the buoyancy effects on the low-density balloon. The balloon was then submerged to the specimen level to obtain the accurate volume with a greater difficulty. However, determination of balloon volume up to different marked levels is impractical. (iii) The applied air suction, during the volume measurement,

exerted an additional pressure on the specimen and caused a slight distortion to the specimen (i.e., heaving at the top surface of the specimen). The distortion was more significant during the initial stages of the shrinkage process. The influence of suction application on the volume measurement was presented in Table 4.1 on a duplicate specimen of B_2 and an initial volume of 32.39 cm^3. The volume was recorded by submerging in water up to a fixed marked level near the balloon's mouth. The volume of the specimen decreased with the application of the suction at the beginning of the test where the specimen water content was higher than the liquid limit water content and specimen maintained good contact with the balloon. The volume changes due to suction application were mainly owing to shearing of the sample under the applied suction which was evident from the sample distortion (heaving at the top surface of the specimen). (iv) a small percentage of soil specimen was stuck to the surrounding walls of the balloon during the soil placement which inflicted error in the volume measurement. Cornelis et al. (2006b) prepared a saturated soil specimen in the balloon itself. However, this method is not practical for preparation of a saturated bentonite specimen at the liquid limit consistency (ASTM D4318, 2010).

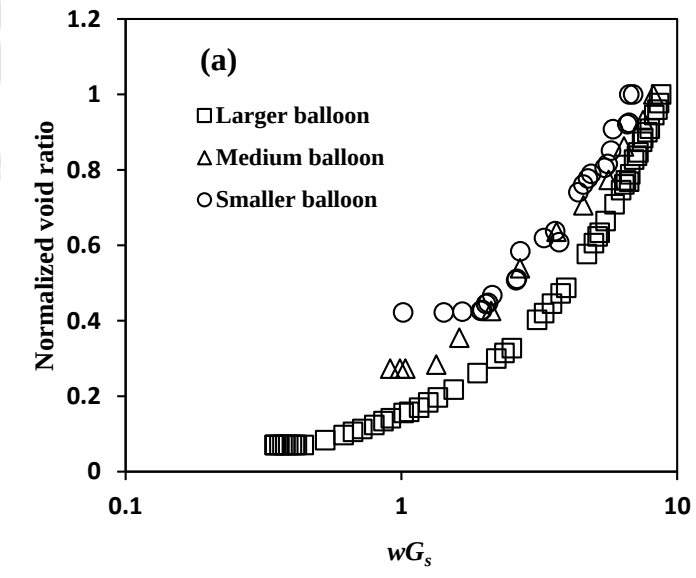

Fig. 4.2a Effect of balloon size on VSC data of B2

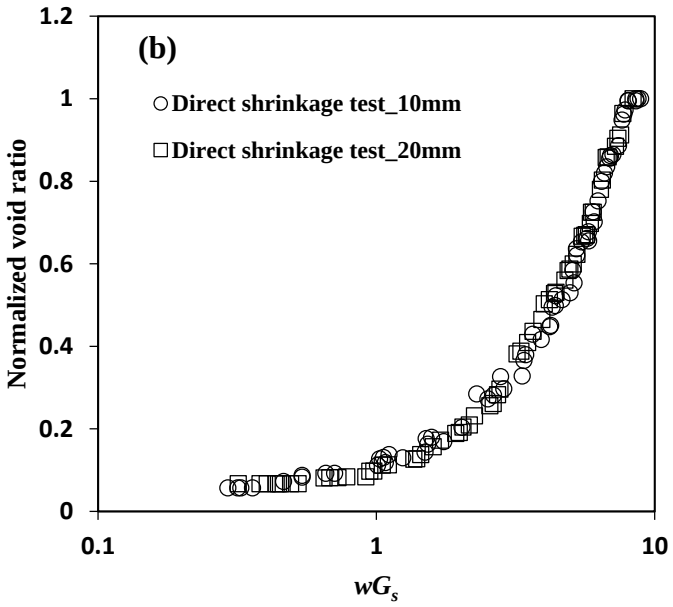

Fig. 4.2b Effect of Perspex dish sizes on VSC data of B2

Table 4.1 Influence of suction application on the volume measurement by balloon method

Reading No.	Time from the start of the experiment (*h*)	Specimen mass (*g*)	Measured specimen volume (cm^3)	
			With suction application	Without suction application
1	0	34.95	30.66	32.99
2	11.5	31.79	29.11	31.93
3	22.5	30.16	27.19	29.29
4	37.5	26.47	23.80	NA (Specimen floats)

The VSC data with different initial volumes by DVM technique (Fig. 4.2b) showed that the measured data obtained from two tests were consistently followed the same trend over the entire water content range. The influence of initial volume was not significant in this technique. However, cracks appeared in all the clay soils (Fig. 4.3a) after the AEV and broken into small pieces which made volume measurement difficult. Further, accurate measurement of volume was not possible as the geometry of the specimens was

not uniform due to anisotropic shrinkage process (Fig. 4.3b). While the volume was measured by considering the specimen dimensions at different elevations and numerically integrating them, the error in the volume measurement was significant. Further, tracking small changes in the specimen volume in the initial saturation zone was very difficult and changes were not measurable by the direct measurement. Due to the inability to measure changes in the initial volume of the specimen by this method, the specimen volume on the VSC data appeared to be following a structural phase which was not expected in clay soils (Chertkov, 2003). The DVM class of techniques is also not useful, therefore, for establishing the shrinkage curve of bentonites due to geometrical effects in bentonites.

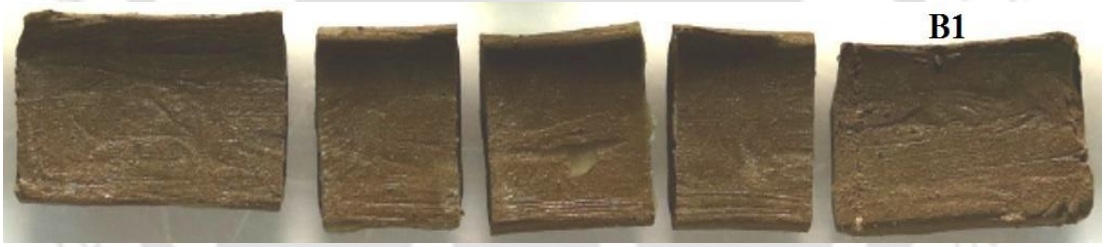

Fig. 4.3a Bentonite specimen in DVM technique during shrinkage process

Fig. 4.3b Cross-sectional view of a clod specimen of DVM technique

The variation in normalized void ratios with water content for all the bentonites was presented in Fig. 4.4 using DVM technique. The shrinkage characteristics such as water contents corresponding to air-entry value and shrinkage limit for all the bentonites were presented in Table 4.2. Water contents corresponding to air-entry value and shrinkage limit were estimated approximately by joining the data points with a straight line in the normal phase and noting the corresponding water contents when the data deviated from the straight line. As the obtained data by different techniques, except for clod test, did not follow 1:1 line in the normal phase, a line connecting the data points before the residual phase was drawn. The estimated w_s and w_{AEV} by WC, Balloon method, and DVM technique were, therefore, only approximate. The deviation in the air-entry value and w_S for different techniques was due to the measurement errors. The water content at desaturation varied from 17% to 25% for different bentonites by clod technique. The shrinkage characteristics of the bentonites were influenced by the chosen method. However, the discrepancy in the measured data was not significant. The shrinkage limit increased with the plasticity of the bentonite, but the AEV was not influenced by the plasticity. The clod test is a reliable and simple technique for obtaining the VSC data. However, the volume data in the initial saturation zone cannot be obtained by this technique. Further, the time required for drying the glue encasement around the wet specimen is high and it was difficult to obtain the VSC data until the glue drying process.

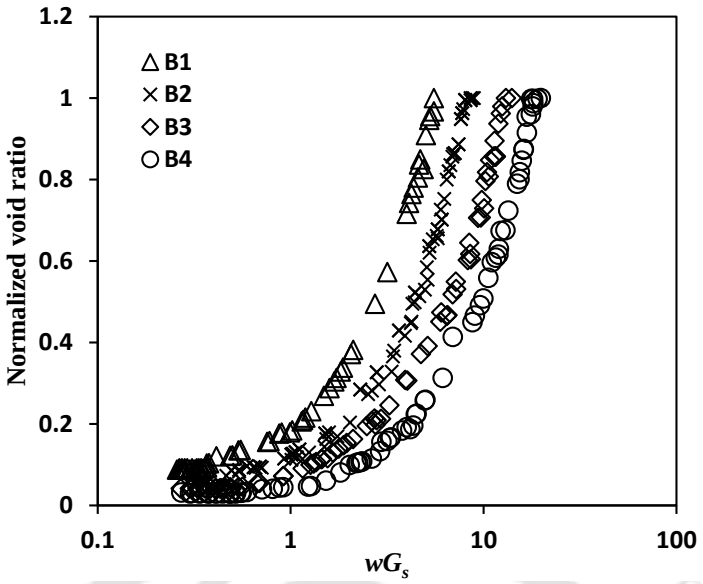

Fig. 4.4 Comparison of VSC data of different bentonites using direct shrinkage measurement technique

Table 4.2 Shrinkage characteristics of the bentonites from measurement techniques

	Bentonite	WC	Clod	Balloon	DVM
w_{AEV} (%)	B1	20	17	20	36
	B2	19	22	16	25
	B3	25	20	20	25
	B4	27	25	30	30
w_{SL} (%)	B1	15	15	15	13
	B2	15	18.5	16	18
	B3	17	20	18	18
	B4	24	23	25	24

4.3 Theoretical VSCs

Theoretical VSCs were obtained by fitting the Kim et al. (1992) and Fredlund et al. (2002) models to the measured data using the gradient based optimization technique (Bharat et al., 2009). The "*fmincon*" MATLAB® program, featuring a constrained optimization of a multivariable function, was used to find the model parameters that

provided the best-fit to the measured data. The theoretical best fit VSCs along with the observed data of B2 and B4 using DVM and clod techniques were shown in Fig. 4.5a-4.5b, respectively.

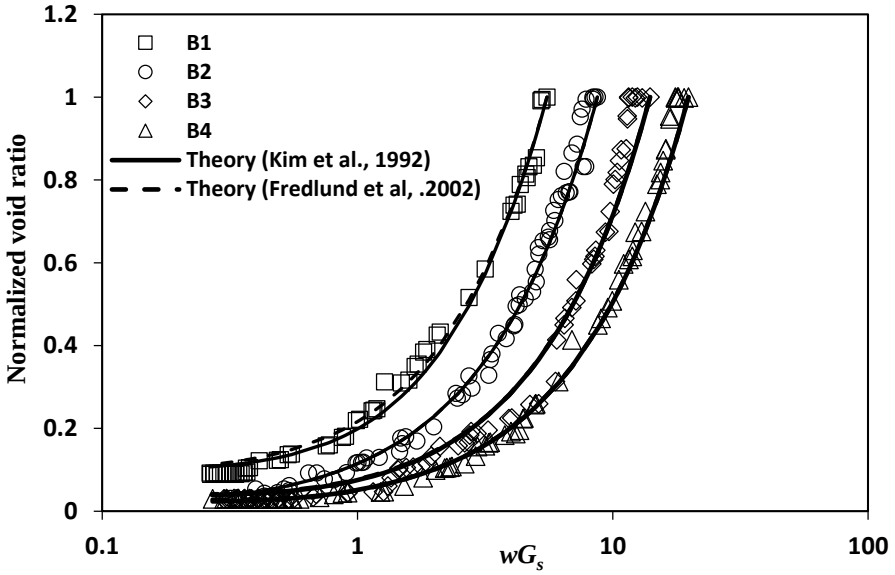

Fig. 4.5a Experimental VSC data using DVM method along with the theoretical curves

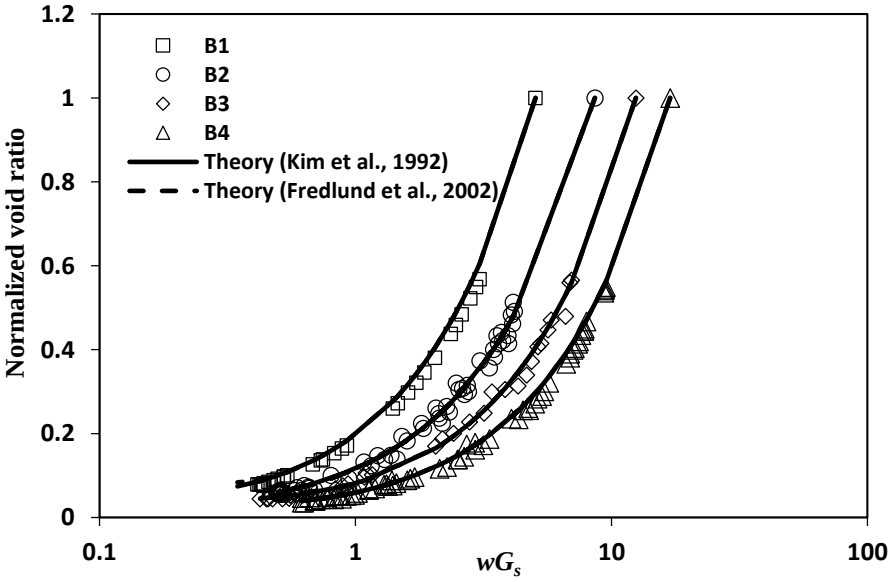

Fig. 4.5b Experimental VSC data using clod method along with the theoretical curves

Theoretical VSCs by both the models were in good agreement with the data. The coefficient of determination, R^2, varied between 0.987 and 0.999 for different tests indicating a very good agreement between the theory and the measured data by different methods. The model parameters were presented in Table 4.3 along with the R^2 values. The model parameter m_2 of Kim's model was close to unity for all the bentonites by clod and DVM techniques. This model parameter signifies the rate of volume shrinkage during the linear-shrinkage phase. The volume of water lost from the specimen is equal to the decrease in pore volume at this stage. Therefore, the predicted m_2 values were justified with the data obtained by clod and DVM techniques. However, the predicted value was consistently higher than unity with balloon and WC techniques. The discrepancy was due to the limitations associated with the test methodologies. The parameters β, which depends on the AEV, varied from 1 to 9.91 for different tests, but for the same clay soil, indicating the inconsistency of the test methodologies.

Table 4.3 Fitted model parameter on the measured VSC data

Bentonite	Method	Kim et al. (1992)			Fredlund et al. (2002)			
		β	m_2	R^2	a_{sh}	b_{sh}	c_{sh}	R^2
B1	WC	1.00	1.06	0.987	0.66	0.24	1.27	0.994
	Clod	9.91	0.99	0.999	0.40	0.15	9.95	0.999
	Balloon	1.00	1.14	0.993	0.54	0.18	1.25	0.995
	DVM	1.67	0.99	0.994	0.49	0.19	1.58	0.990
B2	WC	2.13	1.08	0.993	0.53	0.18	2.11	0.993
	Clod	8.96	1.04	0.994	0.49	0.17	9.81	0.993
	Balloon	1.08	1.11	0.996	0.66	0.20	3.39	0.999
	DVM	3.07	0.95	0.992	0.46	0.17	4.02	0.992
B3	WC	9.94	1.49	0.993	0.43	0.11	9.99	0.993
	Clod	3.25	1.01	0.996	0.56	0.20	3.75	0.995
	Balloon	3.35	1.14	0.996	0.57	0.10	6.03	0.997
	DVM	2.49	0.99	0.997	0.52	0.20	2.64	0.997
B4	WC	9.72	1.00	0.993	0.34	0.13	9.05	0.992
	Clod	3.95	1.04	0.998	0.65	0.23	6.69	0.998
	Balloon	3.35	1.14	0.996	0.57	0.19	1.14	0.996
	DVM	3.89	1.01	0.997	0.54	0.20	7.86	0.997

A slight variation in the a_{sh} parameter, which is a measure of minimum void ratio, was observed with different test methods. However, the model parameter, c_{sh}, related to curvature of the desaturation zone was significantly varied with the adopted method. The variation is consistent with the β parameter, which is an AEV parameter in the Kim's model. The b_{sh} parameter was estimated from a_{sh} using the relationship in Eq. 4.6. The predicted b_{sh} parameter along with the other parameters using the optimization technique on the test data resulted similar values (varied between 0.08 and 0.24) and, therefore, not presented. The model parameters from different theoretical models only provided consistency of different methods. The influence of these parameters on the influence of unsaturated soil behavior cannot be readily estimated. The $SWCC_{SR}$ was established to understand the accuracy of estimated VSC data.

4.4 $SWCC_w$ data

Desorption data of different bentonites obtained by different suction measurement techniques on initially saturated specimens were presented in Fig. 4.6. The water content corresponding to any suction was highest for B4 followed by B3, B2, and B1 in the low-medium suction range (ψ< 5000 kPa). As the initial (saturated) water content of the bentonites was at the slurry state (i.e., 1.15 times the liquid limit); the liquid limit (w_L) was highest for B4 and lowest for B1, the water content varied for different bentonites according to their plasticity in the low –medium suction range. The specific moisture capacity (slope of the SWCC, $d\theta/d\psi$) in this suction range also varied proportional to the plasticity of the bentonite. Specific moisture capacity decreased for different bentonites with increasing suction and attained a constant value at suction value ψ = 5000 kPa. The water content for different bentonites coincided with each other at high suction range, therefore. The water exists as a thin film around the clay platelets and very large suction

is required to decrease the water content in this suction range. The influence of plasticity on the SWCC behaviour was insignificant in this pendular zone as the influence of hydrated cations on the water content at high suction is insignificant (Khorshidi and Lu, 2016). The SWCCs of all the bentonites were, therefore, merged in this suction range.

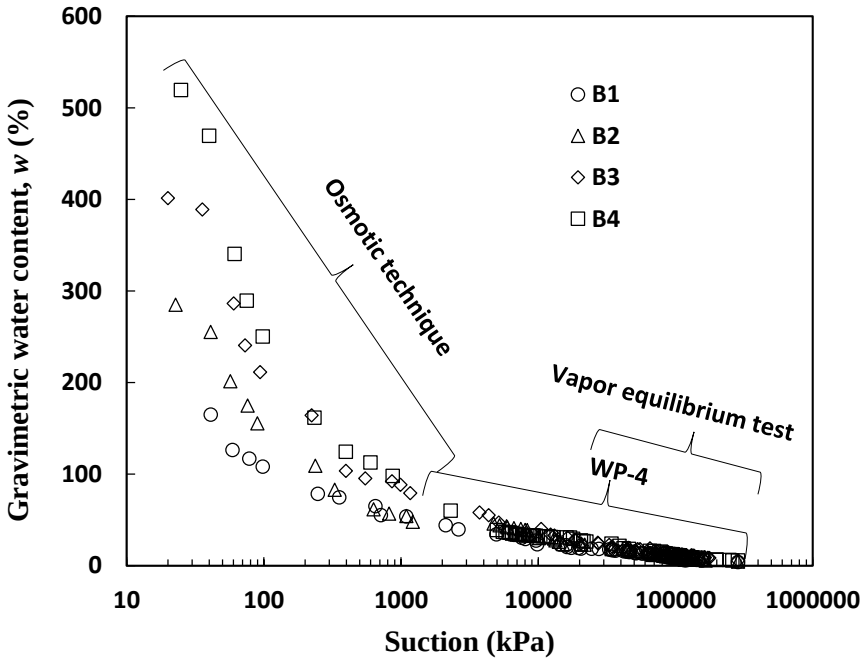

Fig. 4.6 Drying soil water retention data of different bentonites

4.5 SWCC$_{SR}$ Estimation

The measured data of drying gravimetric water content vs. matric suction of the initially slurried bentonites (B2 and B3) were considered in this study for SWCC$_{SR}$ estimation. Sensitivity of the measured VSC data on the estimated SWCC$_{SR}$ for B2 bentonite was analyzed using the measured SWCC$_w$. The gravimetric water content on SWCC$_w$ data was converted to degree of saturation, S_r, for establishing the SWCC$_{SR}$ using:

$$S_r = \frac{wG_s}{e} \tag{4.1}$$

where G_s is specific gravity of the clay soil. The void ratio corresponding to given gravimetric water content was obtained from the VSC data. The SWCC$_{SR}$ data was fitted

with van Genuchten (1980) model to obtain a continuous distribution of S_r for a given matric suction.

The estimated $SWCC_{SR}$ data with the help of clod-VSC data was shown in Fig. 4.7a. The estimated trend was smooth and followed a general SWCC trend of bentonite clays (Tripathy et al., 2014). However, a slight discrepancy in the estimated S_r was observed before the air-entry suction value which was unremarkable in the VSC data. The discrepancy was mainly due to entrapment of tiny mercury spheres to the wet encasement during the measurement of volume by mercury immersion method. The theoretical best fit $SWCC_{SR}$ obtained by van Genuchten (1980) model (equation 2.2)) was also shown in the same figure. The theoretical fit was consistent with the experimental data with a constant 100% degree of saturation values up to the inflection point. The estimated AEV from vG model was also consistent with AEV water content estimated from the VSC data.

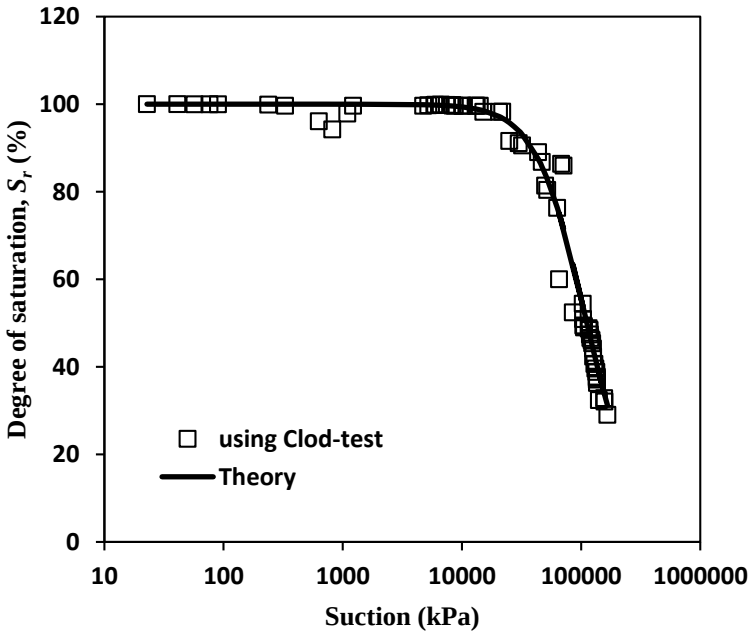

Fig. 4.7a Estimated $SWCC_{SR}$ data of B2 using $SWCC_w$ and Clod-VSC

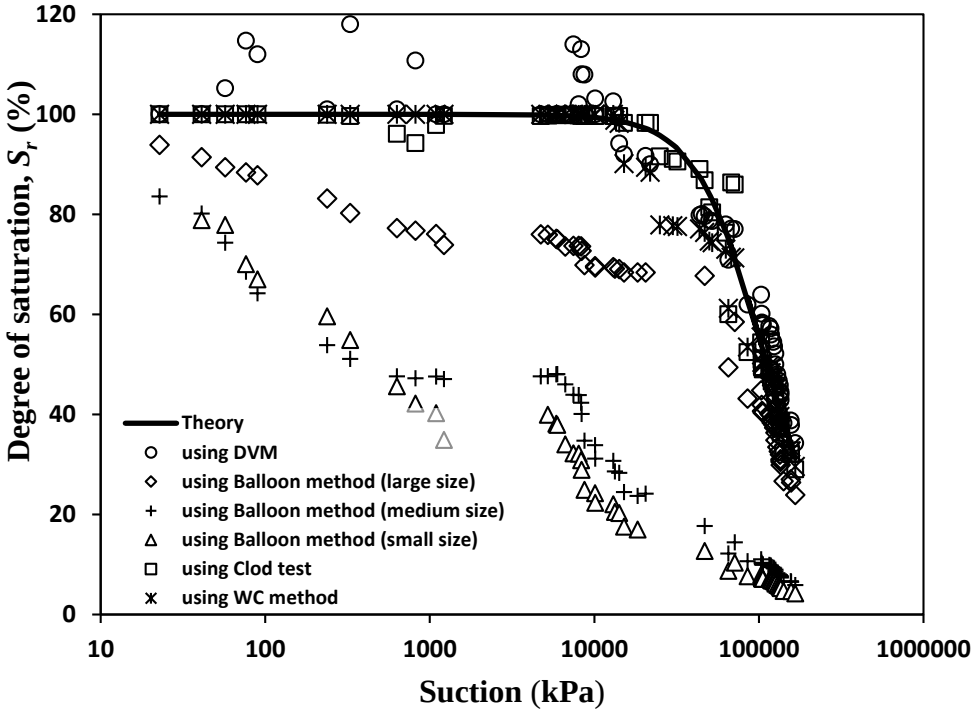

Fig. 4.7b Estimated $SWCC_{SR}$ data for B2 using $SWCC_w$ and different VSC determination methods

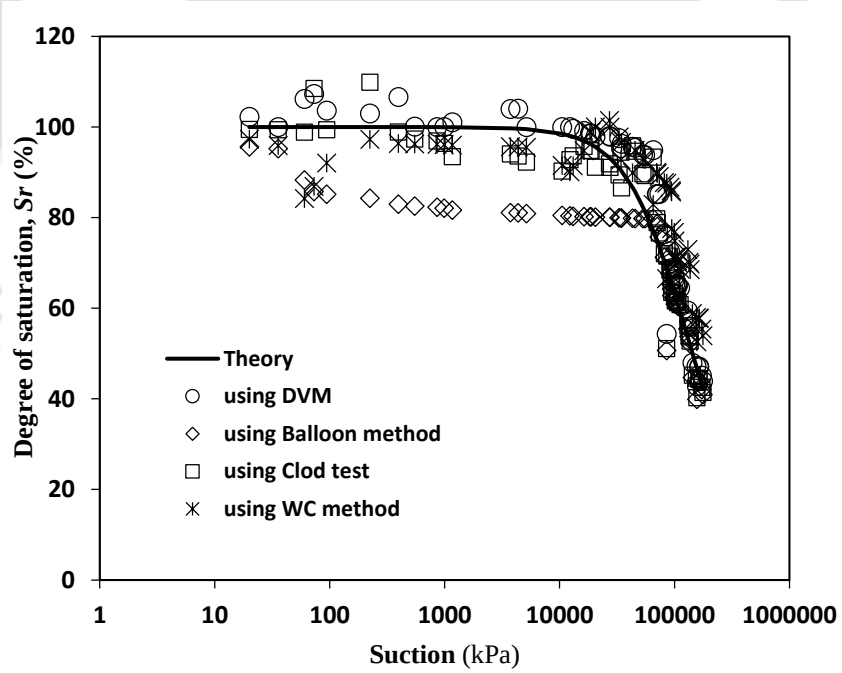

Fig. 4.7c Estimated $SWCC_{SR}$ data for B3 using $SWCC_w$ and different VSC determination methods

The $SWCC_{SR}$ data obtained by different VSC tests were presented in Fig. 4.7b. A significant discrepancy was noticed on $SWCC_{SR}$ using DVM-VSC data. The changes to the initial volume of the specimen were not noticeable by the physical measurement when the water content was in the range of 323-290% for B2. As the constant volume was recorded while the water content decreased in the initial shrinkage phase, the estimated S_r was more than 100% (Fig. 4.7b). The discrepancy beyond the AEV was due to non-anisotropic nature of the shrinkage process as noted before. The $SWCC_{SR}$ using balloon-VSC data with three different initial balloon volumes were also presented in the same figure. The estimated SWCC data significantly deviated from the theoretical SWCC for all the tests. The degree of saturation was consistently less than 100% for all the water contents and decreased consistently. The assumption of zero balloon volume significantly reduced the dry density and increased the void ratio which resulted in smaller values of degree of saturation for any given water content. As the volume of the specimen, inside the balloon, was decreasing during the shrinkage process, the influence of balloon volume was more significant. The error was more significant with smaller initial balloon volume and in residual shrinkage phase as the specimen volume was very small. The balloon volume was significant compared to the specimen volume at this stage. A simple experiment was conducted on a duplicate soil specimen of B2 to verify the volume of the specimen at residual shrinkage state. The volume of the specimen was measured using PVAc coating method. The volume was 1.76 cm^3 and the balloon volume was estimated to be 0.81 cm^3. The mass of the specimen was 3.55 g and the water content was 12.6%. The degree of saturation was estimated to be 36% when the balloon volume was neglected and was 65% when the balloon volume was considered in the calculations. The assumption of zero balloon volume, therefore, significantly underestimates the degree of saturation. However, considering the balloon volume up to

the soil height was not practical at different stages of shrinkage. As discussed earlier, measurement of volume up to a fixed marking level (close to the balloon mouth) was not possible due to the presence of small specimen volume in the residual shrinkage phase. A significant inconsistency in the estimated $SWCC_{SR}$ from WC-VSC data was also observed (Fig. 4.7b) which was expected due to the limitations associated with the method. Similarly, $SWCC_{SR}$ data of B3 obtained using different VSC techniques were shown in Fig. 4.7c. The discrepancy in the estimated S_r corresponding to different suction values using different VSC techniques was qualitatively consistent to B2. Therefore, clod-VSC data alone was consistent and useful to estimate the $SWCC_{SR}$ from $SWCC_w$. Although the initial VSC data was not available from the clod test, the $SWCC_w$ data before AEV helped in establishing the $SWCC_{SR}$ correctly.

4.6 Concluding Remarks

The drying SWCC of four highly plastic bentonites in unrestrained case over a wide suction range was established. The influence of plasticity on the $SWCC_w$ was distinctly visible at the lower suction range, but the $SWCC_w$ data in the higher suction range were not influenced by the bentonite plasticity.

The measurement techniques were found to play important role in the measured volumetric shrinkage data. Several limitations were associated with the shrinkage measuring techniques for expansive clays. However, the VSC models could not identify the correctness of the data and explain the discrepancy in the measured data, but only showed a qualitative disagreement between the data obtained from different methods. Model parameters such as β of Kim et al. (1992) model and c_{sh} of Fredlund et al. (2002) model showed significant difference in the VSC data of the same bentonites by different measurement techniques. The measurement errors from different techniques were significantly reflected on the estimated $SWCC_{SR}$ data which were obtained by combining

the measured VSC and $SWCC_w$ data. The estimated degree of saturation by balloon technique was consistently less than 100% before the AEV and over a wide range of matric suction due to the limitation in balloon volume measurement. The estimated S_r by DVM technique was consistently more than 100% before the AEV due to the limitations associated with the precise volume measurement in the normal shrinkage phase. Significant discrepancy was obtained by WC method due to the application of mechanical stresses by the wax during the solidification process and the requirement for duplicate specimens for establishing the VSC data. The initial specimen volume measurement by clod technique was difficult as the time required for glue drying process was significant and wet-glue does not act as water-repellent material. Therefore, use of water-repellent or non-polar liquids for the volume measurement of the glue-encased clods was unavoidable in this technique in the initial drying stage. Even though the specimen volume measurement by clod technique was difficult in the initial stage of normal shrinkage phase, the measured VSC data by clod method was consistent and established a smooth $SWCC_{SR}$. The clod method is, therefore, a preferred method for establishing the $SWCC_{SR}$ for bentonite clays for engineering applications.

Chapter 5

Wetting SWCC of Bentonites in Volume Restrained Condition

5.1 General

The results obtained in the wetting induced SWCC tests were presented in this chapter. Osmotic technique was used to establish SWCC upto 2000 kPa suction. Vapor equilibrium technique was used for establishing the SWCC data beyond 2000 kPa suction. Due to the importance of vapor sorption data in HLNW repositories under different RH condition, kinetic behavior of vapor sorption data was presented.

5.2. Hydration kinetics of Bentonite clays

The temporal variation of water content in powder bentonite specimens under the influence of saturated vapor pressure was shown in Fig. 5.1. The air-dry clay specimen adsorbs moisture from the ambiance due to the difference in the vapor pressure. The vapor sorption continues to exist until the vapor pressure of the clay specimen reaches the saturated vapor pressure. However, the hydration rate exhibited a stepwise pattern due to the presence of different hydration mechanisms in the expansive clays. The succession of hydration of surface cations, particle surface, and interlayer surfaces at different vapor pressures is found to govern the vapor sorption behavior of smectite clays based on the vapor sorption isotherms (Khorshidi et al., 2016). The hydration kinetics was also influenced by these mechanisms by exhibiting non-unique hydration rate up to 30 – 50 days. The hydration rate was very small and linear beyond this time. The bentonite plasticity also influenced the sorption rate and the equilibrium water content. The sorption rate for different bentonites followed the order of bentonite plasticity i.e., B1 < B2 < B3 < B4 (Table 3.1). Similarly, the time to reach equilibrium water content, w_{eq}, and magnitude of water content increased with the bentonite plasticity.

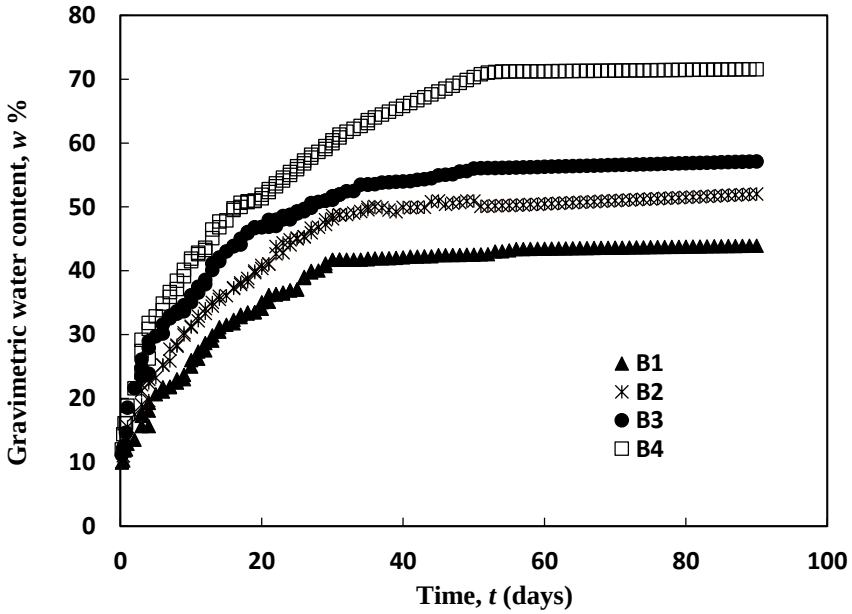

Fig. 5.1 Vapor sorption isotherms for different powdered bentonites specimens under 100% RH environment

Total 84 tests were performed to study the hydration behavior of compacted bentonite specimens under the influence of different vapor pressures. The hydration rate under the influence of compaction density and vapor pressure for different bentonites was shown in Figs. 5.2 – 5.5. Two distinct hydration stages were observed in vapor hydration behavior of compacted specimens. The time for achieving equilibrium water content and completion of individual hydration stages, in compacted specimens, reduced considerably when compared to the powder specimens.

The hydration rate was found to strongly vary with the vapor pressure for a given bentonite and compaction density as seen in Fig. 5.2a. The hydration rate was significantly higher when the vapor pressure is close to the saturated vapor pressure (i.e., vapor pressure of 0.5M KCl solution) when compared to lower vapor pressures (vapor pressure of saturated LiCl solution). The increase in the vapor pressure improves the availability of water vapor for the adsorption by the clay specimen which increased the

water content of the bentonite specimen at any given time. Further, the increase in the vapor pressure gradient across the clay matrix and vapor space of the salt solutions increased the hydration rate. The water hydration rate increased sharply up to nearly 10 days in the vapor pressure environment, but the rate decreased significantly with further exposure. Only a marginal increase in the water content was observed with time beyond the initial equilibrium state. The high vapor sorption rate at the beginning, in the presence of high RH conditions, was reasoned to be due to the hydration of surface cations and accessible external surface area which was considered to be the first stage of hydration. The accessible, external surface area was limited in the compacted specimens due to volume restrained conditions. Hydration of unexposed external surface area was followed in the second stage with a very slow hydration rate. The decrease in the vapor pressure decreases the available water vapor to completely form mono and bi-layer hydration around cations and the external surface which was evident from a nearly monotonous increase in sorption rate under the influence of RH = 53.2%.

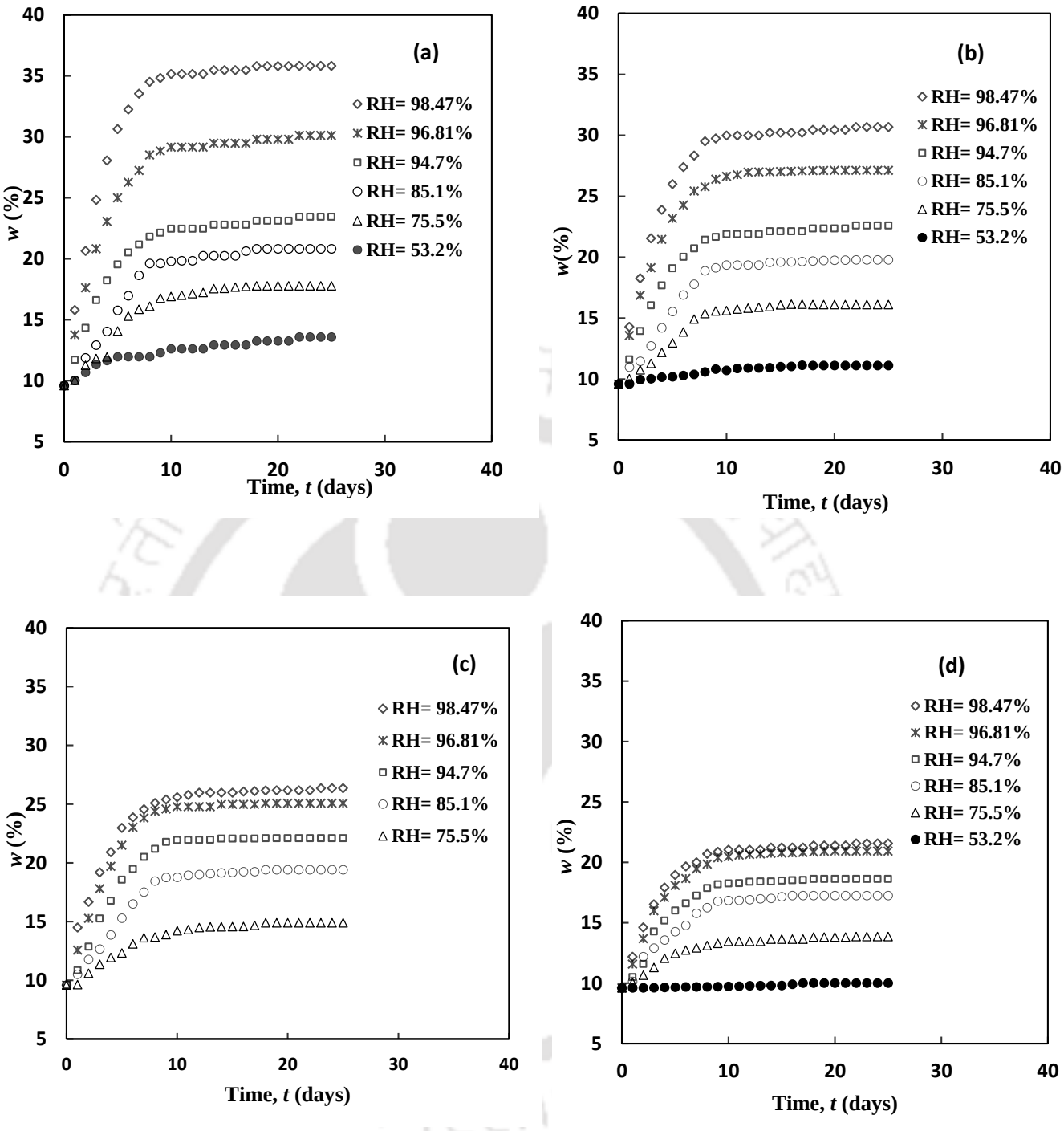

Fig. 5.2 Vapor sorption isotherms for B1 at different compaction dry densities

(*a*) 1.0 g/cm^3 (b) 1.4 g/cm^3 (c) 1.6 g/cm^3 (d) 1.8 g/cm^3

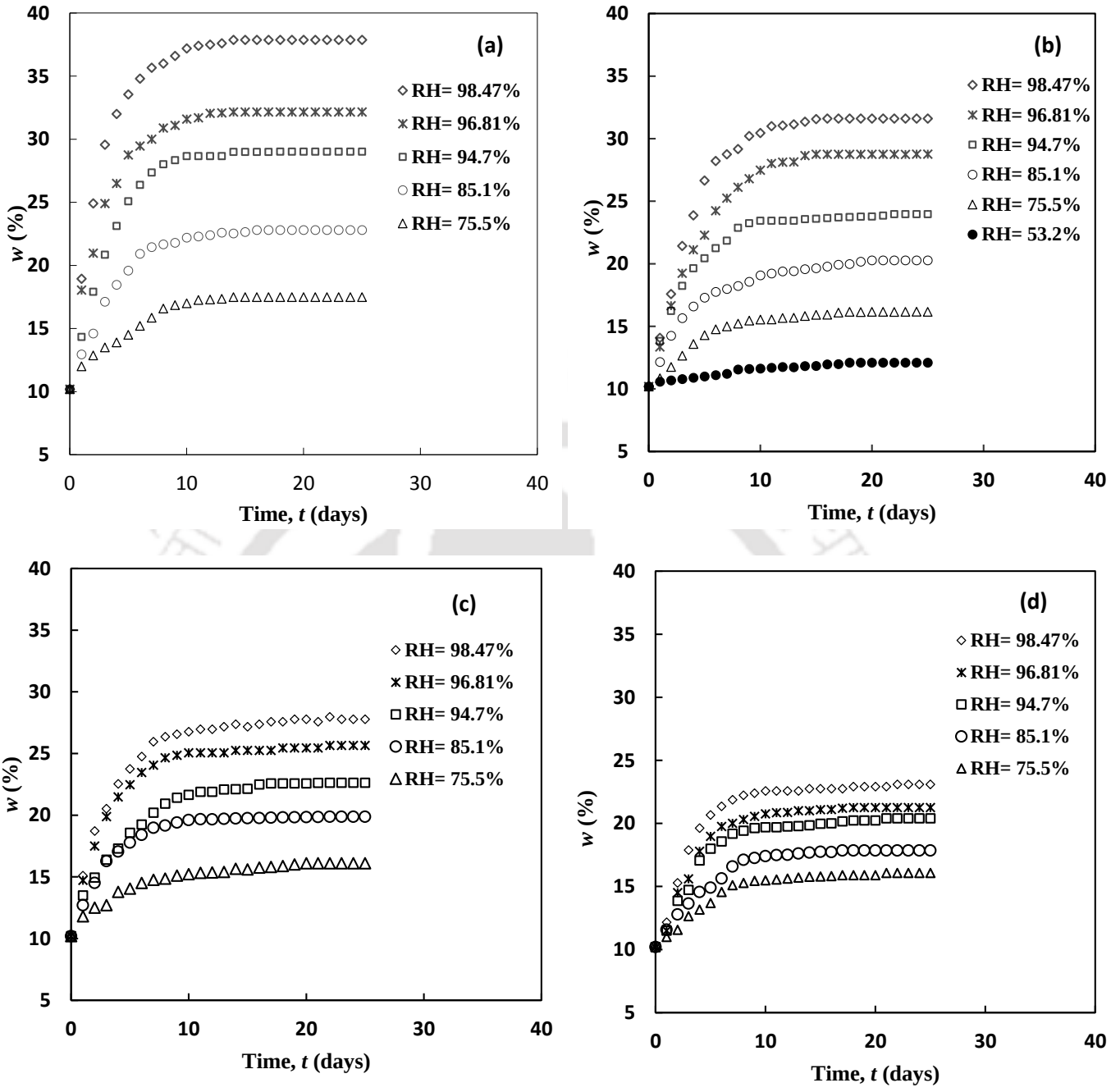

Fig. 5.3 Vapor sorption isotherms for B2 at different compaction dry densities

(a) 1.0 g/cm^3 (b) 1.4 g/cm^3 (c) 1.6 g/cm^3 (d) 1.8 g/cm^3

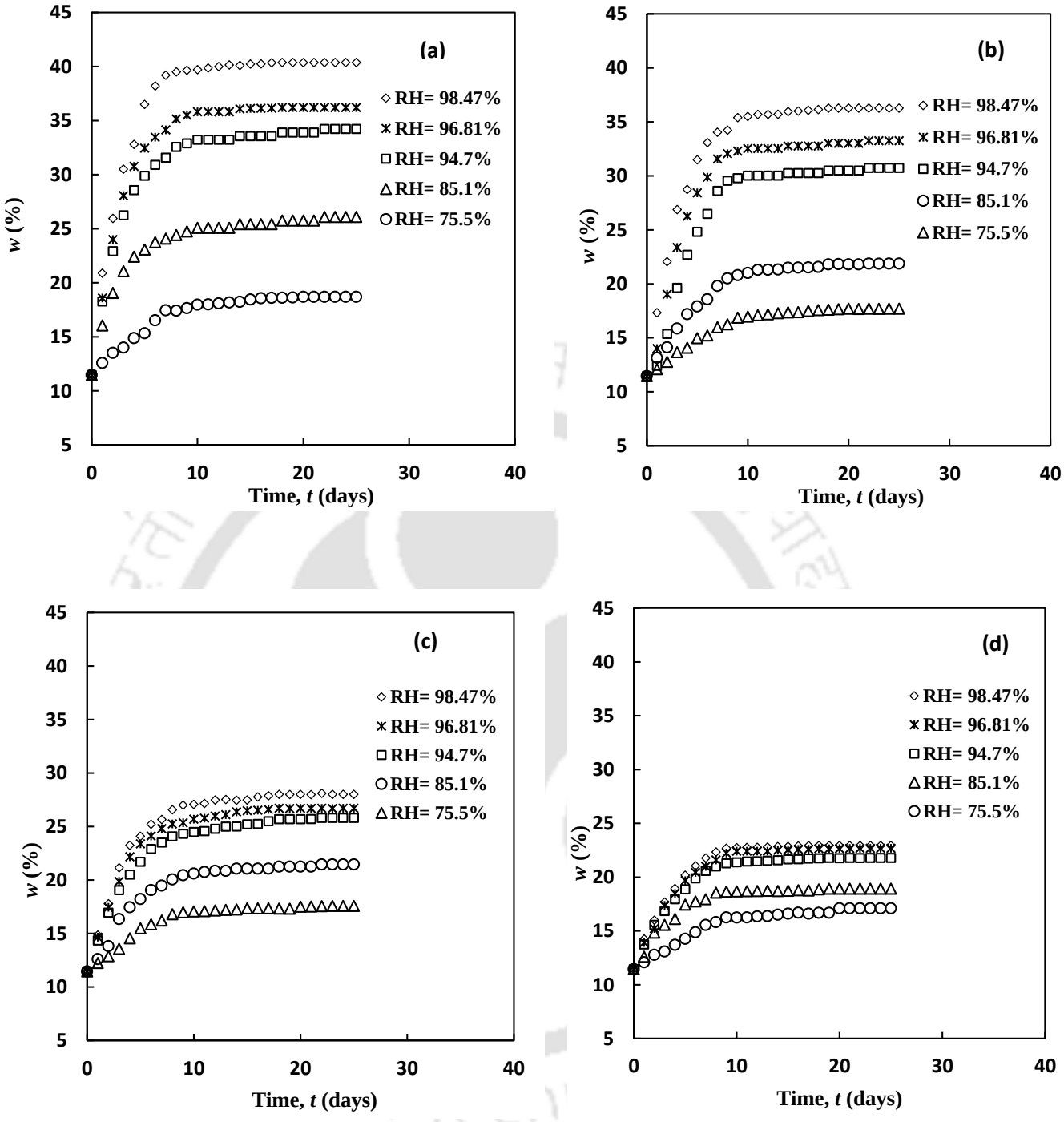

Fig. 5.4 Vapor sorption isotherms for B3 at different compaction dry densities

(a) 1.0 g/cm^3 (b) 1.4 g/cm^3 (c) 1.6 g/cm^3 (d) 1.8 g/cm^3

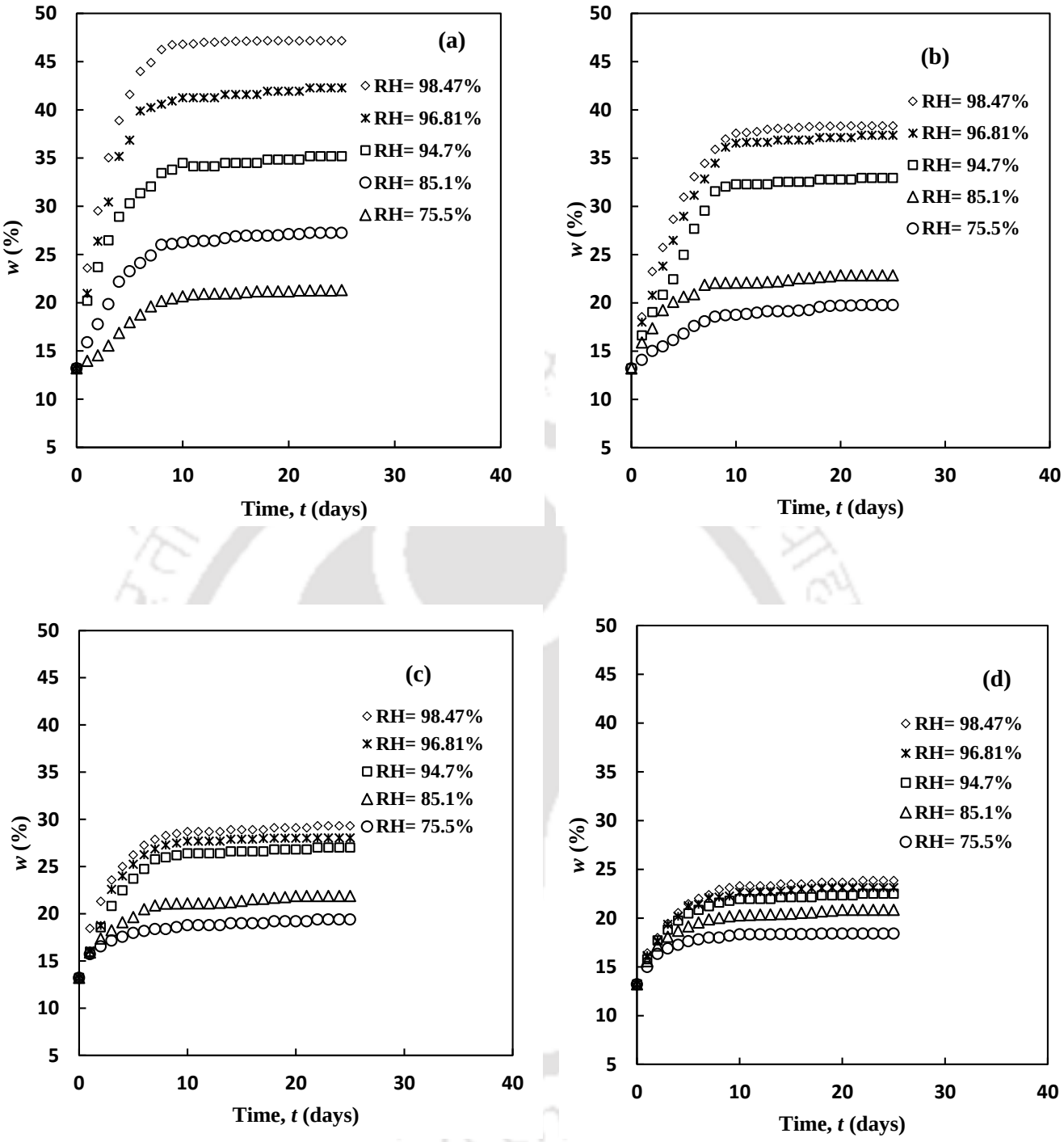

Fig. 5.5 Vapor sorption isotherms for B4 at different compaction dry densities

(*a*) 1.0 g/cm^3 (b) 1.4 g/cm^3 (c) 1.6 g/cm^3 (d) 1.8 g/cm^3

The hydration rate decreased with increase in the compaction density due to reduction in the accessible external surface area of the clay specimen. The reduction in the easily accessible surface area increased the hydration energy. The equilibrium water content also, therefore, decreased with decrease in the vapor pressure and increase in the compaction density. The equilibrium water content remained constant to the initial air-dry water content at ρ_d = 1.8 g/cm^3 when RH was 53.2% and no influence of vapor pressure was observed. Further, the increase in the compaction density contributed in decreasing the equilibrium gravimetric water content (i.e., $w = M_w/M_s$; M_w = mass of water and M_s = mass of solids) as the adsorbed water content was not increased at the same amount as the mass of soil solids. Therefore, the equilibrium water content decreased significantly with increase in the density.

The increase in the bentonite plasticity increased the duration for first stage of hydration and varied from 10 – 12 days for B2 (Fig. 5.3) for different RH conditions. The equilibrium water content, however, increased with the bentonite plasticity due to higher exchangeable sodium percentage (ESP) at the surface and specific surface area. The hydration of sodium dominant smectite clays is higher when compared to the presence of divalent cations at the surface due to significant difference in the hydration energy. The hydration energy of calcium and magnesium cations is five – six orders of magnitude higher than the sodium ions, respectively (Bohn et al., 1985). The hydration rate and equilibrium water content of B4 was highest and B1 was lowest due to higher and lower ESPs, respectively. The hydration rate and w_{eq} were higher in B3 compared to B2 due to higher value of SSA in B3 compared to B2 although ESP of B2 was higher. As the external surface area was considered in the analysis of hydration kinetics on compacted bentonite specimens, the external SSA was assumed to be proportional to the total SSA due to the fact that the same amount of internal surfaces is inaccessible to water vapors at

the same compaction density. The order of plasticity and montmorillonite content was consistent with the hydration rate or w_{eq} for different bentonites.

As the hydration was not significant at RH = 53.2%, the hydration data was not presented for other bentonites and with different compaction densities. Appreciable amount of hydration was not noticed for RH < 50% for all the bentonites and compaction densities. The difference in the hydration rate and equilibrium water content for different vapor pressures decreased with the bentonite plasticity at high compaction densities (Fig. 5.4d and 5.5d). Only a 6% increase in the equilibrium water content was noted with increase in the vapor pressure from 76% to 98.5% for B4 at the compaction density of 1.8 g/cm^3 (Fig. 5.5d) whereas nearly 18% variation was observed for the same variation in vapor pressures in B1 at ρ_d = 1 g/cm^3 (Fig. 5.3a). The influence of RH decreased at higher compaction densities for B4 bentonite, therefore.

5.3 Linearization of Isotherm Kinetics

The adsorption and desorption kinetics in clays are often studied by fitting kinetic models of second order to the measured data (Montes-H and Geraud, 2004). Such curve fitting techniques only provide continuous variation in vapor sorption/desorption with time and are useful for vapor flow simulations. However, the prediction of hydration rate and equilibrium water content data for bentonite specimens is important due to large testing time. A linearization of sorption data was examined in this work. The rectangular hyperbola method (Kondner, 1963; Dakshanamurthy, 1978; Sridharan and Rao, 1981; Sridharan et al., 1987) was explored to linearize the vapor hydration kinetics in bentonite specimens. The equation of rectangular hyperbola is expressed as (Dakshanamurthy, 1978)

$$\frac{X}{Y} = c + mX \tag{5.1}$$

where X and Y are the variables, c is the intercept, and m is the slope of the linear portion. Average degree of consolidation and time factor were used as variables in Eq. (5.1) for linearizing the time rate of consolidation (Kodandaramaswamy and Rao, 1980) which provided useful approach to predict coefficient of consolidation and consolidation settlement (Sridharan and Rao, 1981; Sridharan et al., 1987). Prakash et al. (2014) used rectangular hyperbola representation for temporal variation of adsorbed water on low-plastic natural soils by exposing oven-dry soil specimen to saturated vapor pressures. A unique linear trend is observed until the time to achieve equilibrium water content for natural soils, but the behavior of highly plastic clays such as bentonites is not known. Further, the applicability of rectangular hyperbola method for linearizing the vapor sorption data of bentonites under various compaction states is not known. The presence of multiple hydration mechanisms in plastic clays (Khorshidi et al., 2016), therefore, receives great importance for the applicability of linearization techniques and such studies are useful for nuclear waste repository applications.

In this work, the equation of rectangular hyperbola for sorption data was expressed as

$$\frac{t}{w} = c + mt \tag{5.2}$$

where t is time and w is gravimetric water content. The Eq. (5.2) was utilized in this work for predicting the vapor sorption data over a wide time range and equilibrium water content.

The variation of water content in the powder and compacted bentonite specimens with time appeared to follow a rectangular hyperbola trend in Figs. 5.1 – 5.5. The kinetic data were thus represented as time versus t/w for linearization. The linearized data of vapor sorption kinetics of powder specimens due to exposure to the saturated vapor pressure

were shown in Fig. 5.6. The data followed linear relationship only beyond 40 – 60 days, but they displayed highly nonlinear trend before this time. The nonlinearity was due to the presence of several mechanisms such as monolayer and bilayer hydration of surface cations; surface hydration; and interlayer hydration as discussed earlier. The rectangular hyperbola method was, therefore, not useful for linearizing the sorption kinetic data of powder bentonite specimens.

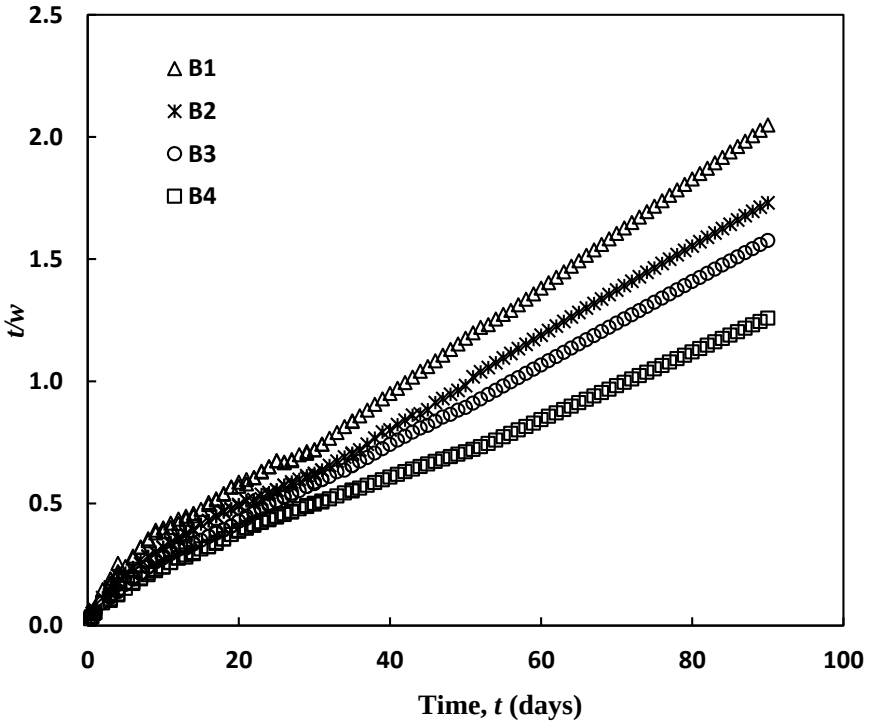

Fig. 5.6 Linearized representation of sorption kinetic data of bentonites in unrestrained condition

Linearization of the kinetic data of B1 compacted at ρ_d = 1 g/cm^3 by rectangular hyperbola approach was presented in Fig. 5.7. The data followed a distinct linear trend after a small initial time of about 4 days (Fig. 5.7 at RH = 53.2%). The initial data deviated from the linear fit due to a very high hydration rate and was distinguishable only in the linearization representation. The preliminary hydration with a high hydration

rate at the beginning might be due to the hydration of surface cations. The time for first stage of hydrations observed in Fig. 5.5, however, was due to both hydration of surface cations (i.e., preliminary hydration) and exposed external surfaces. The time for first stage of hydration was consistently more than 10 days for all the studied tests. The linearization plots for other bentonites and at different compaction densities were qualitatively similar and thus were not presented here for brevity. The preliminary hydration which was part of the first-stage of hydration varied from 1 – 6 days for different compaction densities and vapor pressures.

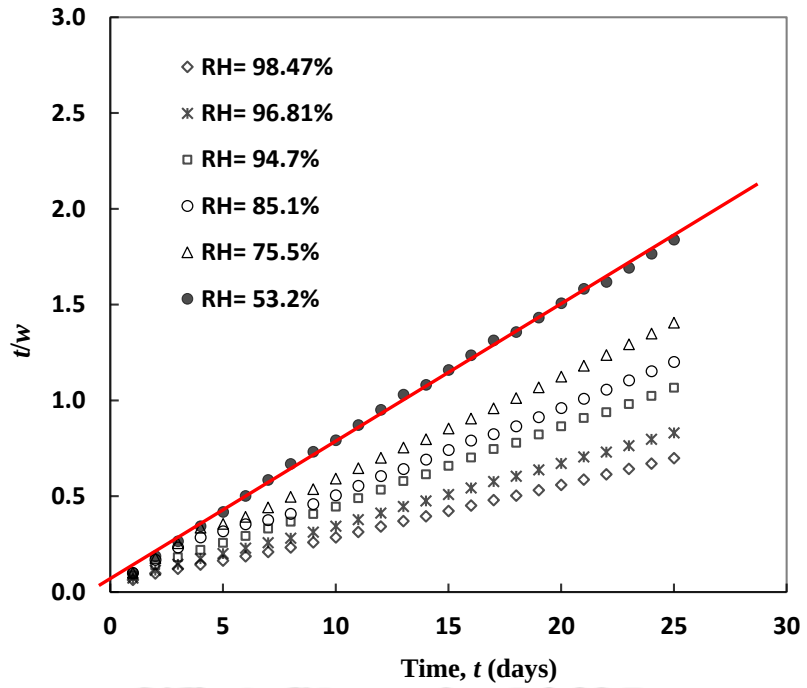

Fig. 5.7 Linearized representation of sorption kinetic data for B1 compacted at 1.0 g/cm^3 and exposed to varying RH environments

5.3.4. Equilibrium Water Content Prediction

The linear portion of the kinetic data after the preliminary hydration (after 1 – 6 days) was utilized for predicting the equilibrium water content due to long testing time in

establishing equilibrium water content of the compacted bentonites. The preliminary hydration may be noted by observing the deviation from the initial kinetic data. Two data points after the preliminary hydration were utilized to establish the equation constants (*c* and *m*) in Eq. 5.2. The linear equations were established using the equation constants and were used to predict equilibrium water content. The equilibrium water content, w_{eq}, was obtained by substituting large value for '*t*' (say, *t* = 25 days) in the derived linear equations. The equation constants for different data sets as well as measured and predicted w_{eq} were presented in Table 5.1 – 5.4. The slope, *m*, of the linear equation increased with decrease in the vapor pressure for a given compaction density and bentonite. Similarly, the slope increased with increase in the compaction density and decreased with the bentonite plasticity at a constant vapor pressure.

The slope of the equation, which indicates the inverse of sorption rate at any given time, well captured the sorption rate and useful, therefore. The predicted and measured equilibrium water contents against RH at different compaction densities and for different bentonites were presented in Fig. 5.8. The prediction was satisfactory and useful for obtaining equilibrium water contents from the early nature of the sorption data.

Table 5.1 Comparison of measured and predicted equilibrium water contents of compacted B1 in the presence of different vapor pressures

ρ_d (g/cm^3)	RH (%)	m	c	Predicted water content (%)	Measured water content (%)
1.0	98.47	0.028	0.001	35.16	35.83
	96.81	0.032	0.028	30.61	30.13
	94.6	0.040	0.049	23.98	23.45
	85.1	0.051	0.001	19.64	20.80
	75.5	0.055	0.054	17.41	17.79
	53.2	0.074	0.046	13.14	13.59
1.4	98.47	0.033	0.001	29.98	30.68
	96.81	0.035	0.029	27.52	27.12
	94.6	0.042	0.036	22.92	22.26
	85.1	0.046	0.056	20.70	19.78
	75.5	0.057	0.098	16.31	16.12
	53.2	0.091	0.039	10.85	11.12
1.6	98.47	0.036	0.032	26.92	26.36
	96.81	0.038	0.023	25.60	25.07
	94.6	0.045	0.003	22.03	22.10
	85.1	0.053	0.003	18.82	19.41
	75.5	0.064	0.076	15.01	14.90
1.8	98.47	0.045	0.037	21.66	21.57
	96.81	0.047	0.017	20.89	20.92
	94.6	0.053	0.018	18.60	18.62
	85.1	0.055	0.074	17.16	17.25
	75.5	0.069	0.055	13.99	13.85
	53.2	0.103	0.004	9.72	10.00

Table 5.2 Comparison of measured and predicted equilibrium water contents of compacted B2 in the presence of different vapor pressures

ρ_d (g/cm^3)	RH (%)	Slope (m)	Intercept (c)	Predicted water content, w_p(%)	Measured water content, w_m(%)
1.0	98.47	0.025	0.016	38.56	37.87
	96.81	0.030	0.016	32.22	32.16
	94.6	0.035	0.001	28.66	29.01
	85.1	0.043	0.027	22.78	22.81
	75.5	0.057	0.06	16.82	17.49
1.4	98.47	0.032	0.007	31.34	31.61
	96.81	0.035	0.004	28.26	28.76
	94.6	0.041	0.04	23.51	23.96
	85.1	0.050	0.05	19.43	20.28
	75.5	0.060	0.044	16.07	16.16
	53.2	0.084	0.034	11.65	12.10
1.6	98.47	0.035	0.025	27.90	27.77
	96.81	0.038	0.023	25.92	25.65
	94.6	0.046	0.001	21.89	22.62
	85.1	0.047	0.048	20.55	19.87
	75.5	0.058	0.068	16.56	16.10
1.8	98.47	0.042	0.025	23.33	23.09
	96.81	0.046	0.027	21.16	21.25
	94.6	0.047	0.036	20.65	20.40
	85.1	0.055	0.055	17.52	17.85
	75.5	0.062	0.057	15.68	16.06

Table 5.3 Comparison of measured and predicted equilibrium water contents of compacted B3 in the presence of different vapor pressures

ρ_d (g/cm3)	RH (%)	Slope (m)	Intercept (c)	Predicted water content, w_p(%)	Measured water content, w_m(%)
1.0	98.47	0.024	0.011	40.79	40.38
	96.81	0.026	0.023	37.71	36.21
	94.6	0.028	0.029	34.79	34.22
	85.1	0.038	0.026	25.51	26.09
	75.5	0.05	0.056	18.99	18.69
1.4	98.47	0.027	0.007	36.05	36.28
	96.81	0.029	0.017	33.58	33.25
	94.6	0.031	0.019	31.06	30.73
	85.1	0.044	0.061	21.66	21.87
	75.5	0.055	0.036	17.65	17.70
1.6	98.47	0.036	0.009	27.45	28.01
	96.81	0.037	0.015	26.30	26.72
	94.6	0.038	0.030	25.63	25.75
	85.1	0.045	0.048	21.22	21.46
	75.5	0.054	0.060	17.79	17.65
1.8	98.47	0.044	0.004	22.87	22.94
	96.81	0.045	0.001	22.40	22.68
	94.6	0.045	0.018	21.88	21.78
	85.1	0.052	0.028	18.29	18.92
	75.5	0.053	0.086	17.76	17.10

Table 5.4 Comparison of measured and predicted equilibrium water contents of compacted B4 in the presence of different vapor pressures

ρ_d (g/cm^3)	RH (%)	Slope (m)	Intercept (c)	Predicted water content, w_p(%)	Measured water content, w_m(%)
1.0	98.47	0.021	0.002	47.07	47.17
	96.81	0.024	0.009	41.83	42.27
	94.6	0.027	0.029	35.46	35.19
	85.1	0.035	0.042	27.45	27.24
	75.5	0.044	0.060	21.46	21.31
1.4	98.47	0.025	0.011	38.59	38.34
	96.81	0.027	0.001	36.63	37.38
	94.6	0.031	0.001	32.29	32.95
	85.1	0.043	0.026	22.58	22.85
	75.5	0.05	0.031	19.52	19.77
1.6	98.47	0.033	0.023	29.85	29.30
	96.81	0.036	0.001	27.69	28.03
	94.6	0.036	0.022	27.29	27.01
	85.1	0.044	0.025	22.08	21.87
	75.5	0.051	0.026	19.40	19.39
1.8	98.47	0.043	0.001	23.30	23.85
	96.81	0.043	0.015	22.78	23.12
	94.6	0.043	0.028	22.77	22.51
	85.1	0.048	0.020	20.70	20.85
	75.5	0.053	0.018	18.55	18.40

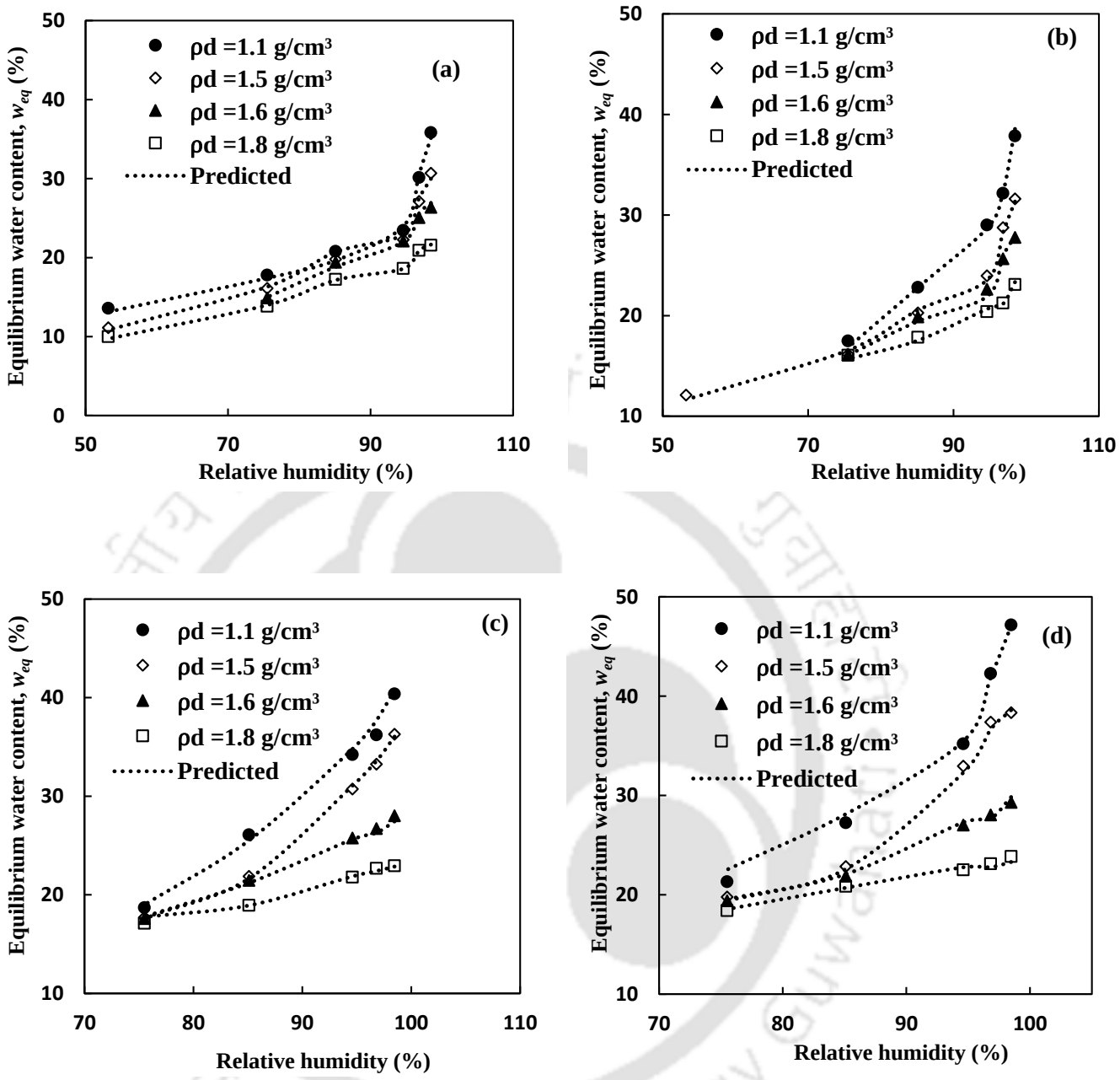

Fig. 5.8 Vapor sorption isotherms using measured and predicted equilibrium water contents for the bentonites

5.5. Wetting SWCC of bentonites in unrestrained and restrained condition

The influence of suction on the gravimetric water content during sorption tests in unrestrained condition was shown in Fig. 5.9 for different bentonites. The $SWCC_w$ data were obtained from three independent wetting tests in different suction ranges as shown in the figure. The measured data using transient water sorption technique in the suction range of 20 MPa – 100 MPa were in good agreement with the data by vapor equilibrium method. The difference in the water content of different bentonites in the lower suction range was significant. The measured water content for a given suction was highest for B4 and lowest for B1. The water content data of B2 and B3 were between these two extreme cases and water content decreased with quality of the bentonite for a given suction. Increase in the plasticity of the bentonite increases the diffuse double layer (DDL) thickness and more water was retained on the clay surface. As the DDL thickness increases with the increase in the water content, the inter-platelet distance increases to accommodate more water in the clay pores. The volume of the specimen, therefore, increases with water content in unrestrained condition at lower suction range. As both DDL thickness and specimen volume are directly proportional to the plasticity of the bentonite, the water content increases with the plasticity of the bentonite. This observation in wetting $SWCC_w$ data for different bentonites in volume unrestrained condition was in accordance with the results by Marinho (2005) where the water content of the drying SWCC is found to be a function of plasticity of the clay soil at any given suction. The difference in water content for different bentonites, however, was insignificant at higher suction values and the $SWCC_w$ data for different bentonites converged to a unique curve beyond 20 MPa. The hydration of surface cations and interlayer surfaces takes place in this suction range and the difference in water content

between different bentonites containing mixed surface cations was insignificant (Khorshidi et al., 2016).

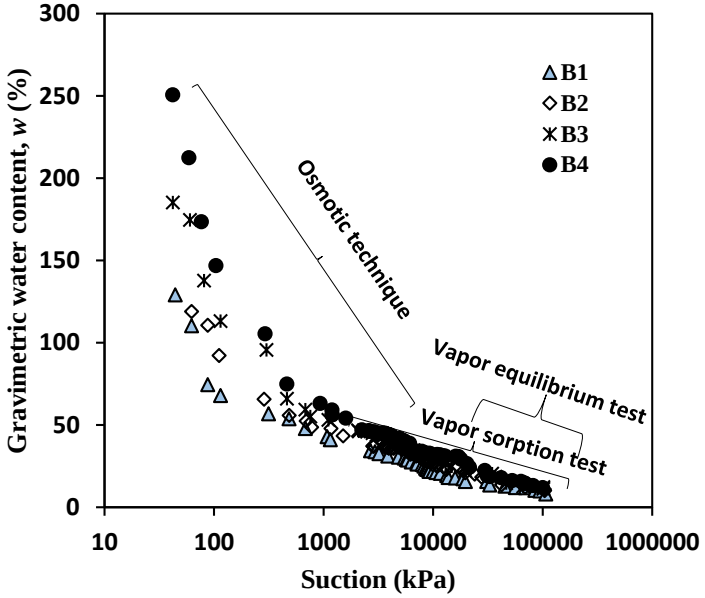

Fig. 5.9 Gravimetric water content versus matric suction ($SWCC_w$) data of bentonites – unrestrained condition

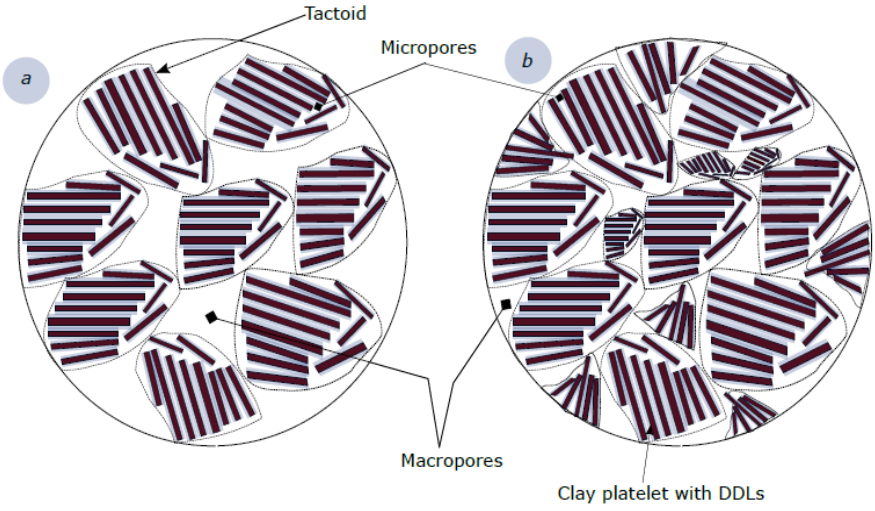

Fig. 5.10 Illustration of clay platelet packing in constrained wetting experiment when specimen is (*a*) loosely compacted and (*b*) densely compacted state

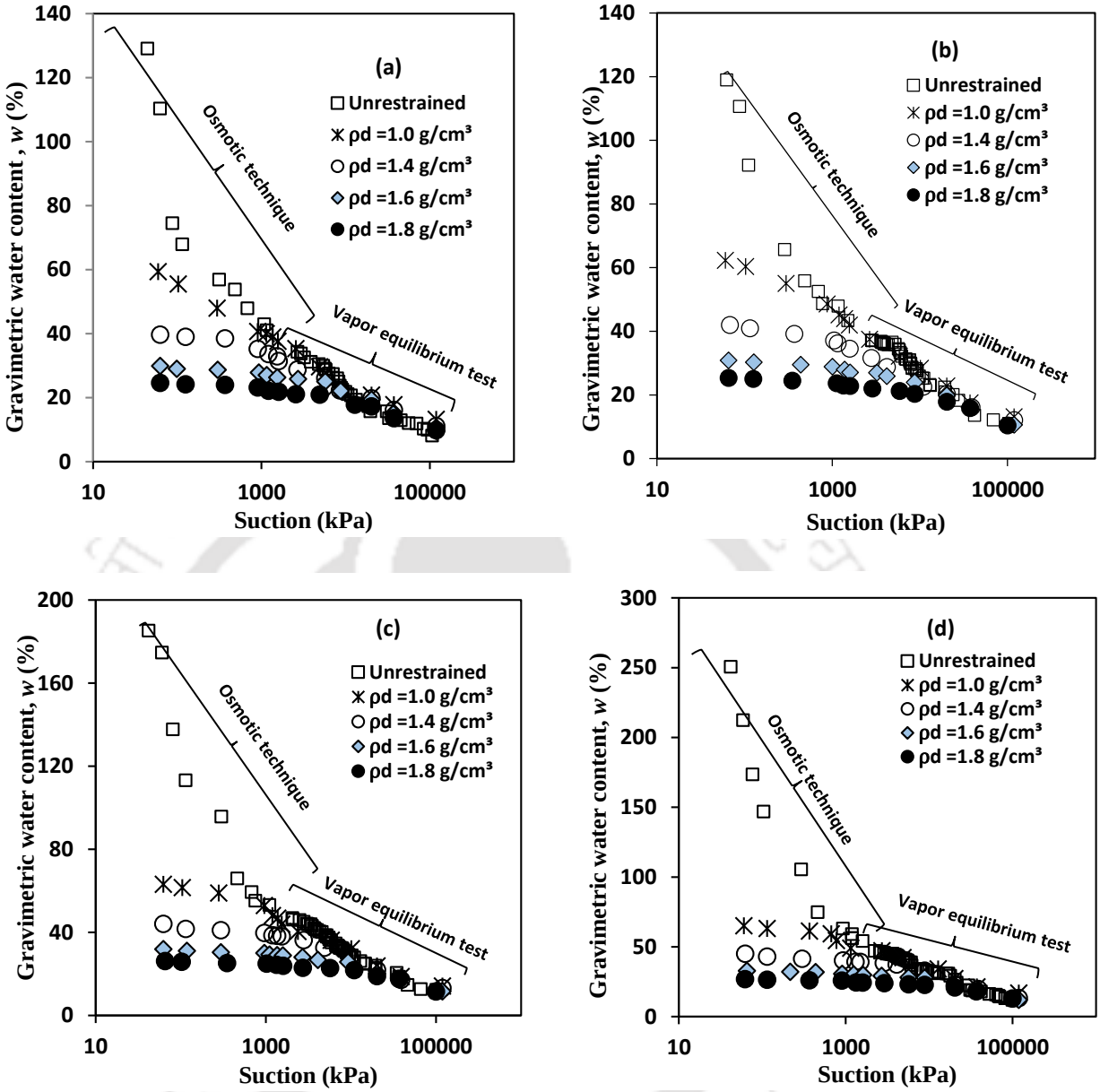

Fig. 5.11 Comparison of Gravimetric water content vs suction ($SWCC_w$) of bentonites under unrestrained and restrained conditions (a) B1 (b) B2 (c) B3 (d) B4

The measured $SWCC_w$ data of B1 at different compaction densities were presented in Fig. 5.11 along with the data obtained in volume unrestrained condition. The data in restrained condition were obtained using two independent wetting tests, over a wide range of suctions that were shown in the figure. The water content decreased with the increase in the compaction density. However, the difference in the water content for

different compaction densities was not significant at higher suction range (> 5 MPa). As the air-dry, compacted bentonite specimens were exposed to different vapors of the salt solutions (i.e., LiCl and NaCl) to induce different suctions, in the higher suction range, only the surface cations and micropores (Fig. 5.10a – 5.10b) got hydrated. The suction required for the saturation of micropores by hydration mainly depends on the specific surface area and exchangeable cations (Khorshidi et al., 2016; Khorshidi and Lu, 2017). As the compaction density can only influence the macropore volume and solid content in double porosity soils (Jacinto et al., 2016), the size of the micropores for specimens compacted at different initial densities is nearly constant. The increase in water content in higher suction range only increased the amount of water in micropores depending on the solid content, the gravimetric water content remained same. The increase in the water content with vapor saturation in this range of suction was, therefore, not significantly different for various compaction densities. The effect of density on the water content at higher suction range (> 5 MPa) was not significant in $SWCC_w$ representation. As the suction decreased further, the micropores were saturated and the volume increased at the expense of macropore volume as the total volume was constant in restrained condition. The loosely compacted specimens contained higher macropore volume when compared to densely compacted specimens and, therefore, more amount of water was accommodated. The repulsive forces between the clay aggregates are also higher for densely packed specimen due to the restriction on the inter-platelet distances in volume restrained condition. Significant increase in the water content was, therefore, not possible by decreasing the suction less than 2 MPa for densely compacted specimens ($\rho_d \geq 1.6$ g/cm^3) due to the development of excessive osmotic pressures. The water content was, therefore, nearly constant with reduction in the suction. The crystallization of the interlayer surfaces was improved with the decrease in the compaction density as the

diffuse double layers' thickness was further allowed to increase with decrease in the compaction density. The water content of loosely compacted specimens for any given suction was, therefore, higher in the lower suction range. Highest gravimetric water content was observed in volume unrestrained condition as the hydration of the mineral surfaces was not restricted and volume change was allowed to full extent. The observations were qualitatively similar for other bentonites in Fig. 5.11. The difference in retention data decreased for B3 and B4 at dry densities of 1.6 and 1.8 g/cm^3 due to increased osmotic pressures between the platelets with the plasticity of the bentonite. The energy for hydration of mineral surfaces increases significantly with the increase in the osmotic pressure in a volume restrained condition. The $SWCC_w$ data of all the bentonites at 1.8 g/cm^3 was similar and significant change was not noted. The data at higher compaction densities, therefore, was not significantly influenced by the bentonite quality.

5.4. Concluding Remarks

Vapor sorption behavior of powdered and compacted bentonite specimens during the wetting process was investigated for understanding the influence of bentonite plasticity, compaction density, and the vapor pressure of the ambience. The kinetic vapor sorption behavior in bentonites was distinctly different in powder and compacted specimens. The mechanisms such as monolayer and bilayer hydration of surface cations, surface and interlayer influenced the vapor sorption behavior of powdered specimens, whereas the interlayer hydration was absent in the compacted bentonite specimens. The sorption rate in bentonites increased with the bentonite plasticity, higher exchangeable sodium percentage and specific surface area. The increase in the compaction density of the bentonite decreased the accessibility of the interlayer surfaces and exposed the external

surfaces to the water vapors and thus decreased both vapor sorption and equilibrium water content.

Rectangular hyperbola method was used for linearizing the kinetic sorption data. The procedure for predicting sorption rate and equilibrium water content using the initial trend was given. The proposed method was satisfactory in linearizing the sorption data and estimating the equilibrium water contents under different compaction densities and humidity conditions on the studied bentonites. The proposed approach reduces the testing time significantly for establishing soil water characteristic curve for the hydro-mechanical studies for nuclear waste facilities.

The $SWCC_w$ data of four bentonites in volume restrained and unrestrained conditions were measured using the equilibrium water content data of vapor sorption technique and osmotic method. The SWCCs in unrestrained condition differed from restrained condition due to difference in the wetting mechanism. The difference was significant in the lower suction range with different compaction densities where the contribution from the macropores was noticeable. The effect of density on the water retention behavior was not reflected at higher suction range (> 5 MPa) in $SWCC_w$ representation. The increase in volume of water as well as solid content with compaction density was not reflected in $SWCC_w$ data as the gravimetric water content was same at different compaction densities in "dry-end" of SWCC, at a given suction. The representation of SWCC data in terms of gravimetric water content was, therefore, not useful to understand the influence of compaction density on the water retention and flow behavior. The measured data were further represented in terms of $SWCC_\theta$ and $SWCC_{SR}$ for volume restrained condition to understand the effect of compaction density which will be discussed in the following chapters.

Chapter 6

Hysteretic Water Retention Behaviour of Bentonites

6.1. General

Estimation of wetting SWCC of compacted bentonites is prerequisite in hydro-mechanical analysis in the design of HLNW as stated earlier. However, due to the long testing time and difficulties associated with the laboratory testing, SWCC data of compacted bentonites were scarce. The drying SWCC data (chapter- 4) from initially slurried state was related to wetting SWCC data using hysteretic models for possible application of the proposed model for predicting wetting data from the published (literature) drying data. Similar to the wetting SWCC data at four densities (chapter- 5), one additional test with ρ_d= 1.35 g/cm^3 with all the bentonites was conducted to relate wetting and drying data using hysteretic model.

6.2. SWCC$_w$ of bentonites at ρ_d= 1.35 g/cm^3

The wetting SWCC data of the studied bentonites, from the initial state of the specimen equal to the residual saturation of the initial drying curve, along the main wetting path in the volume restrained condition was shown in Fig. 6.1. As the residual state of all the bentonites at the chosen point (ρ_d = 1.35 g/cm^3) on the initial drying curve (Fig. 4.6) was nearly same, the initial state of the compacted specimens (compacted at the same density and water content) for all the bentonites was nearly same. The air-dry clay specimen adsorbs water by surface and cation hydration in the higher suction region (Lu and Khorshidi, 2015). The amount of water adsorbed on the bentonite was, therefore, related to the surface properties such as SSA. Therefore, a slight variation in the water content was observed at higher suction range based on their SSA. The water content of the

specimen increased according to the plasticity of the bentonite with decrease in suction in the medium – low suction range due to the formation of the diffuse double layers (DDLs). The DDL thickness was larger in case of higher plastic bentonite which resulted in more retention of water. The specific moisture capacity was higher for more plastic bentonites and followed the trend B4>B3>B2>B1 at low– medium suction range similar to the desorption behavior. However, due to the restriction of the clay volume during wetting process, only slight difference was observed in the gravimetric water content at full saturation.

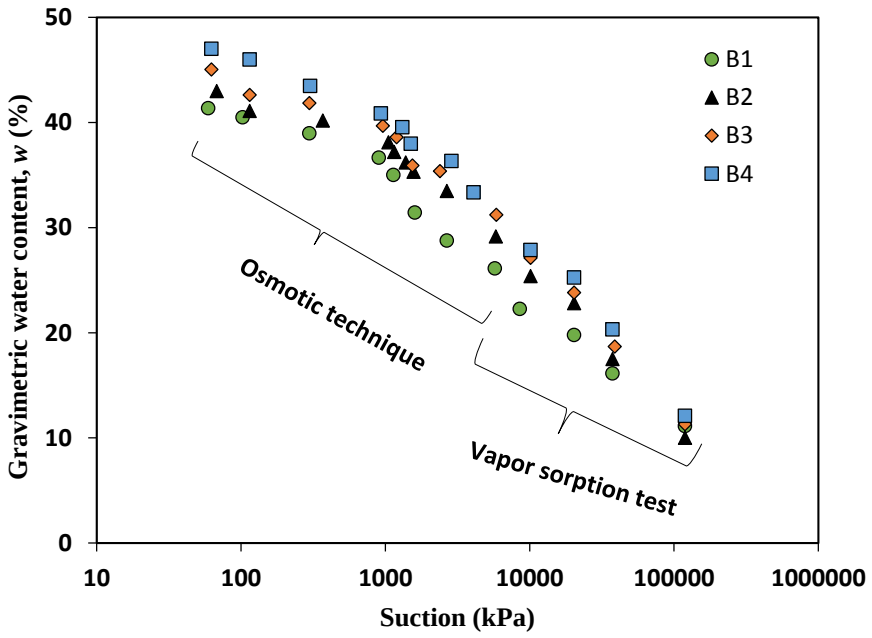

Fig. 6.1 Wetting soil water retention data of different bentonites compacted at dry density, ρ_d = 1.35 g/cm^3

6.3 Hysteretic behavior in clays

The wetting – drying SWCC data of all the bentonites at ρ_d= 1.35 g/cm^3 were presented together in terms of volumetric water content in Fig. 6.2 to represent the hysteretic behavior of the studied bentonites. Drying data of SWCC$_w$ were combined with VSC-

clod to obtain drying $SWCC_\theta$. The wetting $SWCC_\theta$ was obtained by considering constant void ratio as the volume was constant in these tests. The initial drying and main wetting data of a given bentonite were represented by the same marker type for a given bentonite in Fig. 6.2, but the wetting data were represented by filled markers with different colours for different bentonites. The hysteresis effect was predominant in the lower – medium suction range for all the bentonites. Further, highly plastic bentonites exhibited higher variation between the drying and wetting SWCCs (i.e., hysteresis) and followed the trend: B4>B3>B2>B1. When the saturated bentonite specimen is subjected to drying process, air enters into the largest pores of the soil. Since the suction is inversely proportional to pore-radius and the contact angle (α) according to Kelvin's equation, smaller suction force is sufficient to drain the water from the larger pores. The desaturation was, therefore, initiated in the smaller pores only at higher suction. The curvature of the air-water interface within the smaller soil-pores increases during the desaturation until the receding angle. At each drying stage, however, the water content decreases when the applied suction is equalized with the capillary pressure and, at the same time, the pore space decreases to maintain the saturation degree to 100%. The decreased pores sustain more capillary pressure and shrink further with the increase in suction. Significant decrease in the volume ceases as the larger pores at the air-entry suction value undergo desaturation. In contrary, water enters in to the smallest pores of the air-dry bentonite specimen due to wetting process and the saturation of the larger pores initiates only at low suction range. The curvature of air-water interface reduces and the contact angle between the soil-water-air interface starts advancing during the wetting process. In highly plastic clays such as B4 (i.e., the percentage of clay-size fraction was highest), more number of smaller pores are present due to which the water retention capacity was higher. The suction, therefore, was highest for B4 at any given water

content followed by B3, B2, and B1. The pore-water predominantly exists in the microstructure (intra-aggregate pore space) at high suction range. The water content for the hydration of surface cations and intra-aggregate pores at this suction range does not significantly vary with the dehydration process (Khorshidi and Lu, 2016). Therefore, the wetting SWCCs of all the bentonites nearly coincides with the drying SWCCs in the higher suction range.

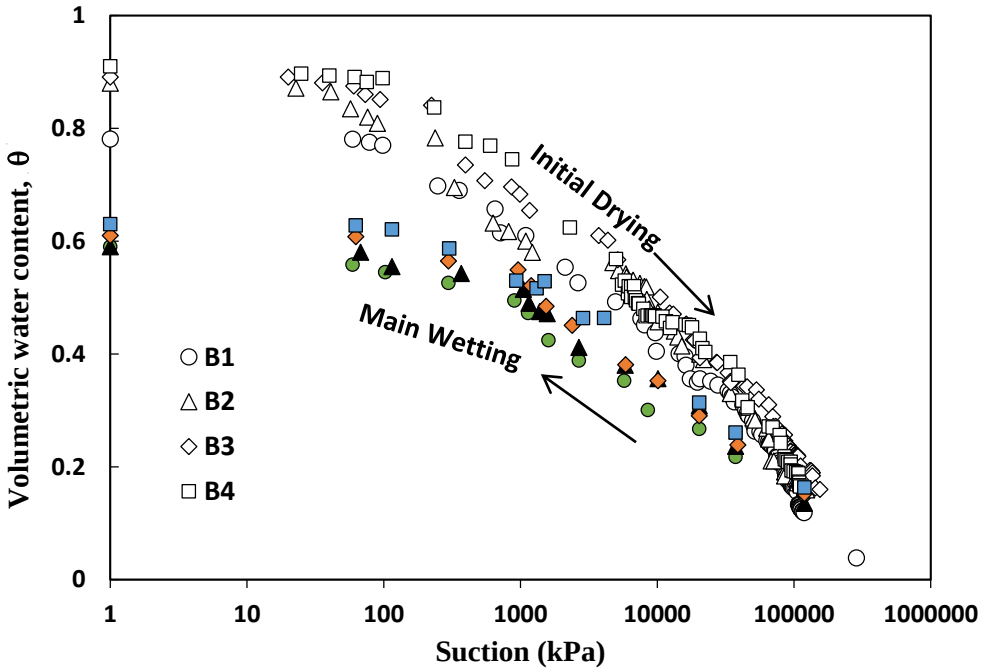

Fig. 6.2 Hysteresis of soil water retention data of different bentonites

6.4 Prediction of boundary wetting curve

In this work, the boundary wetting curves were predicted from the initial drying data and two additional data points along the boundary wetting curve using the proposed approach which was based on Pham et al. (2003) model. In Eqs. (2.9) – (2.13), either gravimetric water content or volumetric water content were used in place of degree of saturation similar to the earlier work (Pham et al., 2003), depending on the availability of the data for model validation. The water content corresponds to lowest controlled/measured suction using osmotic technique (20 – 60 kPa) was used for water content corresponds to

zero suction on the initial drying data (w_s, θ_s, or S_s) and on the boundary wetting curve (w_u, θ_u, or S_u) in Eq. 2.9. Locations of the two data points on the main wetting curve were obtained from Eqs. (2.10) – (2.11) and the fitting parameters of the main wetting curve were obtained using Eq. (2.12) – (2.13). The proposed method did not require any scaling factors and the method was simple. The predicted boundary wetting curve was compared with the measured data of plastic clays from the current study and the literature.

The curve-fitting parameters of the initial drying data (b_{id}, c_{id}, and d_{id}) and boundary wetting data (b_w, c_w, and d_w) in Eq. 2.9 were independently estimated by minimizing the error between theoretical and measured data (Bharat et al., 2009). The theoretically estimated SWCCs by optimization were shown in Fig. 6.3 using the solid lines along with the measured data. Equation (2.9) was found to approximate the measured data well for all the bentonites. The optimized fitting parameters of the initial drying and boundary wetting SWCC data were shown in Table 6.1. The fitting parameters b and d were directly proportional to the plasticity of the bentonites as they depend on the air-entry suction value and slope of the linear portion in SWCC, respectively. The air-entry suction value increased with the plasticity of the bentonite and the optimized parameters were higher for B4. The slope parameter was higher for drying SWCC compared to the wetting SWCC as the specific moisture capacity on the drying path was higher compared to wetting path at any given suction.

The wetting SWCC curves of the bentonites were predicted using two measured data points on the main wetting curve and the curve fitting parameters of the initial drying SWCC data (i.e., b_{id} and d_{id}) using the proposed approach. The predicted curves were presented for all the studied bentonites in Fig. 6.3 using broken lines along with the measured data. The predicted wetting curves were in good agreement with the measured

wetting data and fitted curves for all the bentonites. The coefficient of determination, R^2, between the measured and predicted wetting data varied between 0.985 and 0.994 for different bentonites.

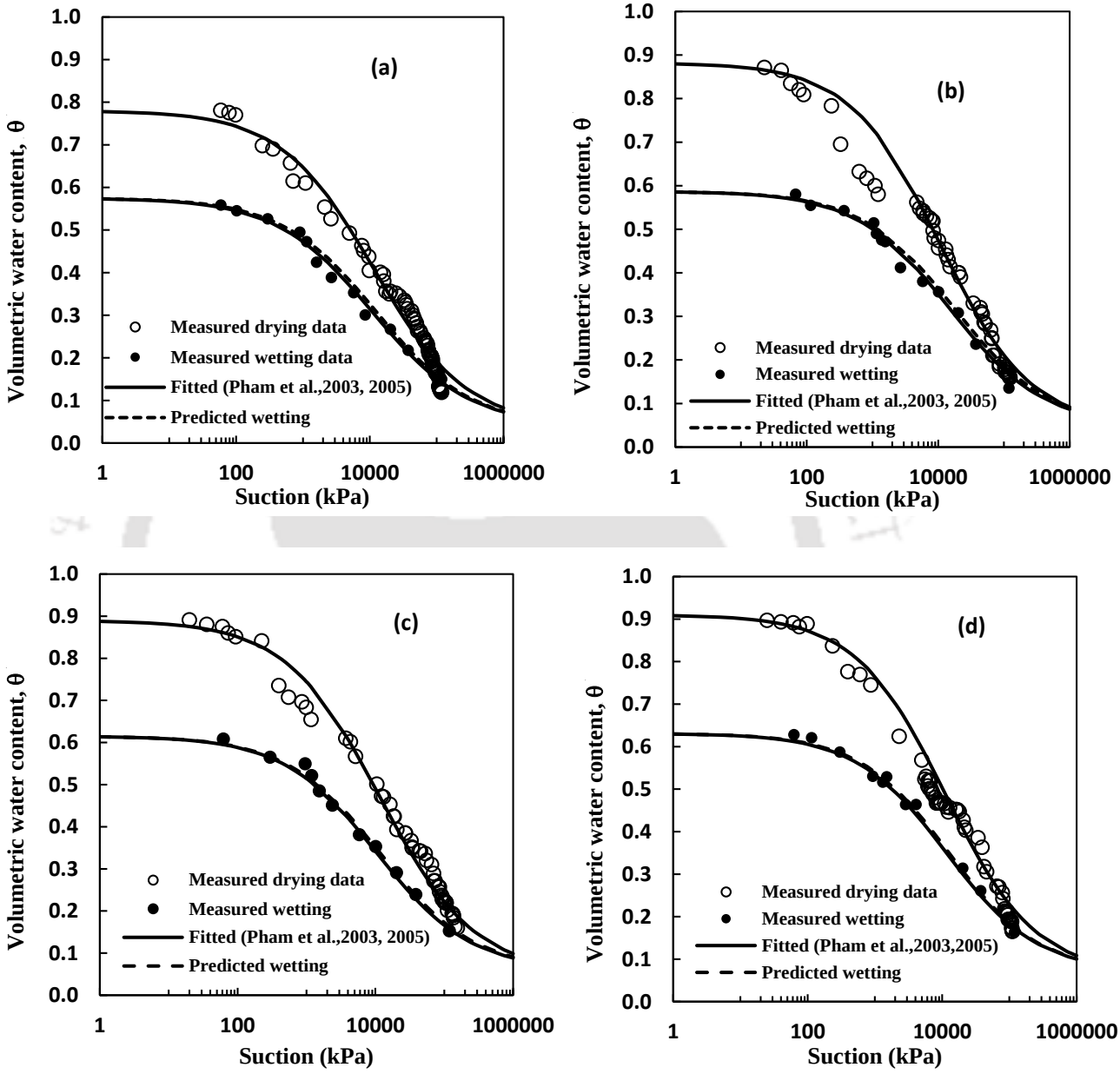

Fig. 6.3 Predicted hysteretic behaviour for bentonites (a) B1 (b) B2 (c) B3 (d) B4

The hysteresis data of clay soils from the literature were also utilized to validate the proposed approach. The published water retention data of montmorillonite, white clay, and FoCa clay (Fleureau et al., 1993, 2002) were considered. These three clays were

included in this study as the data along the initial drying and boundary wetting paths are available which would facilitate the validation of proposed method for predicting the main wetting curve from the initial drying data. The measured data and predicted hysteresis curves for these three clays were presented in Fig. 6.4a- 6.4c.

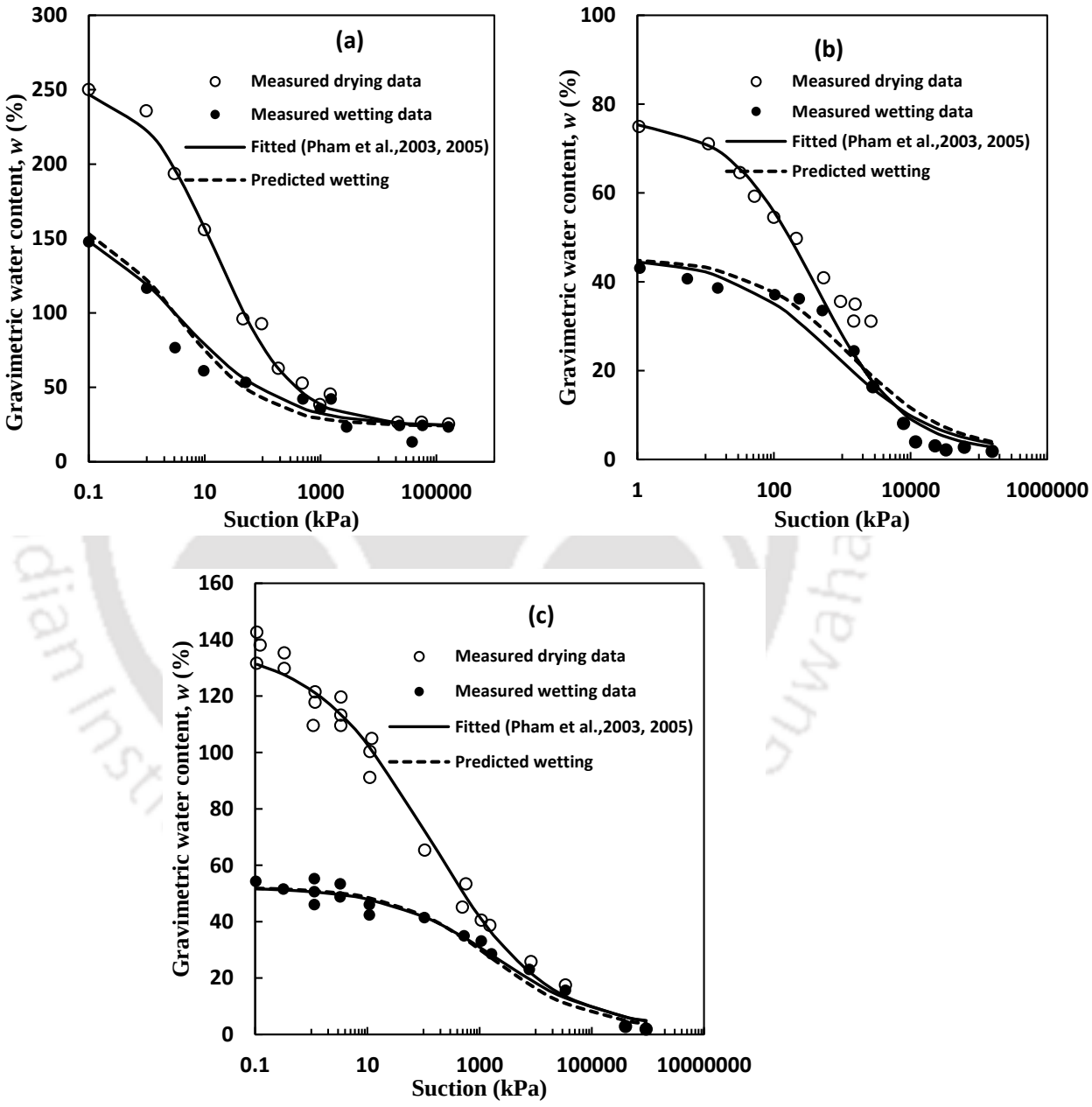

Fig. 6.4 Predicted hysteresis behaviour of (a) montmorillonite (Fleureau et al., 1993) (b) White clay (Fleureau et al., 1993) (c) FoCa (Fleureau et al., 2003)

The optimized curve fitting parameters of hysteretic SWCC data along with the details of additional data points on the main wetting path were given in Table 6.2. The measured and predicted main wetting data of all the clays showed good agreement and the R^2 varied between of 0.945 and 0.975. Therefore, the proposed approach was useful for predicting the main wetting curve from the initial drying data of clay soils using the proposed approach. This approach is useful for understanding the hysteretic behavior of bentonite clays under different stress states using (initial) drying data of slurry specimen. The wetting behavior along the boundary wetting or scanning paths could be predicted under various stress conditions (i.e., compaction conditions and volume restrained-unrestrained conditions) using limited measurements. In this work, the wetting behavior under volume restrained condition and from the residual state on the initial drying curve was successfully predicted.

Table 6.1 Predicted curve fitting parameters of soils

Soil type			B1	B2	B3	B4
Initial drying SWCC (Fitting)	θ_s		0.78	0.882	0.89	0.91
	c		0.04	0.05	0.06	0.07
	b_{id}		343	358	382	429
	d_{id}		0.625	0.633	0.64	0.66
	R^2		0.969	0.969	0.986	0.982
Main wetting SWCC (Fitting)	θ_u		0.58	0.59	0.62	0.63
	b_w		273	353	375	401
	d_w		0.60	0.61	0.63	0.64
	R^2		0.988	0.987	0.993	0.992
Main wetting SWCC (Predicted)	Position of two additional points	ψ_{1w}	285	284	309	310.33
		θ_1	0.53	0.55	0.56	0.59
		ψ_{2w}	22449	21519	22943	2067.49
		θ_2	0.26	0.30	0.27	0.31
	b_w		324	382	398	456.88
	d_w		0.61	0.61	0.64	0.64
	R^2		0.985	0.987	0.993	0.992

Table 6.2 Predicted curve fitting parameters of soils taken from published literature (Fleureau et al., 1993, 2002)

Soil type			Montmorillonite	FoCa clay	White clay
Initial drying SWCC (Fitted)	w_s		255	138	76.55
	c		24	1.8	1.55
	b_i		6.06	10.56	60
	d_i		0.65	0.47	0.68
	R^2		0.993	0.991	0.965
Main wetting SWCC (Fitted)	w_u		169.57	52.23	45.40
	c		24	1.8	1.50
	b		1.88	30.22	45.00
	d		0.49	0.45	0.57
	R^2		0.944	0.969	0.957
Main wetting SWCC (Predicted)	Position of two additional points	ψ_{1w}	0.46	1.12	13.94
		w_1	135.22	51.10	42.00
		ψ_{2w}	27.10	302.40	816.40
		w_2	57.86	37.45	24.12
	b_w		2.07	46.49	71.47
	d_w		0.58	0.52	0.59
	R^2		0.945	0.965	0.975

6.5 Influence of bentonite plasticity on the hysteresis

Hysteresis behavior is often quantified by average degree of hysteresis (D_h) signifying the average water content difference between drying and wetting SWCCs (Lu and Khorshidi, 2015; Al-Mahbashi et al., 2016). The average degrees of hysteresis over suction range between data points j to k is expressed by (Lu and Khorshidi, 2015):

$$D_h = \frac{\sum_{i=j}^{i=k} \frac{w_{di} - w_{wi}}{w_{mi}}}{k - j + 1} \quad (6.1)$$

where w_{di} is the gravimetric water content at point i on drying curve, w_{wi} is the gravimetric water content at point i on wetting curve, and w_{mi} is the average gravimetric water content at point i between the wetting and drying states. The D_h value of all the

bentonites were estimated using Eq. (6.1) and were presented in Table 6.3. The D_h values varied between 0.3 and 1.01 for different clays indicating a water content difference of 30% – 100% of the mean water content for drying and wetting SWCCs. Relatively large D_h values were obtained for the bentonites and D_h values increased with the plasticity of the bentonites.

The variation of D_h with liquid limit was shown in Fig. 6.5. The degree of hysteresis increased non-linearly with the plasticity of the bentonite. The larger D_h values for the bentonites were due to large volume changes during drying – wetting cycles as the expansiveness increased with the plasticity of the clay. The volume restrained condition in wetting tests also limited the volume expansion of the bentonites which increased the estimated average D_h.

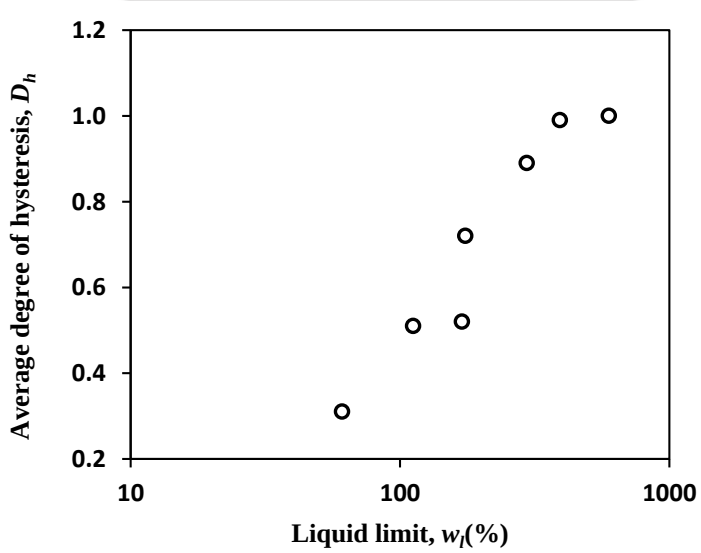

Fig. 6.5 Variation of degree of hysteresis of soil water characteristics curve in soils with liquid limit

Table 6.3 Degree of hysteresis in soil water characteristic curves for the soils

Clay type	Liquid limit (%)	Degree of hysteresis, D_h
B1	175	0.72
B2	296	0.89
B3	393	0.99
B4	597	1.01
Montmorillonite	170	0.52
White clay	61	0.31
FoCa clay	112	0.51

6.6 Concluding Remarks

The hysteretic SWCC data of bentonites with different plasticity were established over a wide suction range using different laboratory suction controlling techniques on independent bentonite specimens. The type of surface cations and clay content did not influence the drying SWCCs at higher suction range due to the insignificant influence of surface cation hydration. The influence of plasticity on the wetting SWCCs of bentonite specimens in volume restrained condition is insignificant as the adsorptive storage mechanism controls the water retention behavior when the volume expansion is curbed.

The degree of hysteresis, which is a qualitative representation of difference between drying and wetting SWCCs for different bentonites was controlled by the drying SWCCs in the present work due to the insignificant influence of plasticity on the wetting SWCCs in volume restrained conditions. The degree of hysteresis is proportional to the plasticity of the bentonites. The degree of hysteresis was higher than 100% (i.e., the average water content difference between the wetting and drying SWCCs with respect to the mean water content) for B4 due to volume restrained condition in wetting.

A theoretical model based on Pham et al. (2003) was proposed to predict the hysteresis in SWCCs. The proposed model was simple and was accurate in predicting the boundary wetting curve directly from the initial drying data and two additional data points along

the wetting path for the bentonites and clay soils studied in this work. The proposed method did not require any scaling factors between the two boundary curves used in the earlier studies. The proposed method is useful in understanding the wetting behavior of bentonites under volume restrained conditions using the drying data of an initial slurry specimen. The method can be advantageously utilized for predicting the wetting SWCCs of soils in the absence of measurements over a wide suction range.

The proposed method is not useful for understanding the constitutive behavior of clays following cyclic drying – wetting cycles. The physically-based models such as Gallipoli (2012) and Pham and Fredlund (2011) are useful for understanding the changes in stress-state of the soil in drying – wetting cycles. The hysteretic behavior of the bentonites in this work was studied by considering the initial condition of the boundary wetting data to be equal to the compaction condition of the specimen at residual state on the initial drying curve using independent specimens. The same specimens could not be used for establishing the entire hysteresis data unlike non-plastic soils due to the limitations associated with the suction controlling techniques. The boundary wetting behavior of the specimen may differ quantitatively (it will be same qualitatively), if the same specimen on the initial drying curve is subjected to wetting due to the influence of surface forces. Experimental methodology to establish hysteretic behavior of bentonites over a wide suction range is required for understanding the micromechanical cyclic behavior.

Chapter 7
Wetting Hydraulic functions

7.1 General

The previous chapters have discussed the effect of soil plasticity and compaction density on water retention curve expressed in terms of gravimetric water content. However, the SWCC representation in terms of θ or S_r is required in solving the flow equation. Further the effect of density is evident in $SWCC_{\theta}$ and $SWCC_{SR}$ representation. Therefore, this chapter investigated the influence of compaction density and soil plasticity on $SWCC_{\theta}$ and $SWCC_{SR}$ of compacted bentonites. Hydraulic conductivity functions were obtained from the SWCC data using a statistical model. The influence of compaction density and bentonite plasticity on the estimated HCFs was discussed. The present study is very important for understanding wetting mechanism in restrained, compacted clays of different plasticity and is useful in the design of waste repositories.

.

7.2 SWCC in terms of volumetric water content and degree of saturation

The gravimetric water content data at different suction values were expressed in terms of S_r by considering a constant dry density ($\rho_d = M_s/V$, where M_s is mass of solids and V is the total volume of the specimen) during the wetting process. The volume of the extruded specimens from the osmotic cells, after the tests, were estimated using paraffin-wax coating method (ASTM D4943-08, 2008) to understand the effect of perspex material expansion on the specimen volume during the wetting process. The dry densities were slightly smaller to nearly same for different saturation conditions. The slight decrease in the dry density at near saturation was reasoned out to be due to slight swelling of the specimens when the stresses were released during the extrusion. The

swelling potential of the specimens due to release of stresses varies with the water content (Tripathy et al., 2014). The mould volume was, therefore, used in the estimation of S_r as the difference between mould volume and extruded specimen volume was insignificant. The estimated S_r in the lower suction range was higher than 100% for denser specimens (ρ_d > 1.0 g/cm^3) as shown in Fig. 7.1 for different bentonites.

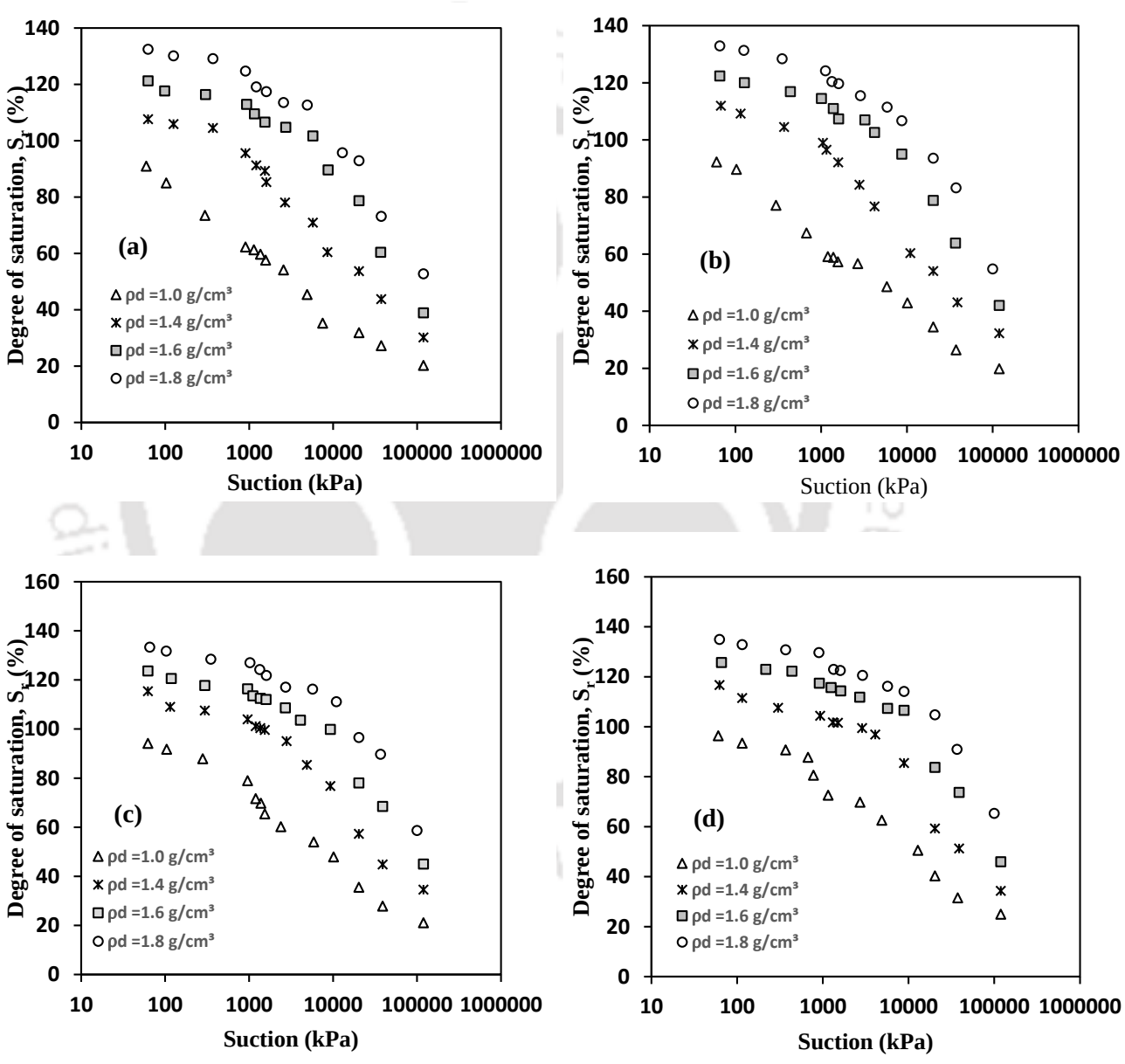

Fig. 7.1 Comparison of Degree of saturation vs suction (SWCC$_{SR}$) of bentonites for (a) B1 (b) B2 (c) B3 (d) B4

The S_r data for ρ_d = 1.0 g/cm^3 were below 100% for any given suction. The maximum suction corresponding to S_r > 100% increased with the increase in the compaction density and plasticity of the bentonite. The observed S_r data above 100% was attributed to the changes in the water density in the compacted condition. The attribution was similar to the recent interpretations by Jacinto et al. (2012, 2016) for the density of water in the volume restrained condition near saturation. The density of water in the adsorbed layers of clay minerals is reported to be higher than 1.0 g/cm^3 (Martin, 1960; Low, 1976; Sposito and Prost, 1982; Hueckel, 1992; Villar and Lloret., 2004, 2008). The water density varies between free water density and adsorbed layer density for different suction values. The water density approaches unity at near saturation for unrestrained condition, similar to lower compaction density (ρ_d = 1.0 g/cm^3). As the increase in the water content during sorption tests, the macropores (contain free water with ρ_w = 1 g/cm^3) were saturated and the average density was higher than 1 g/cm^3. However, as the adsorbed water dominates in the volume restrained condition, the water density for any given suction was higher than unity. The water density in the saturation portion of the SWCC$_{SR}$ was estimated by assuming S_r = 1 for the gravimetric water content corresponding to lowest measured suction (~ 60 kPa) by osmotic technique. The estimated water densities for different bentonites and compaction densities were given in Table 7.1. The water density variation with the compaction density was shown in Fig. 7.2. The water density increased with the compaction density and with the plasticity. The water density was highest for densely packed system as the amount of free water was less. Similarly, surface charges are higher for plastic clays that adsorb water tightly on the mineral surfaces. The effect of plasticity, however, reduced with the increase in the compaction density. The water density increased by 10% when the compaction density increased to 2 g/cm^3 for B3 and B4 bentonites.

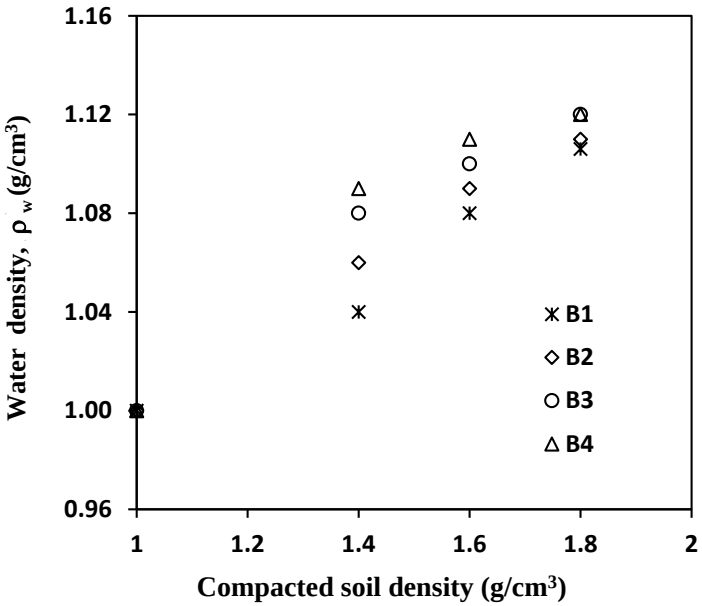

Fig. 7.2 Variation of water density with initial compaction density.

Table 7.1 Void ratio as a function of water density.

Soil	Compaction density ρ_d (g/cm^3)	e (Water density, ρ_w =1 g/cm^3)	Adjusting S_r =100%	
			e	Water density, ρ_w (g/cm^3)
B1	1.0	1.80	1.80	1.00
	1.4	1.02	1.10	1.04
	1.6	0.68	0.82	1.08
	1.8	0.51	0.68	1.11
B2	1.0	1.83	1.83	1.00
	1.4	1.04	1.16	1.06
	1.6	0.70	0.85	1.09
	1.8	0.53	0.70	1.11
B3	1.0	1.86	1.86	1.00
	1.4	1.06	1.22	1.08
	1.6	0.71	0.88	1.10
	1.8	0.54	0.72	1.12
B4	1.0	1.87	1.87	1.00
	1.4	1.07	1.25	1.09
	1.6	0.72	0.91	1.11
	1.8	0.55	0.74	1.12

The corrected $SWCC_{SR}$ data were shown in Fig. 7.3 for different bentonites. The water entry suction value, which is the maximum suction required for water to enter in to the smallest pore opening, was higher for the densely compacted specimen due to the availability of smaller pores (Fig. 5.10b). The degree of saturation of densely compacted specimens was higher than loosely compacted specimens at any given suction. The observed trend was completely opposite to the trend in w vs. ψ representation (Fig. 5.2) where the gravimetric water content of densely compacted specimens was lower than the loosely compacted specimens at any suction. Densely compacted specimens contained lesser void volume (smaller macropore sizes) when compared to loosely compacted specimens as illustrated in Fig. 5.10. The smaller void ratio for given water content ($S_r = wG_s/e$) in the denser packing significantly increased the degree of saturation. The influence of density on the water retention behavior was visible at higher suction range also in this representation. However, the estimated degree of saturation data might be inaccurate due to the fact that the water density depends on the water content in clays (Martin, 1960) and using a constant water density over the entire suction range is erroneous. Jacinto et al. (2016) suggested using weighted average density of water by considering density of interlayer and external water. The water density, with this assumption, decreases with the increase in water content and reaches to 1 g/cm^3 near saturation. The predicted trend is opposite to the laboratory observations (Fig. 7.1), where the deviation from $S_r = 1$ was more evident near saturation, and the literature studies (Martin, 1960). As the water density could not be estimated for different suction values accurately, the S_r vs. ψ representation was not useful for flow analysis through compacted bentonites and data were not used for hydraulic conductivity estimation in this work.

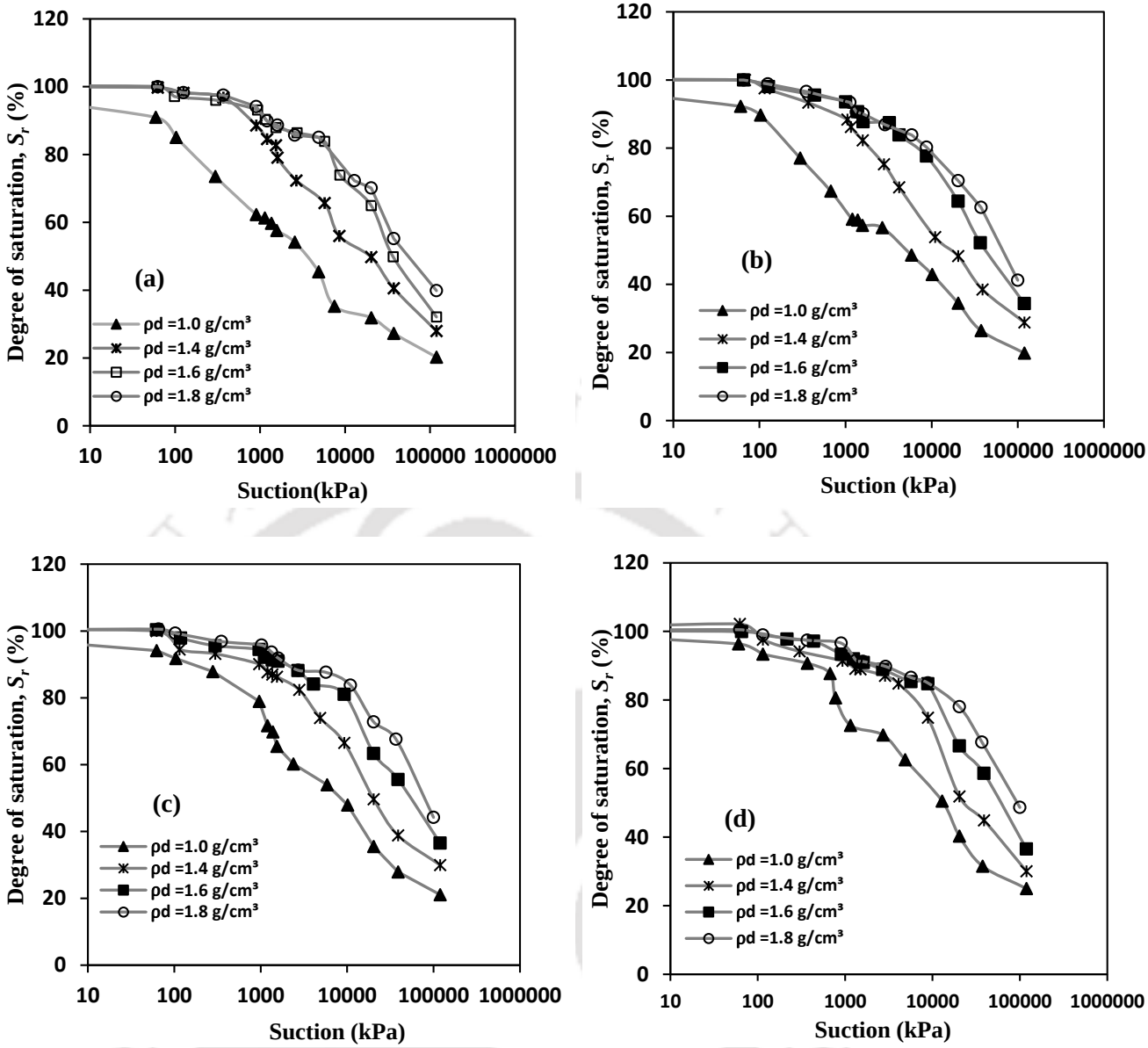

Fig. 7.3 Comparison of $SWCC_{SR}$ of bentonites after adjusting water density for (a) B1 (b) B2 (c) B3 (d) B4

The measured retention data were presented in terms of volumetric water content ($SWCC_{\theta}$) in Fig. 7.4 for establishing theoretical $SWCC_{SR}$ and hydraulic conductivity functions. As the densities of the compacted specimens were constant during the sorption tests, the following relationship between the volumetric and gravimetric water content was utilized for establishing $SWCC_{\theta}$.

$$\theta = \frac{w\rho_d}{\rho_w} = \frac{w\rho_b}{(1+w)\rho_w} \tag{7.4}$$

where ρ_w is the density of water, ρ_d is the dry density, ρ_b is the bulk density, and w is the gravimetric water content. The effect of density on the water retention behavior was significantly evident over the entire suction range. The retention data crisscrossed at different suction values exhibiting lower water content in the higher suction range in loosely compacted specimen, but higher water content in the lower suction range when compared to the densely compacted specimens, for all the bentonites. The observations in the higher suction range (> 10 MPa) were in contrast to the measured SWCC$_w$ data (Fig. 5.2) where the specimens with different densities exhibited the same gravimetric water content in the higher suction range. As the volumetric water content is defined as the ratio of volume of water to the total volume, the total volume of water at higher suction range was higher in denser packing due to the presence of higher solid content even when w was same at the same suction in both compaction conditions. For example, the gravimetric water content (w = 12%) of the air-dry specimens compacted at two different compaction densities was same, but the volumetric water content nearly doubled for density ρ_d = 1.8 g/cm^3 when compared to ρ_d = 1.0 g/cm^3 as the total volume was constant (V = 22.67 cm^3) as evident from Eq. (7.4). Although gravimetric water content (Fig. 5.2) was not significantly affected by the compaction density at higher suction range, the volumetric water content was significantly higher for denser packing as observed in Fig. 7.4 for B1. As the suction was decreased, the accommodated water volume was lesser in denser packing due to the development of higher amount of osmotic pressures. The volumetric water content decreased for denser packing with the decrease in matric suction, therefore, exhibiting crisscross behavior. The observations on the retention data for other compacted bentonites were similar as seen in B2, B3 and B4

(Fig. 7.4). The $SWCC_\theta$ data were used to estimate the model parameters of the van Genuchten (vG) equation (Eq. 2.3) by optimization. The model parameters using *m*, *n* dependent ($m = 1 - 1/n$) and *m*, *n* independent cases (Vogel et al., 2001) were obtained using RETC computer code (van Genuchten, 1994). The estimated model parameters for different bentonites and compaction densities were shown in Table 7.2. The α parameter was represented in kPa^{-1} instead of m^{-1} here, which represents the inverse of the air-entry suction. The air-entry suction increased with the compaction density for a given bentonite. As the pore size of the soil matrix (macropore volume) decreased with the compaction effort (Fig. 5.10), the largest pore diameter in densely compacted bentonite is smallest among the other compaction densities. As the air-entry value (AEV) is defined as the suction corresponding to water content at which the air enters into the largest pore of the clay specimen, ψ_{AEV} increased with the compaction density. The ψ_{AEV} also increased with the bentonite plasticity for lower compaction densities. Due to the presence of higher clay content in the plastic clays, the average pore-size decreased with the plasticity. At higher compaction densities, the optimized model parameters were same for different bentonites and the effect of plasticity was not seen. The observation was in accordance with the $SWCC_w$ representation. The theoretical fit was in good agreement with the measured data and the coefficient of determination (R^2) varied between 0.93 – 0.998 for *m*, *n* dependent case; varied between 0.945 – 0.999 for *m*, *n* independent case. However, *n* parameter takes the values less than unity for the plastic clays in unrestrained *m*, *n* case (Vogel et al., 2001; Ippisch et al., 2006). As the *n* parameter is required to be restricted to unity to avoid singularity near saturation portion of SWCC (van Genuchten and Nielsen, 1985), the *n* parameter for most of the bentonites and compaction densities was same and was nearly unity. The theoretical $SWCC_\theta$ data using only *m*, *n* dependent case was utilized for HCF estimation, therefore, although the

theoretical fit improved using *m*, *n* independent case. Theoretical SWCCs using the optimized model parameters (*m*, *n* dependent case) were shown in Fig. 7.4 along with the measured data. The theoretical fit was in good agreement with the measurements for different bentonites.

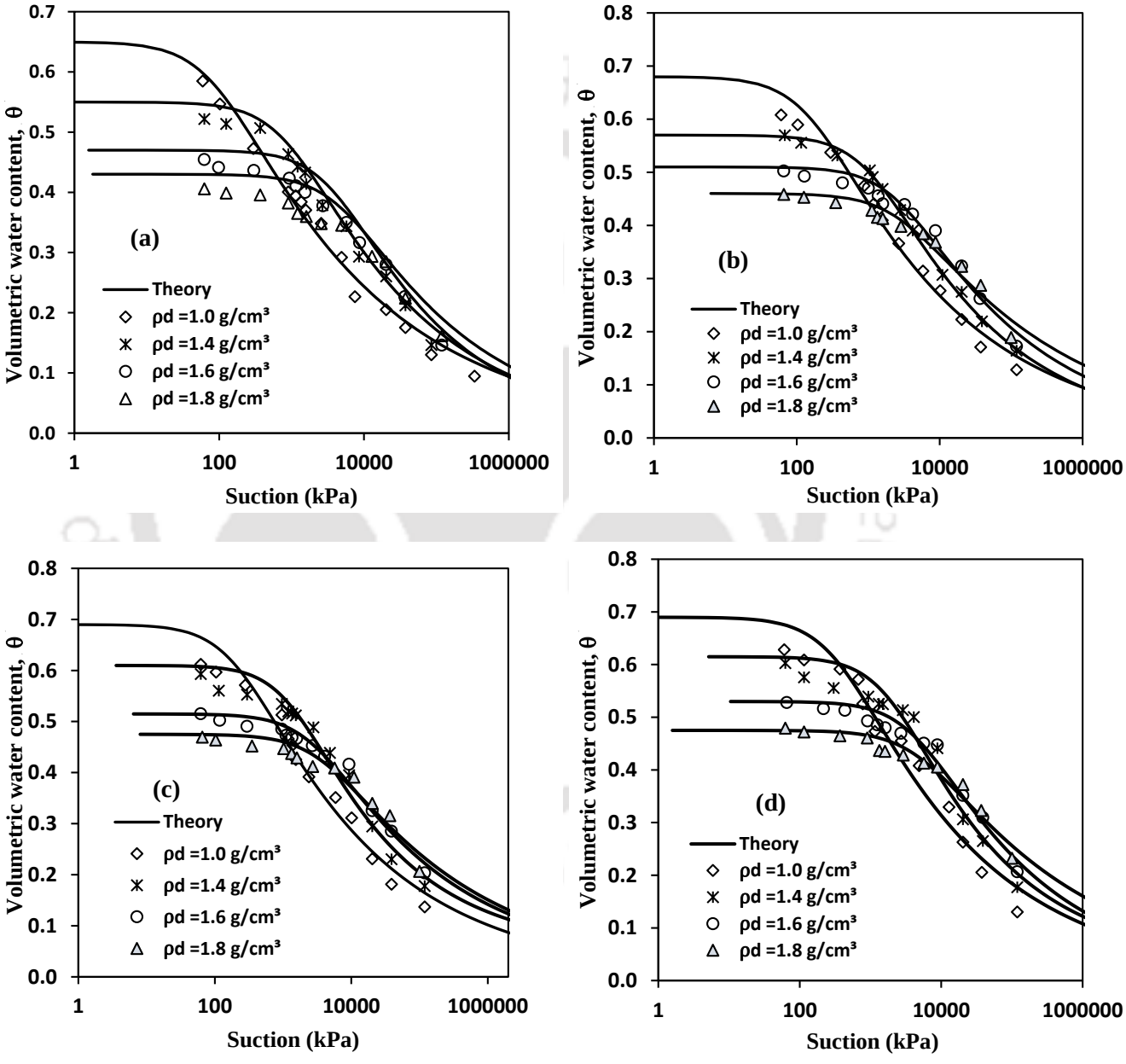

Fig. 7.4 Experimental and fitted SWCC $_{\theta}$ of bentonites under restrained conditions (compacted at different densities) for (a) B1 (b) B2 (c) B3 (d) B4

Table 7.2 Optimized vG model parameters for bentonites obtained by RETC

Soil type	Density (g/cc)	m, n dependent			m, n independent			
		α (m^{-1})	n	R^2	α (m^{-1})	n	m	R^2
B1	1.0	0.098	1.21	0.986	0.075	1.01	0.23	0.989
	1.4	0.011	1.25	0.992	0.009	1.09	0.24	0.992
	1.6	0.003	1.29	0.988	0.001	1.01	0.37	0.990
	1.8	0.002	1.25	0.974	0.001	1.01	0.32	0.978
B2	1.0	0.062	1.23	0.980	0.047	1.01	0.24	0.987
	1.4	0.009	1.26	0.998	0.007	1.06	0.27	0.999
	1.6	0.004	1.25	0.967	0.002	1.01	0.31	0.978
	1.8	0.003	1.21	0.954	0.002	1.01	0.26	0.966
B3	1.0	0.048	1.23	0.964	0.033	1.01	0.25	0.972
	1.4	0.007	1.3	0.964	0.004	1.01	0.37	0.976
	1.6	0.004	1.24	0.973	0.002	1.01	0.29	0.982
	1.8	0.003	1.21	0.930	0.001	1.01	0.27	0.945
B4	1.0	0.029	1.23	0.958	0.021	1.01	0.26	0.965
	1.4	0.005	1.30	0.952	0.003	1.01	0.38	0.966
	1.6	0.002	1.26	0.963	0.001	1.01	0.28	0.975
	1.8	0.002	1.20	0.950	0.001	1.01	0.24	0.955

7.3. Hydraulic conductivity functions (HCFs)

The effect of density on $SWCC_w$ data was not reflected in the higher suction range (> 5 MPa) and the water density at different saturation values was not available in the $SWCC_{SR}$ representation. Therefore, hydraulic conductivity functions of different bentonites and at different compaction densities were estimated using the vG model parameters obtained by fitting $SWCC_\theta$ data only. Mualem's (1976a) statistical model was utilized to estimate the HCFs in terms of relative hydraulic conductivity (k/k_s) vs. suction. The measured saturated hydraulic conductivities for different bentonites at various compaction densities (Table 3.3) were utilized to establish hydraulic conductivity vs suction as shown in Fig. 7.5. The saturated hydraulic conductivity at a compaction density of 0.5 g/cm^3 was utilized for establishing HCF from unrestrained - $SWCC_w$ data for comparison with the restrained HCFs. The hydraulic conductivities of different

bentonites in unrestrained condition were, however, not accurate as the effect of volume changes were not incorporated. Further, the volumetric water content and degree of saturation data for unrestrained condition could not be established for powder specimens from the measured gravimetric water content as the measurement of density variation in the specimen during wetting tests was not possible.

The estimated HCFs for different bentonites followed a standard trend with sharp reduction in the conductivity after air-entry suction and continuous decrease in the conductivity by several orders of magnitude of its k_s value (Hillel, 1980). Hydraulic conductivity of B1 (Fig. 7.5) at high suction range in densely compacted specimen was higher due to the presence of higher volume of water and availability of continuous channels. On the other hand, the larger macropores with lesser water volume in loosely compacted specimens resulted in discontinuous water channels with the presence of significant air volume. The water entry suction of the loosely compacted specimens was smaller than the densely compacted counterparts, therefore, which was also evident from Kelvin's equation (Eq. 3.1). The increase in k with reduction in suction in densely compacted specimens was not significant for suction less than 2 MPa for different bentonites as the free water in the pore space did not increase considerably. The osmotic pressures were significantly higher in the densely compacted specimens at this suction range. The available free water in denser packing was, therefore, smaller in the lower suction range (average $\rho_w > 1$) due to the availability of smaller macropores which decreased the hydraulic conductivity significantly relative to the specimen at looser packing. As the hydraulic conductivity of the denser packing was higher than the loosely compacted specimen at higher suction and the trend was reversed at lower suction range, the HCFs of specimens compacted at different densities crisscross each other.

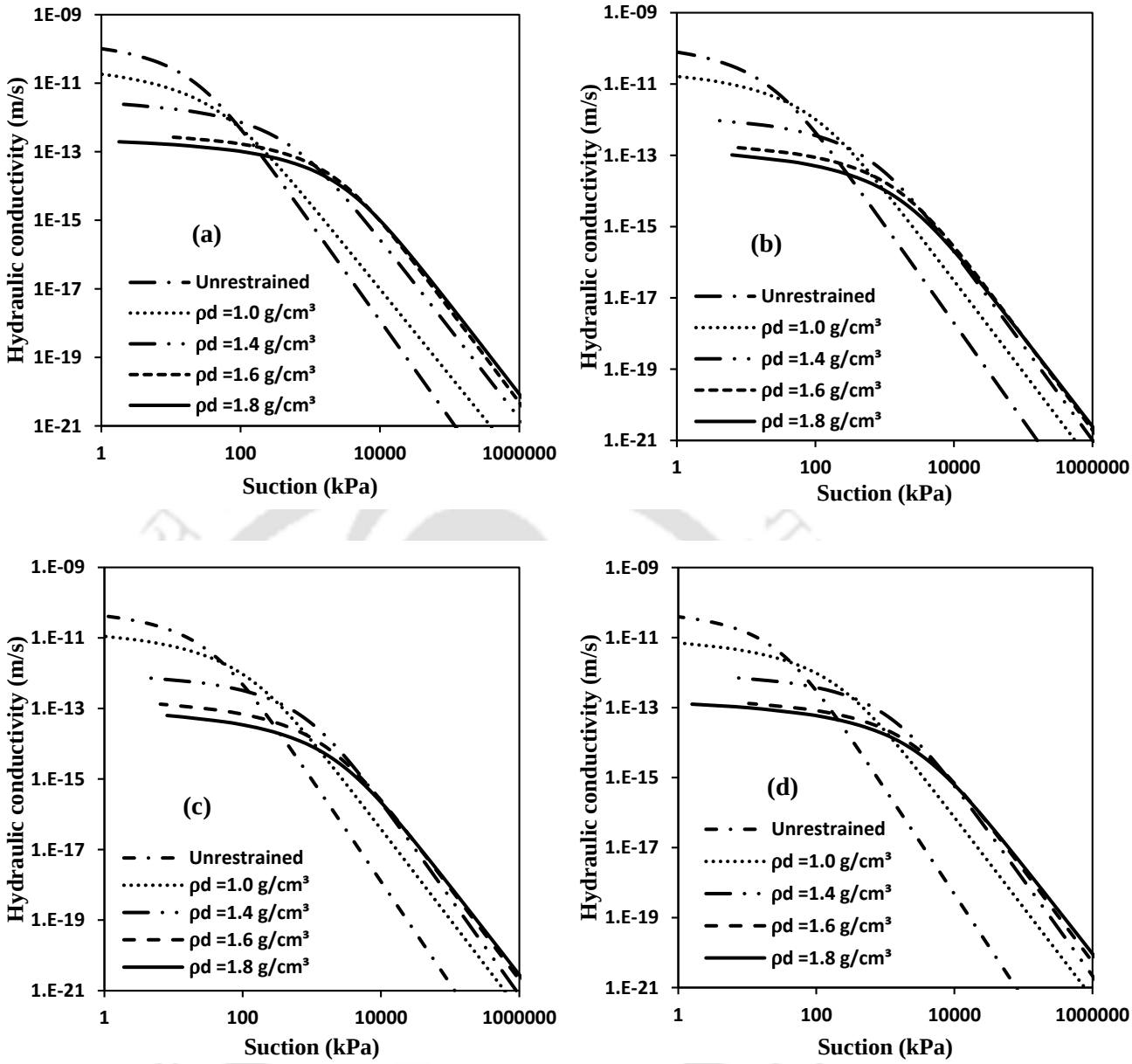

Fig. 7.5 Comparison of hydraulic permeability (k_{unsat}) of bentonites under restrained conditions (compacted at different densities) for (a) B1 (b) B2 (c) B3 (d) B4

The observed trend of HCFs was similar to the hydraulic conductivities of texturally different soils or soils with varying density in natural deposition that often studied for understanding capillary barrier retention mechanism (Hillel, 1980; Huang et al., 2011; Harnas et al., 2014). The estimated HCFs of the specimens compacted at higher densities (ρ_d = 1.6 g/cm^3 and ρ_d = 1.8 g/cm^3) were similar and no significant difference in the

permeability was found. The observed trend of HCFs of other bentonites was qualitatively similar to B1, but the conductivities smaller by few orders of magnitude near the saturation. The difference in the estimated HCFs of B3 and B4 specimens at higher compaction densities (ρ_d= 1.6 g/cm^3 and 1.8 g/cm^3) were insignificant. As the volumetric water content data at higher compaction densities and for different bentonites in "dry-end" suction range were significantly different, the conductivities were nearly the same. The HCFs of bentonite specimens compacted at higher densities were, therefore, not effected by the clay plasticity (Fig. 7.5). Overall, the SWCC$_\theta$ data provide accurate HCF estimation of the bentonites in volume restrained conditions.

7.4 Concluding Remarks

The measured water retention data were represented in terms of SWCC$_\theta$ and SWCC$_{SR}$ for volume restrained condition to understand the influence of compaction density. The vG model was used to fit the estimated data to obtain a smooth distribution. HCFs were estimated from the theoretical SWCCs using a statistical model. The SWCCs and HCFs in unrestrained condition differed significantly from the restrained condition due to the difference in the wetting mechanism discussed earlier. The difference was significant in the lower suction range with different compaction densities where the contribution from macropores was noticeable. The influence of compaction density was evident in SWCC$_\theta$ and SWCC$_{SR}$ representation. The water density was higher than 1 g/cm^3 for specimens compacted at ρ_d > 1.0 g/cm^3 in SWCC$_{SR}$ representation. The water density was estimated from SWCC$_{SR}$ data by adjusting S_r value, corresponding to lowest measurable suction, to unity. The variation in the water density with other suction values in the moderate to high suction range could not be estimated and thus a constant value was used. The representation of SWCC data in terms of degree of saturation was also not useful to

understand the influence of compaction density on the water retention and hydraulic behavior. The SWCC$_\theta$ data of specimens at different compaction densities accurately depicted the effect of density at lower suctions and pore-size effects at higher suction range. The retention data of specimens compacted at different densities, therefore, crisscrossed and exhibited the influence of different mechanisms in different suction ranges. The estimated HCFs from the SWCCs using statistical model provided a standard "S-curve" trend similar to the other soils reported in the literature where the variation of conductivity with suction was not significant up to air-entry suction, but decreased by several orders of magnitude with the increase in suction. The observation was in contrast to the recent observation on GMZ bentonite by Ye et al. (2009, 2016) which seems to be due to neglecting the mass conservation. The estimated HCFs using SWCC$_\theta$ data provided the influence of compaction density. The HCFs estimated at different compaction densities also crisscrossed each other, similar to the unsaturated permeability behavior of texturally dissimilar soil layers. The HCFs estimated from the SWCC$_\theta$ alone provide accurate unsaturated flow characteristics in the numerical analysis through compacted plastic clays, therefore. The estimated HCFs of the specimens compacted at higher densities (ρ_d = 1.6 g/cm^3 and ρ = 1.8 g/cm^3) were not influenced by the compaction density and bentonite quality.

Chapter 8

Infiltration characteristics of compacted bentonites

8.1 General

In this work, one-dimensional water infiltration studies of the bentonites compacted at four different densities were investigated. The influencing factors such as hydraulic head, plasticity of soils and compaction densities on infiltration rate and moisture content distribution through the compacted bentonites were investigated. The effect of water density on the water retention behavior, hydraulic conductivity function and water movement in the compacted bentonite were also studied in detail. The spatial and temporal variations of water content in the compacted bentonites were theoretically validated using unsaturated flow equation and the estimated hydraulic functions from the present study.

8.2 Numerical model

Water flow through unsaturated soils is often modelled (Zettl et al., 2011; Qi and Vanapalli, 2015; Bashir et al., 2016; Oh et al., 2016) using Richards' (1931) equation, which combines the Darcy's law with the mass conservation principle. Several software packages such as Hydrus – 1D and SEEP/W incorporate flow simulation in porous medium using Richards' equation. The flow behaviour was modelled in this study using Hydrus–1D software (Šimunek et al., 2013), which is a finite element program developed for simulating the transport of water in variably saturated porous media using Richards' equation. The Richards' equation for one dimensional horizontal flow is expressed as

$$\frac{\partial \theta(\psi)}{\partial t} = \frac{\partial}{\partial x}\left(k(\psi)\frac{\partial \psi}{\partial x} \right) \tag{8.1}$$

where θ is the volumetric water content, ψ is the matric suction, k is the hydraulic conductivity of the soil, x is a spatial variable, and t is the time. The optimized model parameters of the unsaturated hydraulic properties for all the studied bentonites were taken from Table 3.3 and Table 7.2.

One-dimensional model of the soil profile (38 mm diameter and 100 mm length) was considered in Hydrus – 1D with initial water content equal to the air-dry water content of the given bentonite. Convergence and stability of the model were verified by adjusting the nodal spacing and time-step increments. A constant-water content condition at the upper boundary and free-drainage condition at the lower boundary were considered in the model to simulate the laboratory experimental conditions. As the theoretical results from Hydrus – 1D and measured data were not in good agreement, another finite element software, SEEP/W (Geo-slope, 2012), was also used to validate the experimental data. A homogenous soil domain of 38 mm diameter and 100 mm long was considered (Fig. 8.1). The mesh dimensions were varied to test the solution convergence. The initial condition was activated by specifying the activation pore water pressure corresponding to the air-dry state of the bentonite specimen. A 'zero pressure head' condition at the upper boundary and 'free–flow' condition at the lower boundary were used. No flow boundary condition was used on the sides of the model as shown in Fig. 8.1. The temporal and spatial variation in the moisture content was obtained to theoretically study the transient flow behavior of water through the compacted bentonites.

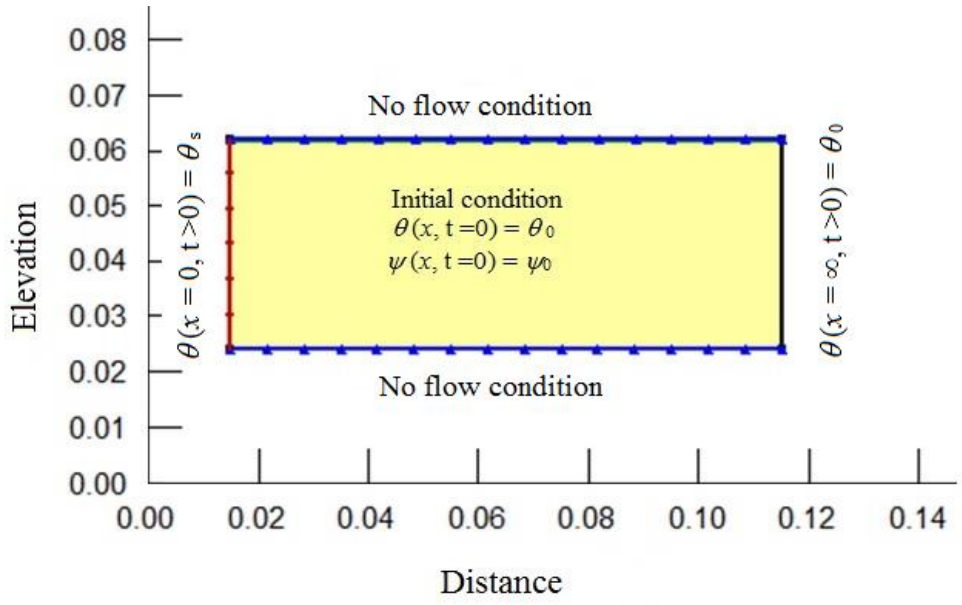

Fig 8.1 Soil column domain for unsaturated seepage modelling in SEEP/W (Geostudio)

8.3 Infiltration characteristics 1 D laboratory tests

The water content variation along the column length at different testing durations was obtained from the laboratory infiltration tests for different bentonites and at different compaction densities. As the transparent Perspex material was used as columns for infiltration tests, the moisture movement was clearly noticed with the changes in the specimen colour. The colour of the bentonite specimen changed to darker with water wetting and the colour varied from dark to light from the source to infinite boundary, respectively, as shown in Fig. 8.2 for B1 (ρ_d = 1.4 g/cm^3) at t = 120 h. Although the intensity of the colour is a measure of water content, the direct measurement of water content by slicing and oven-drying technique was considered in the analysis. The influence of compaction density and the plasticity were analyzed on the infiltration characteristics.

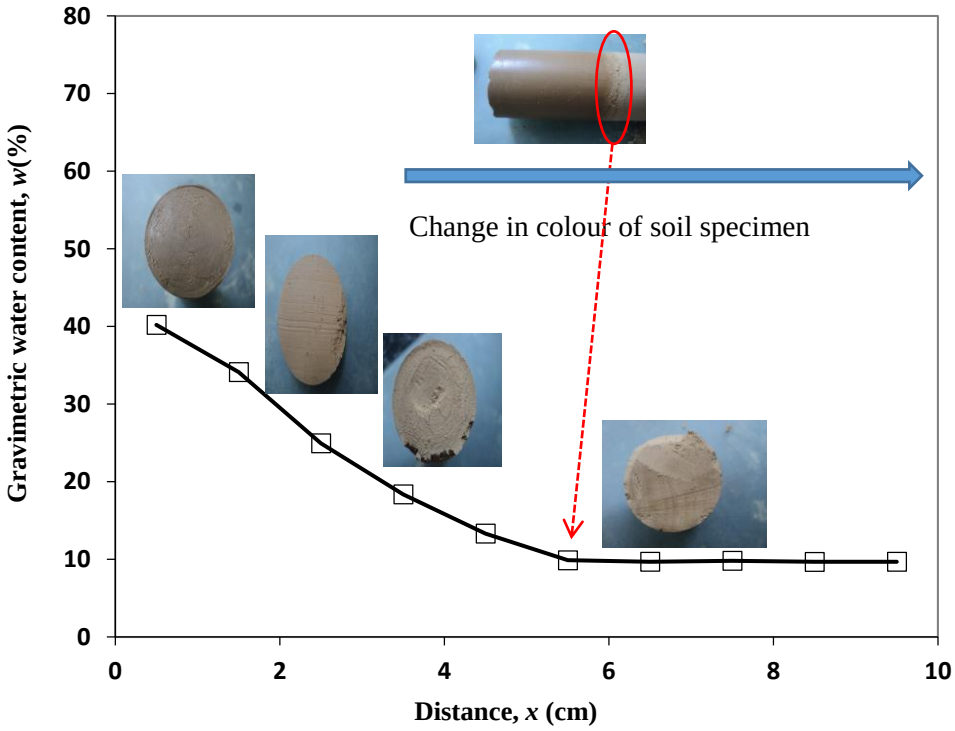

Fig. 8.2 Pictorial analysis of moisture distribution across B1 bentonite compacted at ρ_d= 1.4g/cm^3 and for time t =120 hours

The influence of compaction density on the spatial distribution of water content for B1 was presented in Fig. 8.3a–8.3c for different testing durations. The variation of gravimetric water content along the specimen length from the source boundary to infinite boundary was presented in these figures. The variation in moisture distribution along the specimen length for different bentonites was qualitatively similar as shown in Fig. 8.3-8.6. As the water moves towards the infinite boundary with time (t = 72 h and t =120 h), the transient water content variation spreads to wider distance as shown in Fig. 8.3b – 8.3c by keeping a constant water content near the source boundary. The water content from the source boundary to towards the infinite boundary (i.e., initial water content) varied significantly for lower compaction densities, but decreased with the increase in density. As the water infiltrates into the clay specimen, the surface cations and external surfaces get hydrated. Due to the presence of high suctions gradients between the

macropores and micropores (L1oret et al., 2003), the interlayer spacing gets hydrated. The formation of diffuse double layers (DDLs) around the clay plates eventually decreases the macropore volume (Burton et al., 2015). The specimens compacted at higher compaction densities contain less macropore volumes and thus limited formation of the DDLs was possible. The gravimetric water content at any distance from the source reservoir was highest for specimens compacted at lower compaction densities and least for the densely compacted specimens. The flow rate was slightly faster in the specimens compacted at lower densities due to availability of more flow paths.

The influence of bentonite plasticity on the spatial distribution of moisture content at t = 72 h and different compaction densities was shown in Fig. 8.7a – 8.7d. The moisture distribution profiles of different bentonites at the same compaction density were given in the same figure for understanding the plasticity effect. The effect of plasticity on the moisture distribution was marginal for any given density albeit the moisture content at any given distance from the source reservoir was higher for higher plasticity bentonite (i.e., in the order of B4 > B3 > B2 > B1). The results were similar at other testing durations, but only t = 72 h were presented here for brevity. As the water retention capacity of the bentonite increases with the increase in the plasticity, an increase in the moisture content at any distance was observed. The percentage variation of water content for different bentonites, at any given compaction density, varied only in the range of 3 – 6%. The same variation nearly existed throughout the specimen length at any given time. However, the moisture variation with plasticity was restricted by the volume constrained condition in the testing. Therefore, the moisture variation in volume restrained condition was insignificant unlike huge variations in gravimetric water contents observed for bentonites in unrestrained condition.

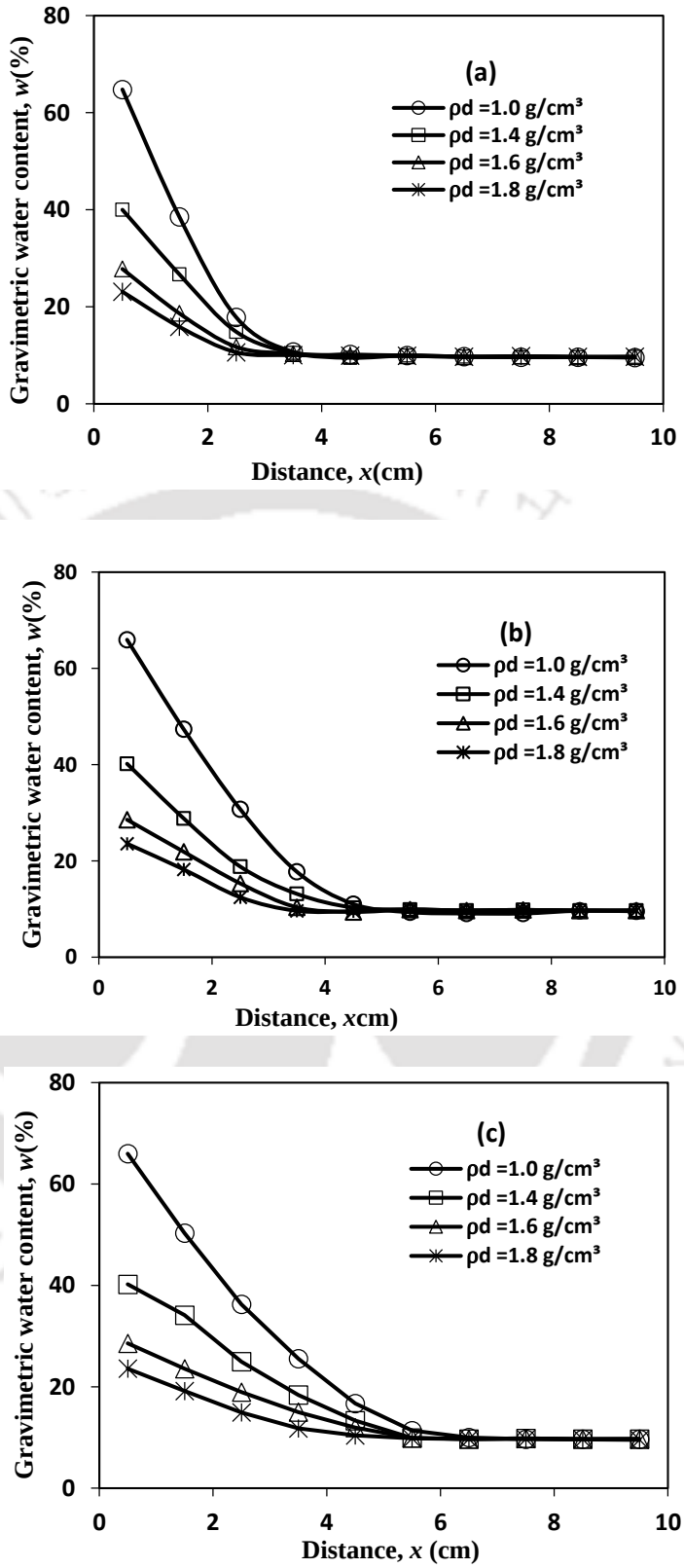

Fig. 8.3 Influence of density on the flow behavior (gravimetric water content) of B1 compacted at different densities for time (a) t = 24 hours (b) t = 72 hours (c) t = 120 hours

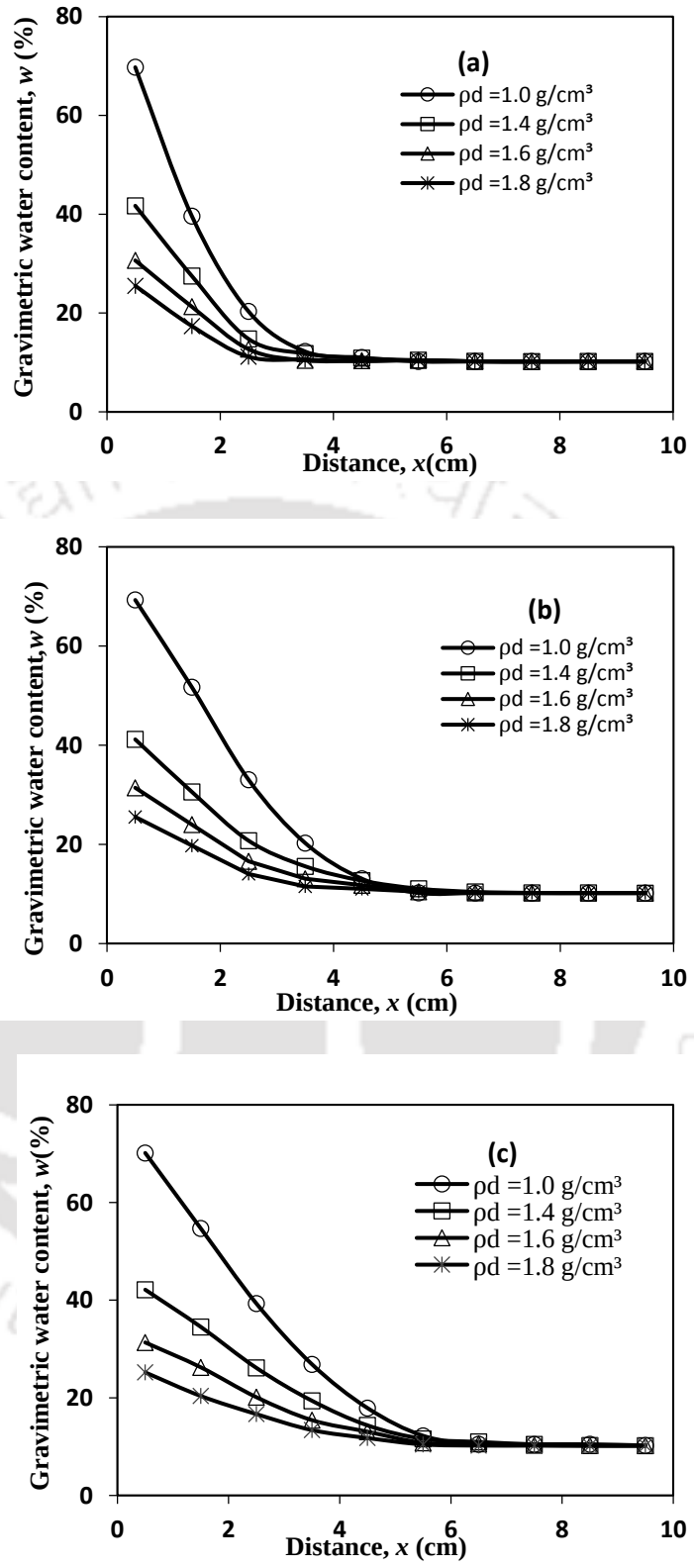

Fig. 8.4 Influence of density on the flow behaviour (gravimetric water content) of B2 compacted at different densities for time (a) t = 24 hours (b) t = 72 hours (c) t = 120 hours

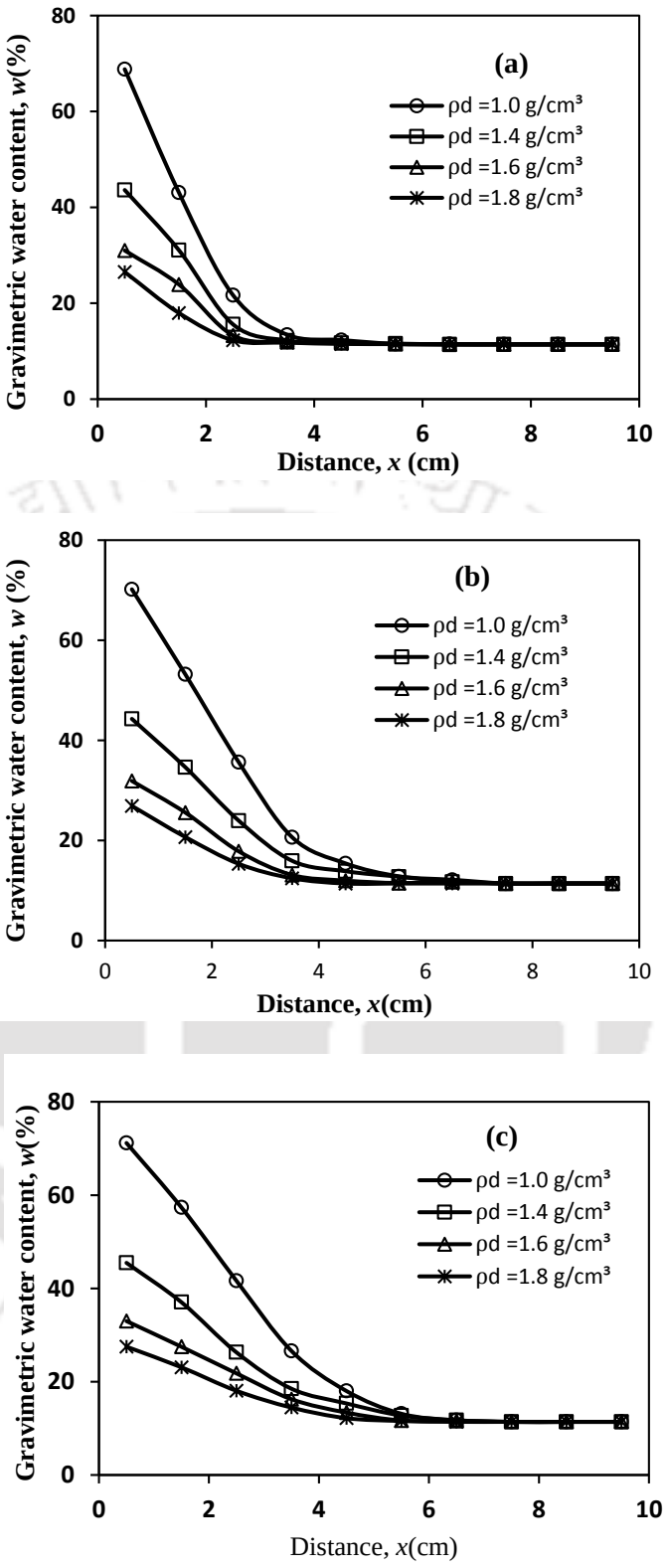

Fig. 8.5 Influence of density on the flow behaviour (gravimetric water content) of B3 compacted at different densities for time (a) t = 24 hours (b) t = 72 hours (c) t = 120 hours

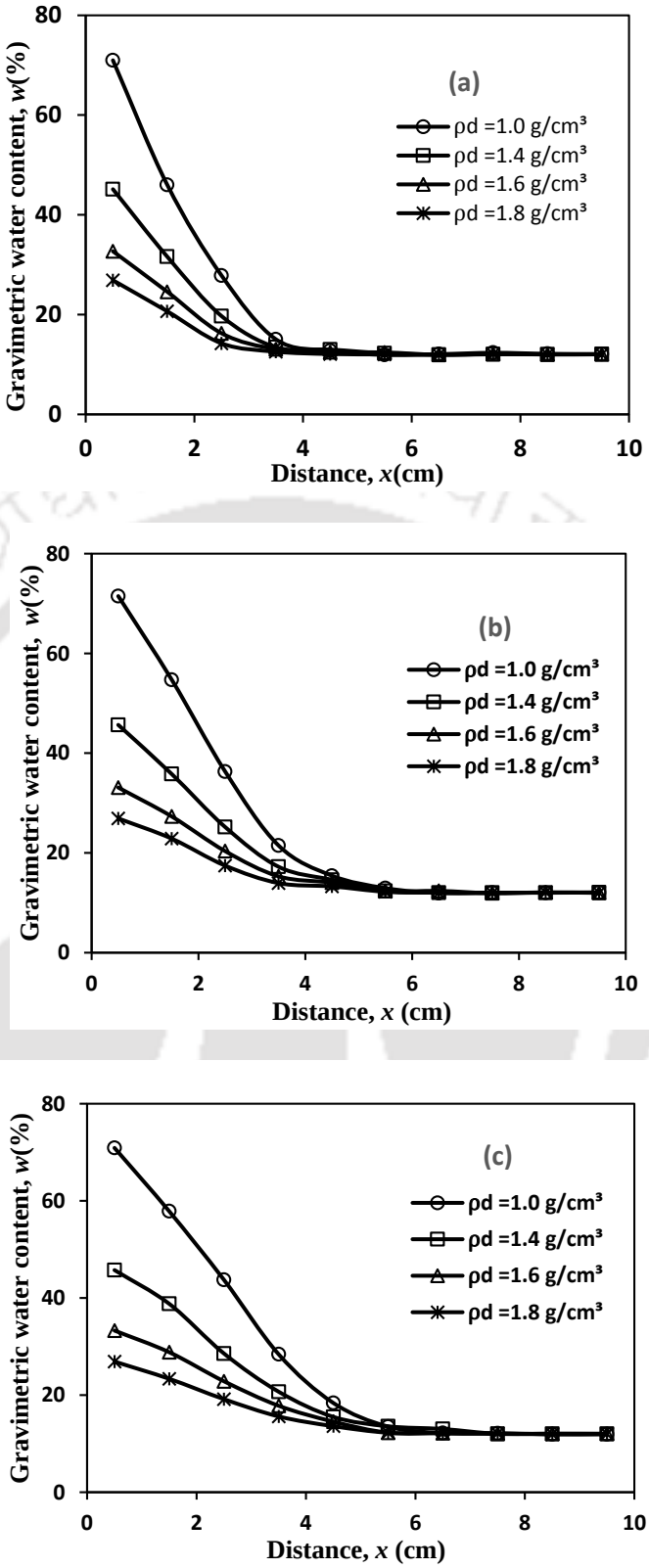

Fig. 8.6 Influence of density on the flow behaviour (gravimetric water content) of B4 compacted at different densities for time (a) t = 24 hours (b) t = 72 hours (c) t = 120 hours

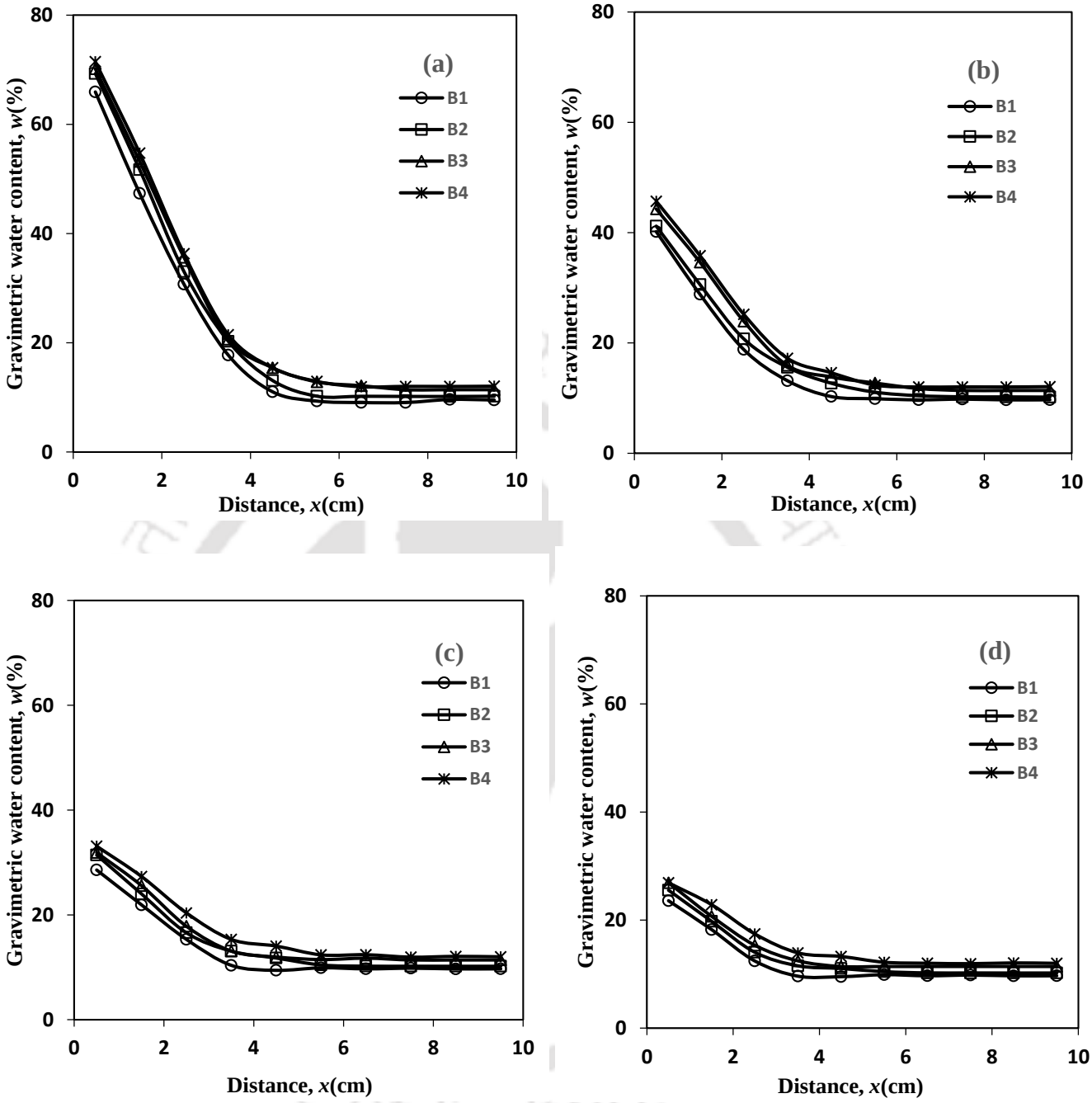

Fig. 8.7 Influence of plasticity on flow behaviour (Gravimetric water content) of bentonites compacted at different dry densities (a) 1.0g/cm^3 (b) 1.4 g/cm^3 (c) 1.6 g/cm^3 and (d) 1.8 g/cm^3 for time t =72*h*

8.4 Influence of water density on the hydraulic characteristics of bentonites

The water density may be different from the standard value (ρ_w = 1 g/cm^3) in bentonites due to the presence of strong electrochemical forces (Martin, 1960). The density of water is higher (1.5 g/cm^3 < $\rho_w \leq$ 1 g/cm^3) than the standard value when it exists in the form of adsorbed water around the clay platelets due to which the degree of saturation, at low matric suction, is often estimated from the gravimetric water contents to be higher than 100% in compacted bentonites (Villar and Lloret, 2008; Jacinto et al., 2012). As the water density depends on the water content (Martin, 1960) and compaction density (Villar and Lloret, 2008), the following four cases/possibilities were considered in representing the moisture distribution in terms of volumetric water content.

Case – 1: Water density was assumed to be constant and equal to the standard value, ρ_w = 1 g/cm^3.

Case – 2: Water density was estimated by adjusting the degree of saturation corresponds to the lowest measurable suction to 100%. The water density of B1 compacted at ρ_d = 1.6 g/cm^3 was found to be 1.08 g/cm^3 at ψ = 121 kPa. The estimated water density was used as a constant for different water contents.

Case – 3: A constant water density was used based on the relationship between water density and compaction density from the literature (Villar and Lloret, 2008) (Fig. 8.8a). The estimated water density was 1.13 g/cm^3 based on this relationship for B1 at ρ_d = 1.6 g/cm^3.

Case – 4: Water density was dynamically estimated by adjusting the degree of saturation, at each suction value, to 100% until the air entry suction value. The water density was assumed to be constant and equal to the standard value beyond the air-entry suction value as shown in Fig. 8.8b.

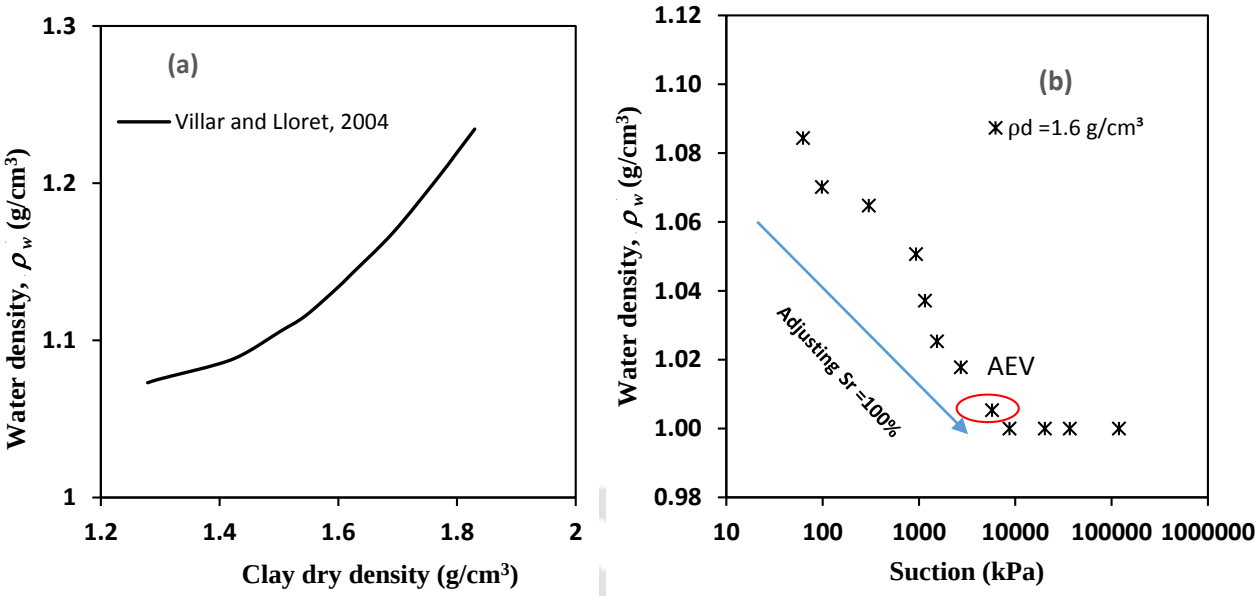

Fig. 8.8 Variation of water density with (a) clay density of bentonite (After Villar and Lloret, 2004) (b) suction in B1 compacted at 1.6 g/cm^3, designated in this study as ρ_w= varying with suction

The variation in volumetric water content with distance from the source reservoir was shown in Fig. 8.9 by considering the aforementioned four different cases in estimating the water density. The maximum variation in the volumetric water content was noticed close to the source reservoir as the water density variation in the fully saturated state was significantly high (Fig. 8.8b). The $\theta(x)$ was not significantly affected by the variation in water density thus not important in moisture distribution studies in bentonites.

The volumetric water content distribution with distance for the analysis was, therefore, considered by assuming ρ_w = 1 g/cm^3. The measured $\theta(x)$ data for B1 at different compaction densities crisscrossed (Fig. 8.10a – 8.10c) by exhibiting higher water content near the source and lower water content farther away from the source for specimens compacted at lower densities compared to the densely compacted specimens. As the volumetric water content is the measure of volume of water to the total volume of soil,

more water is present at the air-dry specimen compacted at higher density for a constant gravimetric water content compared to the loosely compacted specimens. Water infiltration increased θ in proportion to the available void space (i.e., macrovolume) which was qualitatively similar to Fig. 8.3 due to Eq. 7.4. The criss-cross point shifted away from the source boundary with the water movement in the specimen. The crisscrossed behaviour in $\theta(x)$ was qualitatively similar when different water density variations were considered and presented from Fig. 8.11-8.13. The $\theta(x)$ data were qualitatively similar for the other bentonites (not shown here).

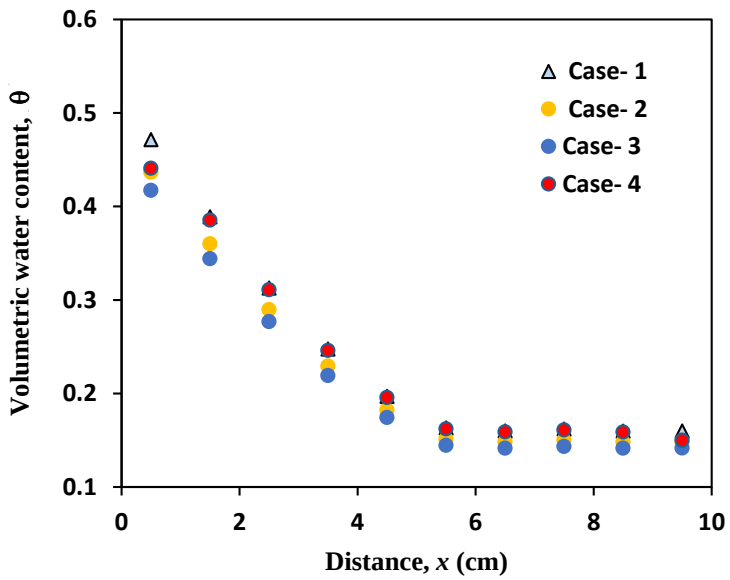

Fig. 8.9 Effect of water density on water movement in B1 bentonite compacted at dry density, ρ_d= 1.6 g/cm^3 for time, t= 120 hours

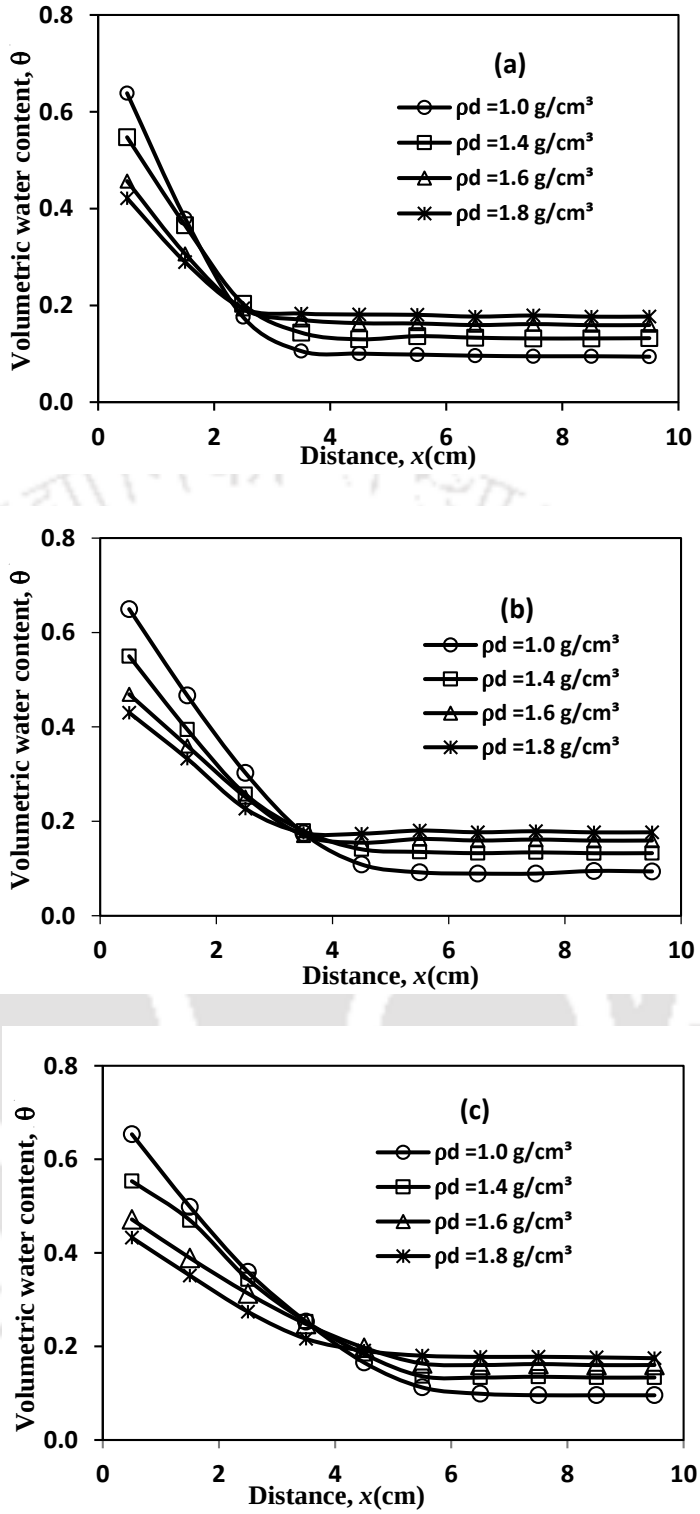

Fig 8.10 Influence of density on the flow behaviour (volumetric water content) of B1 compacted at different densities for time (a) t = 24 hours (b) t = 72 hours (c) t = 120 hours

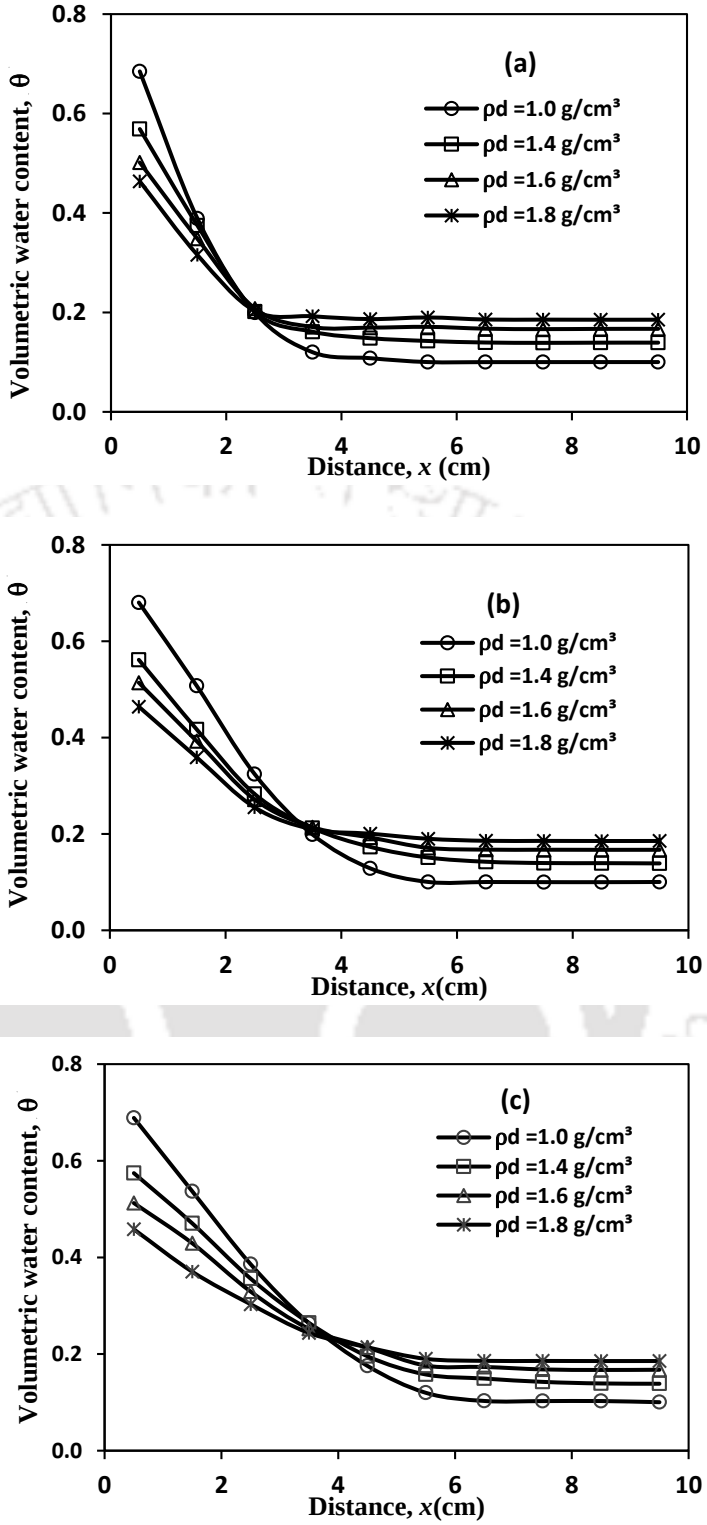

Fig. 8.11 Influence of density on the flow behaviour (volumetric water content) of B2 compacted at different densities for time (a) t = 24 hours (b) t = 72 hours (c) t = 120 hours

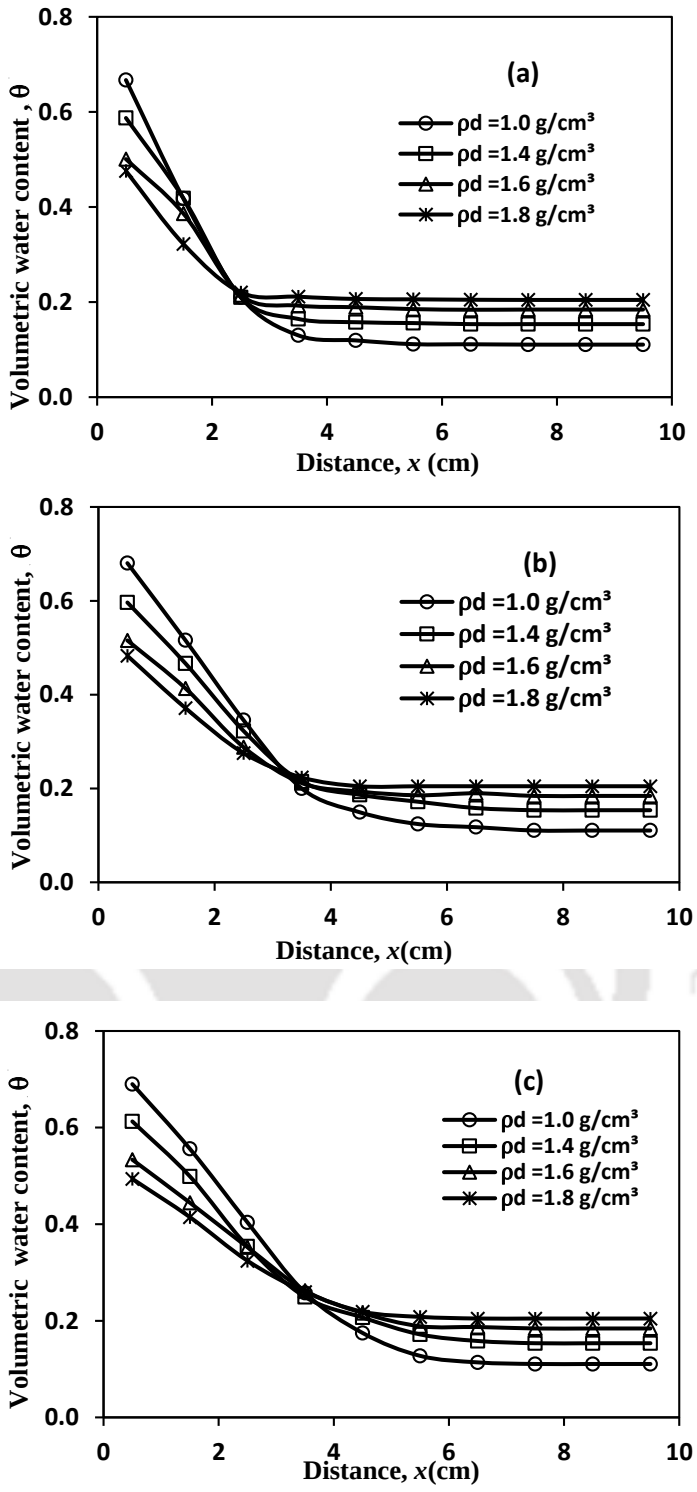

Fig. 8.12 Influence of density on the flow behaviour (volumetric water content) of B3 compacted at different densities for time (a) t = 24 hours (b) t = 72 hours (c) t = 120 hours

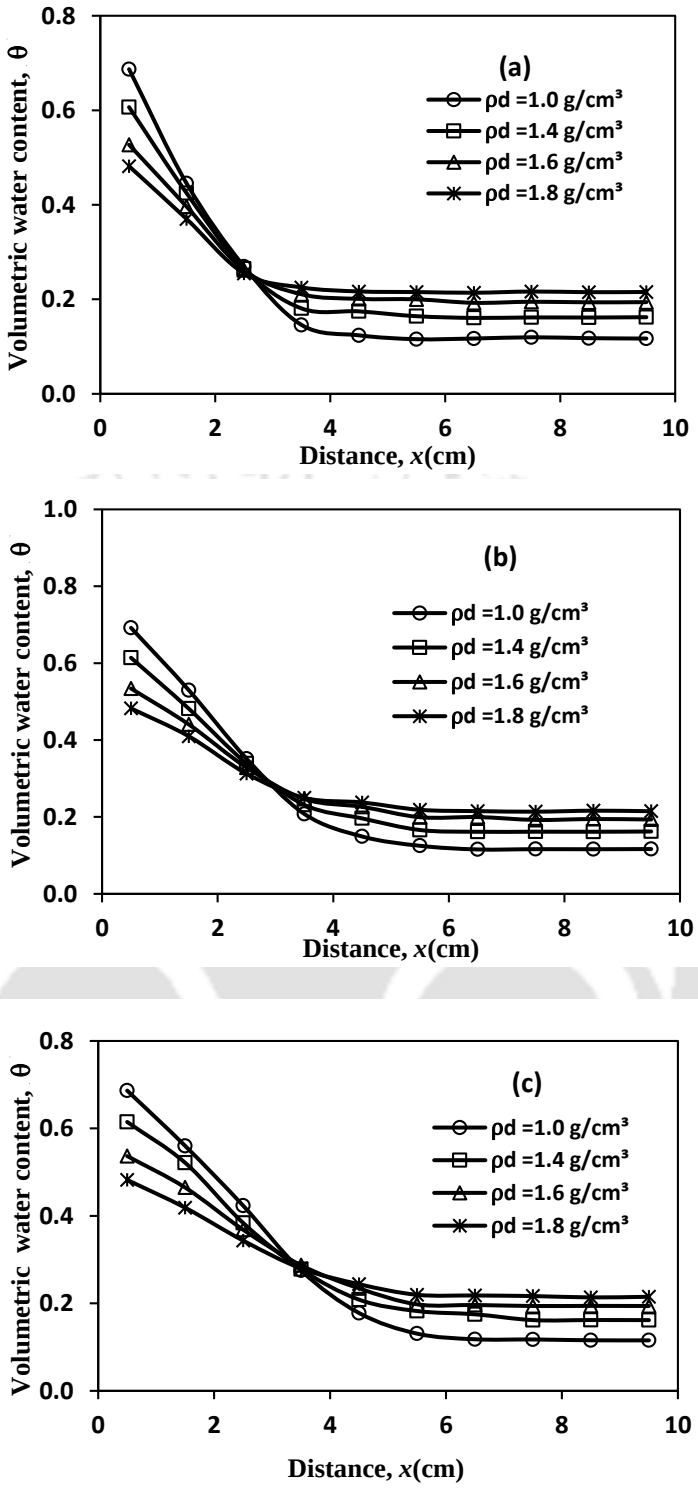

Fig. 8.13 Influence of density on the flow behaviour (volumetric water content) of B4 compacted at different densities for time (a) t = 24 hours (b) t = 72 hours (c) t = 120 hours

8.5 Theoretical Validation

Theoretical model was validated on the measured data of $\theta(x)$ using Hydrus–1D and SEEP/W. Two well-defined hydraulic functions viz. SWCC in terms of θ, $SWCC_{\theta}$, and hydraulic conductivity function are required as input to solve the Richards' equation. The influences of water density on the estimation of $SWCC_{\theta}$ was studied as the adopted experimental procedures yielded SWCC data in terms of gravimetric water content, $SWCC_{w}$. The estimated $SWCC_{SR}$ data (i.e., SWCC data in terms of degree of saturation) for B1 compacted at 1.6 g/cm^3 by considering different water density variations (Fig. 8.9) were shown in Fig. 8.14a. The estimated degree of saturation is 120% at lowest measureable suction by osmotic technique when the standard value for water density was used. The estimated S_r by utilizing the water density as 1.13 g/cm^3 based on $\rho_w - \rho_d$ relationship (Villar and Lioret, 2008) was lower than 100% near saturation. The estimated $SWCC_{\theta}$ data based on Fig. 8.14a and fitted theoretical lines by RETC software (Šimunek et al., 2013) showed a slight variation in θ in the saturation zone. However, insignificant difference was found in the predicted hydraulic conductivity functions (Fig. 8.14c) by different approaches for water density approximation.

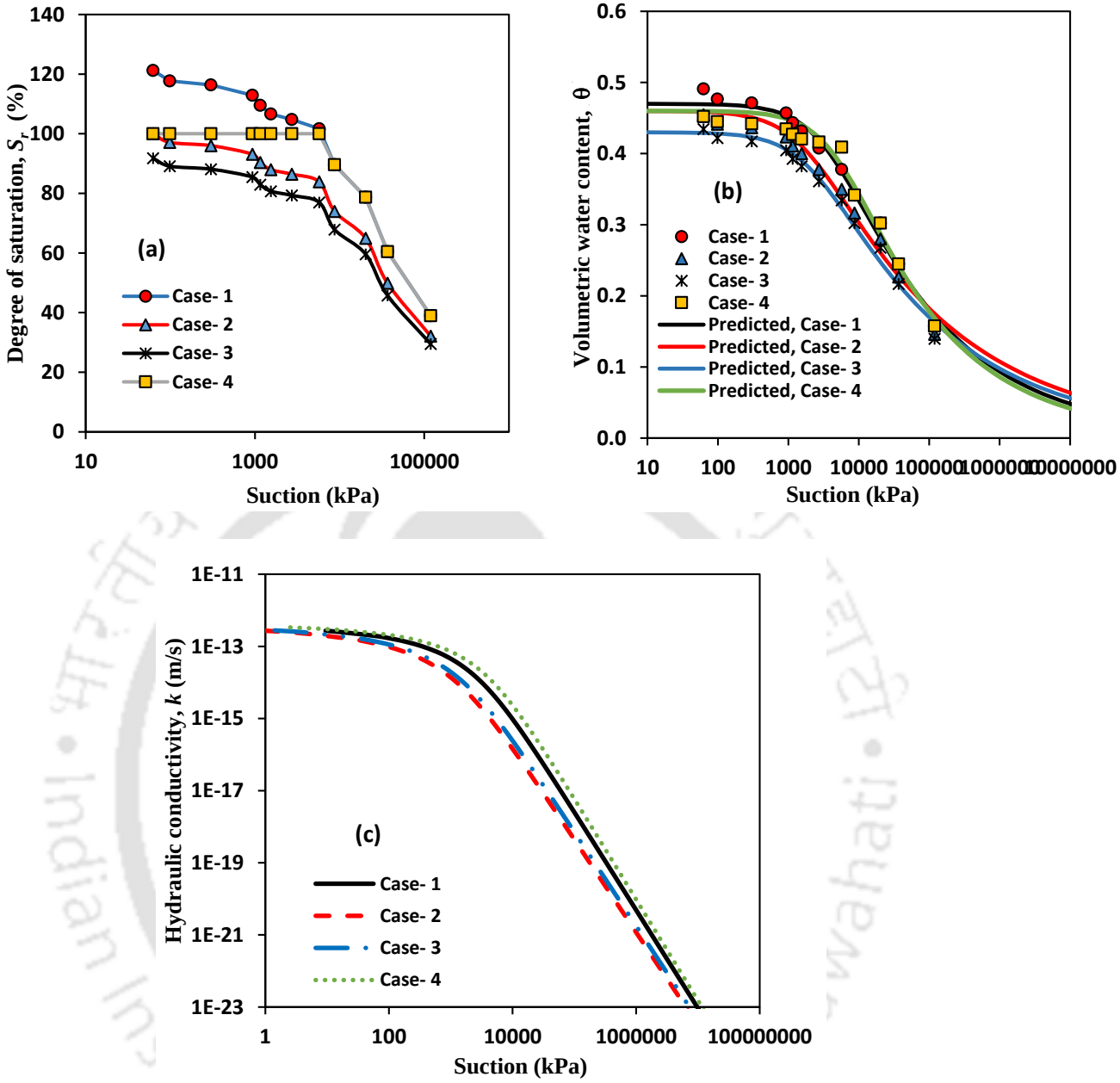

Fig. 8.14 Effect of water density on (a) SWCC$_\theta$ (b) SWCC$_{SR}$ (c) hydraulic conductivity of B1 bentonite compacted at dry density 1.6 g/cm^3

The influence of water density on the theoretical water content distribution was studied for B1 (ρ_d = 1.6 g/cm^3 and t = 120 *h*) in Fig. 8.15. The variation in the measured $\theta(x)$ data due to water density approximation was also shown in the same figure. The variation in the theoretical soil moisture profile was insignificant due to different assumptions made for the water density similar to the experimental observations.

Therefore, the soil hydraulic properties based on the standard value for water density were (Table 8.1) considered for the validation experiments.

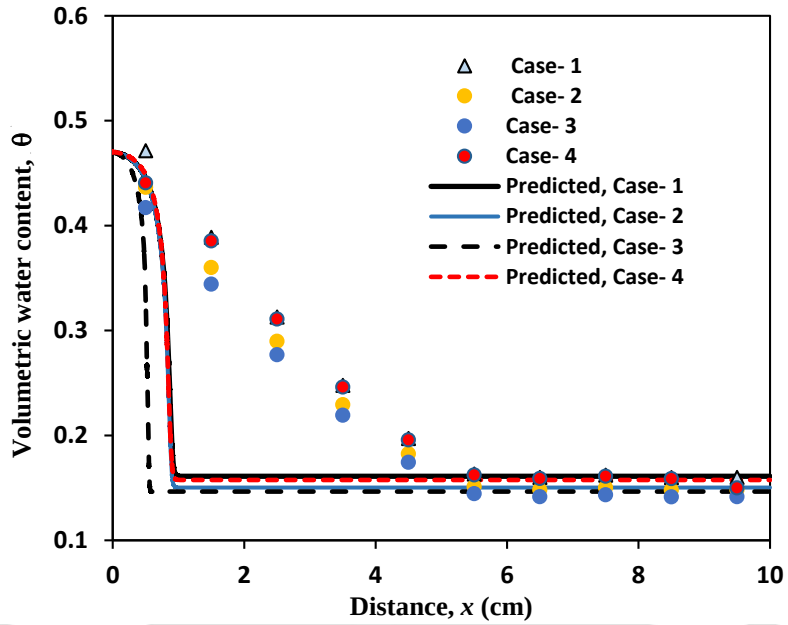

Fig. 8.15 Effect of water density on water movement in B1 bentonite compacted at dry density, ρ_d= 1.6 g/cm^3 for time, t= 120 hours

Table 8.1 Optimized vG model parameters obtained after fitting SWCC θ of bentonite B1 compacted at 1.6 g/cm^3

Soil type	Water density, ρ_w (g/cm^3)	a (kPa^{-1})	n	R^2
Bentonite B1 compacted at ρ_d= 1.6 g/cm^3	1.0	0.00030	1.29	0.988
	1.08	0.00024	1.29	0.979
	1.13	0.00046	1.24	0.984
	Varies with suction	0.00019	1.32	0.969

The numerical solution of Richards' equation by Hydrus – 1D and SEEP/W was compared for B3 compacted at 1.4 g/cm^3 along with the measured spatial distribution of moisture content for different testing durations in Fig. 8.16. Theoretically predicted

results by Hydrus – 1D and SEEP/W were in good agreement with each other and, therefore, only the results from Hydrus – 1D were shown for validation. The validation of theoretical solution with the measured transient moisture distribution in different compacted specimens showed (Fig. 8.17 – 8.20) that the theory severely under predicted the water movement in bentonite specimens for all the different compaction densities. The possible reasons for overly underestimated results by the numerical model were investigated by additional experiments that were discussed in the following section.

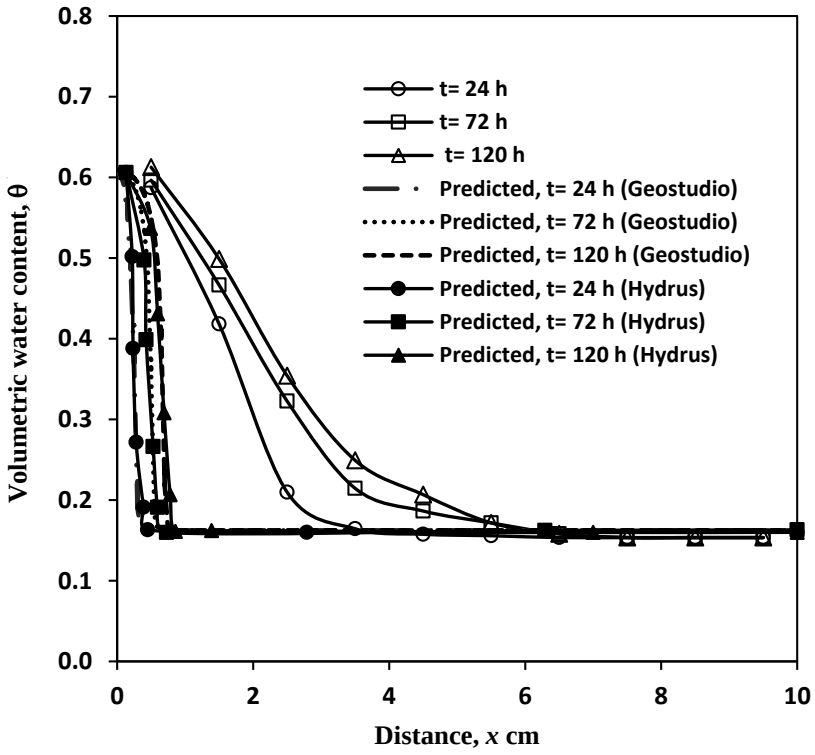

Fig 8.16 Validation of the flow behaviour of B3 bentonite compacted at dry density, ρ_d =1.4 g/cm^3 using Hydrus and SEEP/W

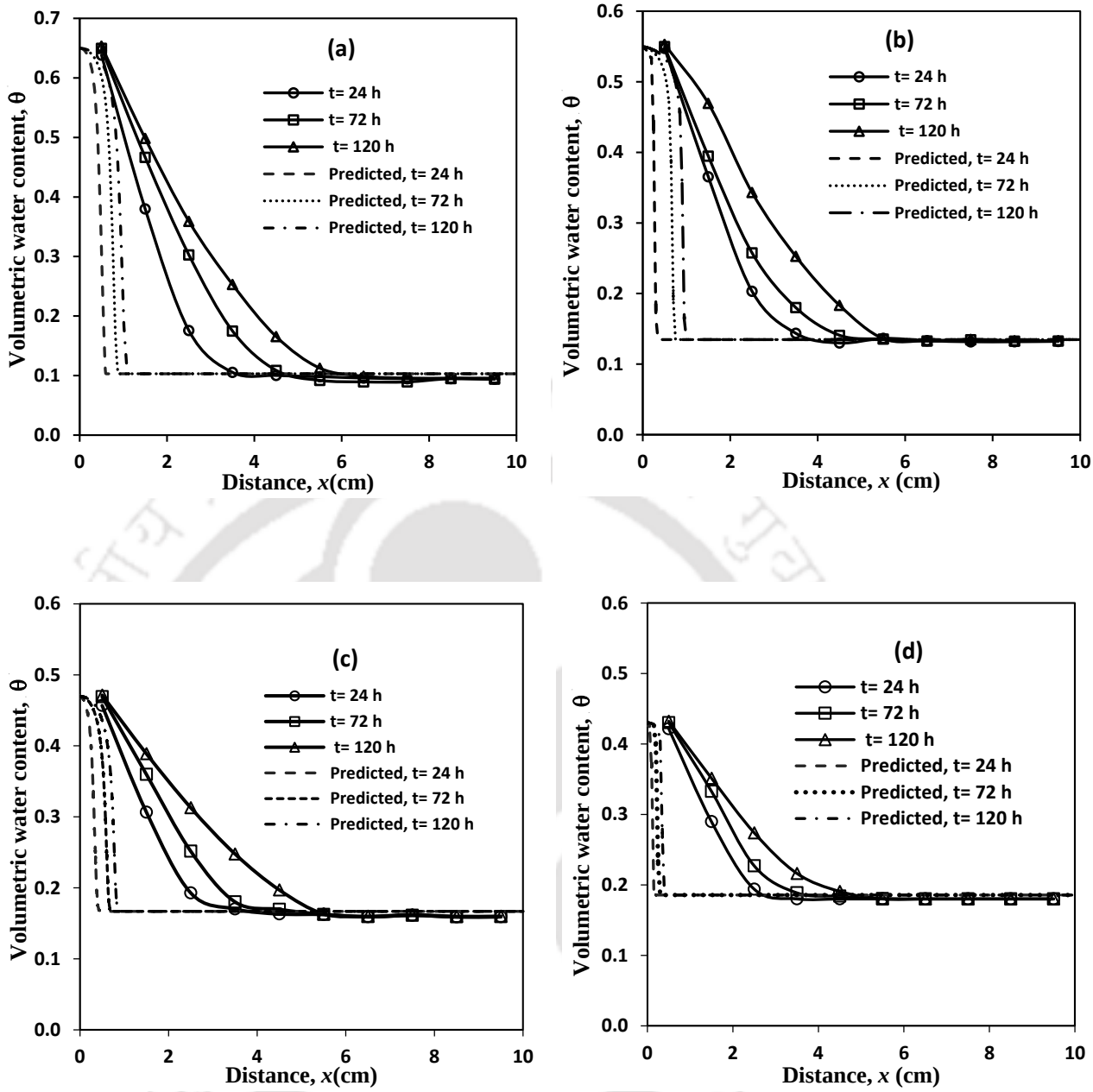

Fig 8.17 Comparison of theoretical and experimental water movement of B1 compacted at (a) ρ_d =1.0 g/cm^3 (b) ρ_d =1.4 g/cm^3 (c) ρ_d =1.6 g/cm^3 (d) ρ_d =1.8 g/cm^3

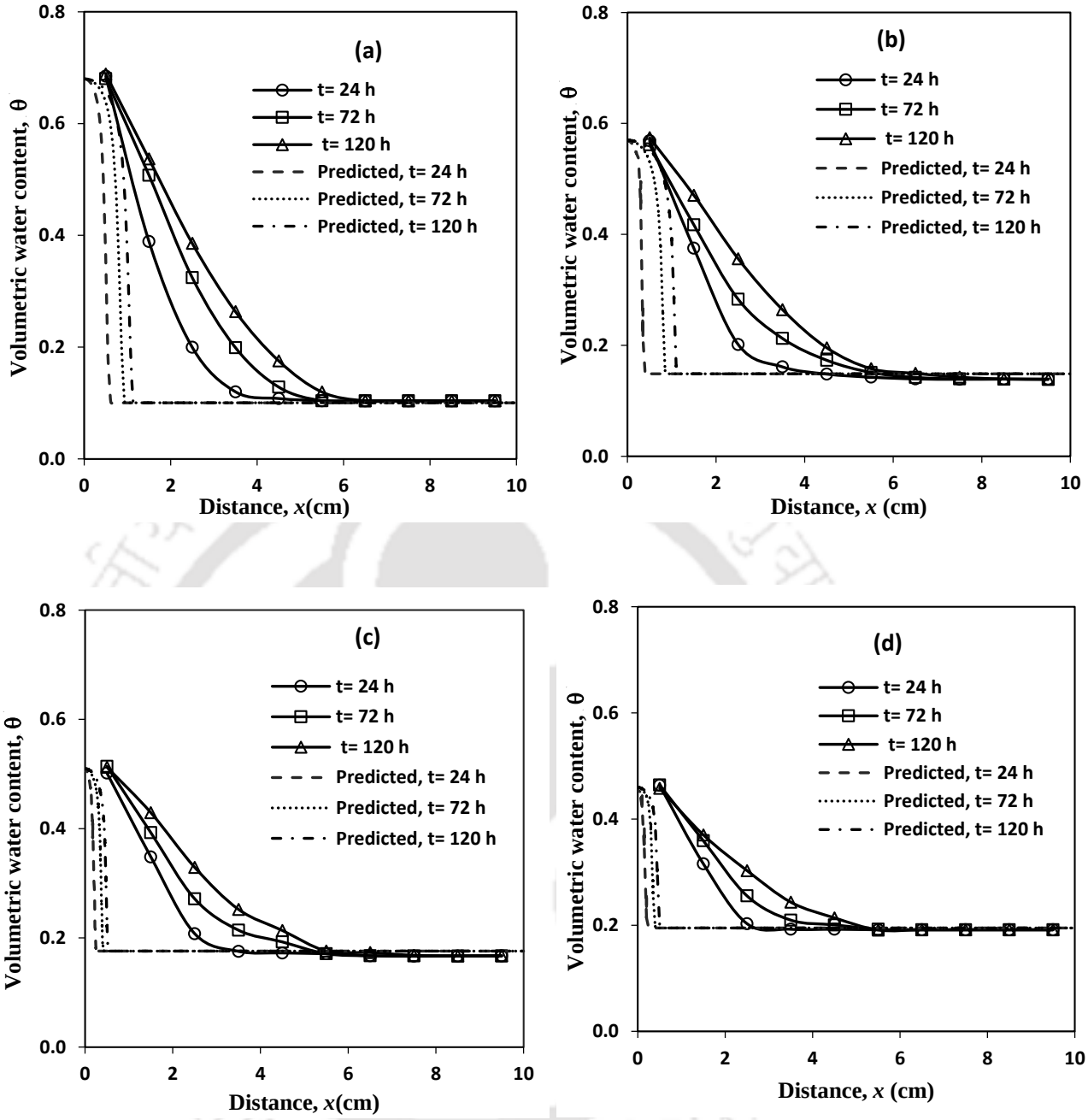

Fig 8.18 Comparison of theoretical and experimental water movement of B2 compacted at (a) ρ_d =1.0 g/cm^3 (b) ρ_d =1.4 g/cm^3 (c) ρ_d =1.6 g/cm^3 (d) ρ_d =1.8 g/cm^3

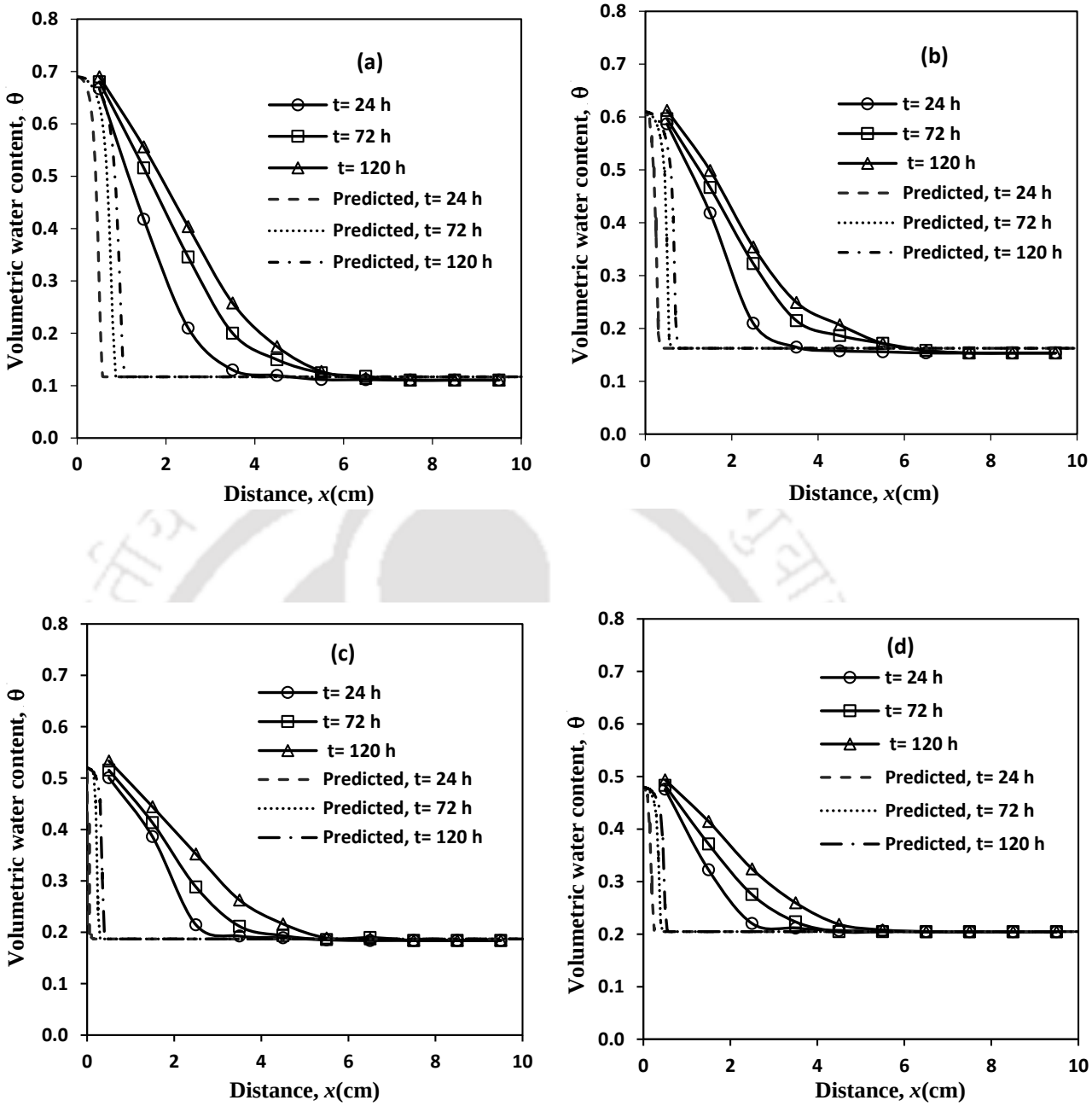

Fig 8.19 Comparison of theoretical and experimental water movement of B3 compacted at (a) ρ_d =1.0 g/cm^3 (b) ρ_d =1.4 g/cm^3 (c) ρ_d =1.6 g/cm^3 (d) ρ_d =1.8 g/cm^3

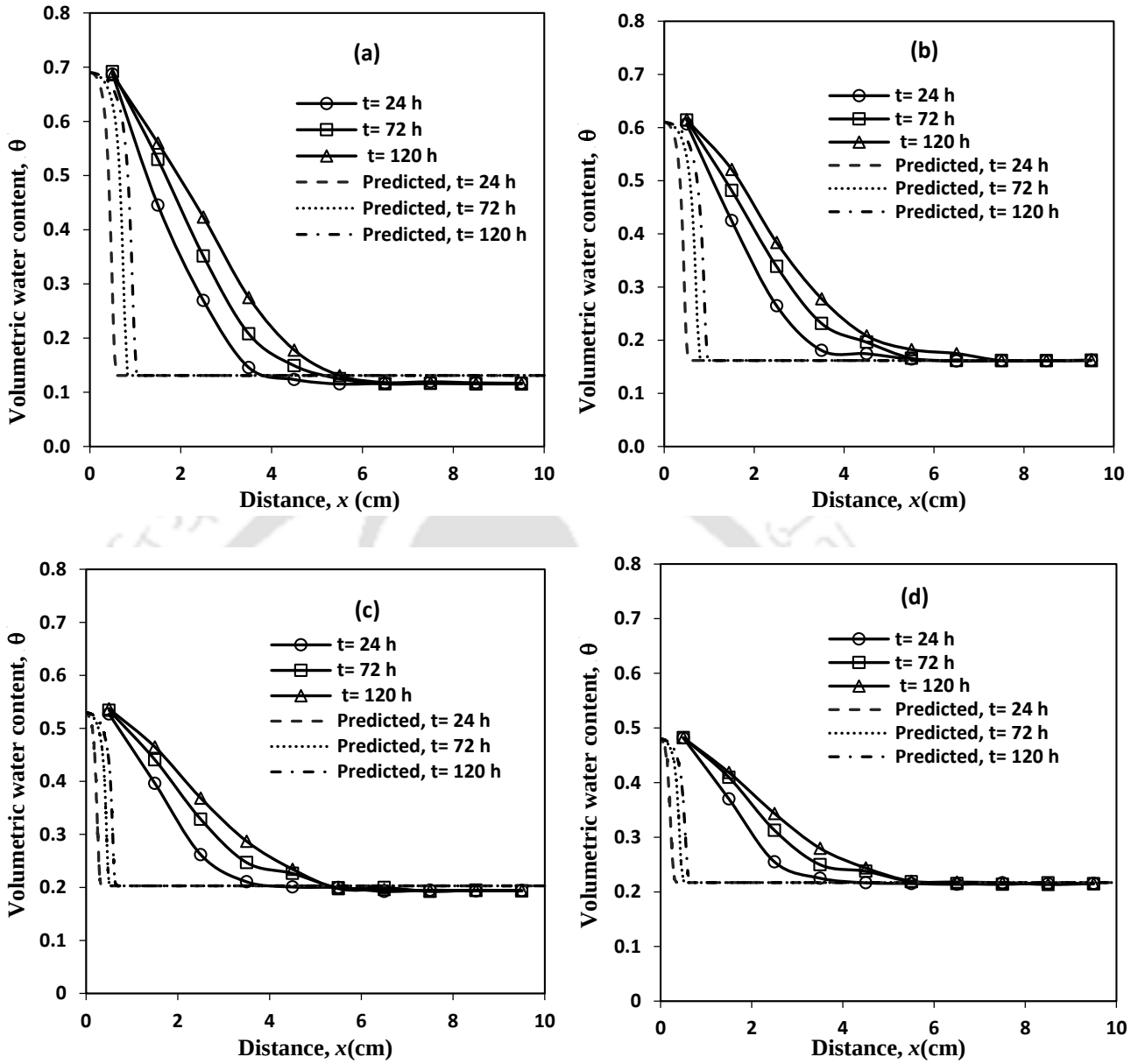

Fig 8.20 Comparison of theoretical and experimental water movement of B4 compacted at (a) ρ_d = 1.0 g/cm^3 (b) ρ_d = 1.4 g/cm^3 (c) ρ_d = 1.6 g/cm^3 (d) ρ_d = 1.8 g/cm^3

8.6 Discussion

Validity of 1D assumption was examined by observing the moisture distribution in the radial direction from centre of the specimen towards the periphery at any given distance from the source boundary. The B4 specimen compacted at ρ_d = 1 g/cm^3 was subjected to water infiltration for a duration of t = 16 h (Fig. 8.22a) and B3 compacted at ρ_d= 1.4 g/cm^3 for time t= 24 h (Fig. 8.22b) . The specimen was extruded carefully and cut into 1 cm thick slices. The specimen at the core part was separated from the periphery with thin blade as shown in Fig. 8.21 for the water content determination separately. The water content data at the core and periphery were same at any given distance from the source boundary indicating a uniform distribution of the water in the radial direction. The 1D flow approximation was, therefore, valid for the numerical analysis.

Fig. 8.21 Water content variation across core and periphery of the soil slice

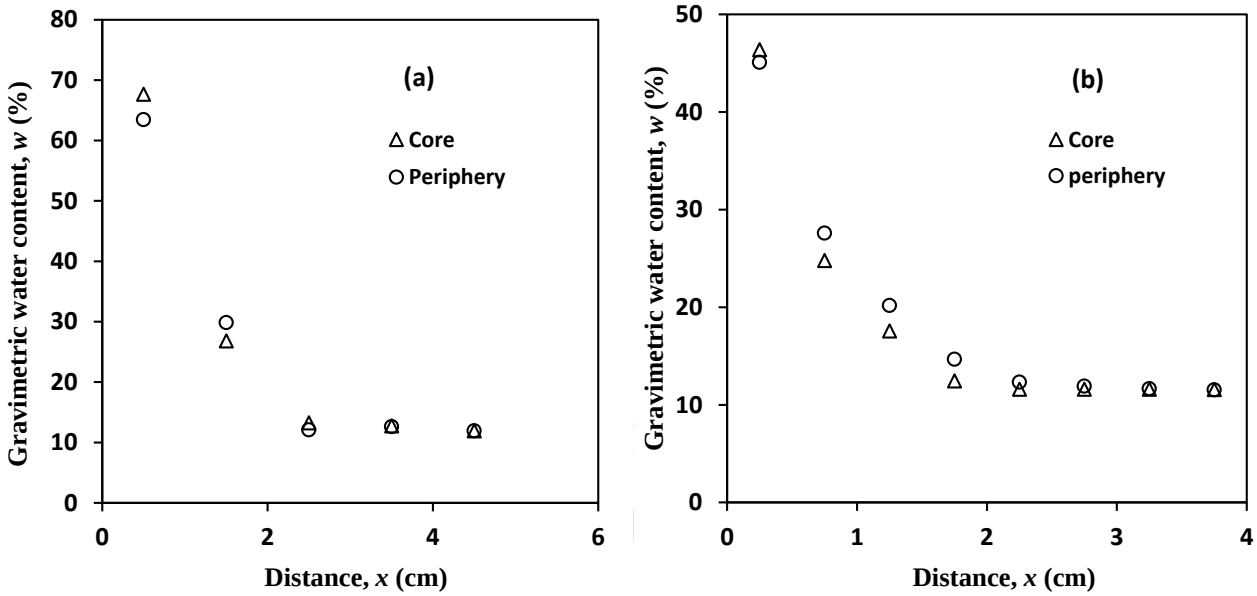

Fig. 8.22 Water content determination across the cross-sectional area of (a) B4 compacted at ρ_d= 1 g/cm^3 for time, t= 16 hours (b) B3 compacted at ρ_d= 1.4 g/cm^3 for time, t= 24 hours

Further, the effect of specimen size on the flow characteristics was studied. An infiltration test on B3 bentonite compacted at 1.4 g/cm^3 was conducted using 60 mm diameter and compared the moisture distribution data with 38 mm diameter at different testing durations as shown in Fig. 8.23. The infiltration rate in the specimen with larger diameter was slower at the beginning (i.e., t = 1 day), but the moisture distribution profiles converged for both the specimens with passage of time (i.e., t = 5 days). The moisture distribution in specimen was expected to be independent of the specimen size at any given time due to one–dimensional nature of the flow (as confirmed from Fig. 8.22) similar to the theoretical results in Fig. 8.23. The deviation in the experimental data at the beginning may be attributed to the inhomogeneity at the source boundary due to the presence of porous disc. Therefore, the 1D flow assumption is valid in the studied tests.

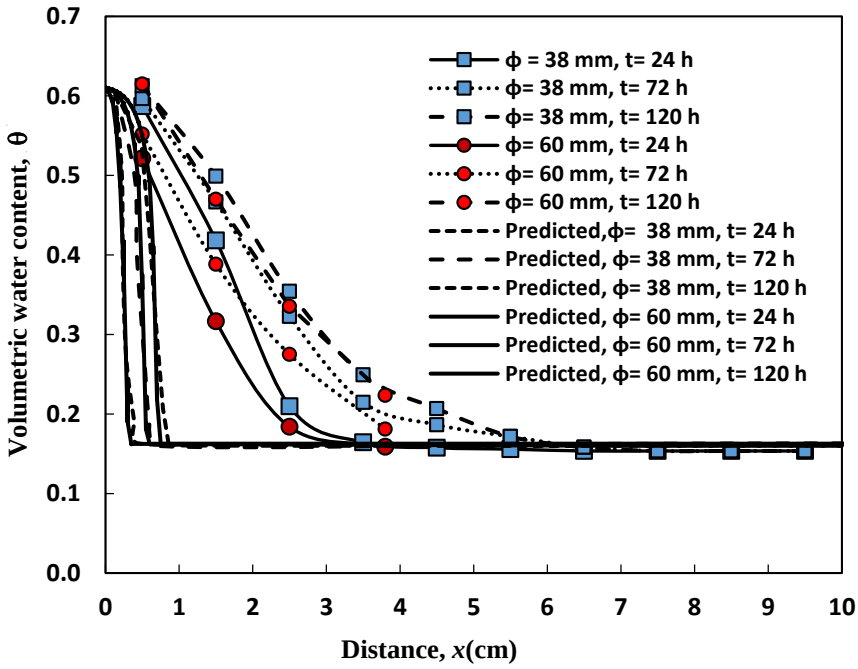

Fig. 8.23 Influence of column diameter on water movement in B3 compacted at dry density, $\rho_{d=}$ 1.4g/cm^3 for (a) t= 24 hours (b) t= 72 hours (c) t= 120 hours

Influence of hydraulic head on the infiltration characteristics of the compacted bentonite specimen was studied to understand the deviation between the experimental observations and theory. The hydraulic head was increased 1 m from 0.1 m in infiltration tests on B3 bentonite compacted at 1.4 g/cm^3. The moisture distribution data for different time durations using two different hydraulic heads were compared in Fig. 8.24. Theoretical moisture distribution profiles for the experimental conditions were also shown in the same figure. An insignificant difference was found in the measured and theoretical data due to increase in the hydraulic head. Therefore, the influence of hydraulic head on the infiltration characteristics in compacted bentonites is not present due to low hydraulic conductivity at any given water content. The flow appeared to be diffusion dominant as the hydraulic conductivity was less than 10^{-11} m/s for different bentonites and compaction densities studied in this work (Table 3.3). Therefore, the flow rate based on the hydraulic gradient was severely underestimated.

Moreover, the statistical hydraulic conductivity model by Mualem (1976a) idealizes the void spaces at each cross-section to be consisting of circular pores of different size classes and considers the probability of water-filled pores of different sizes from each section are connected. Further, the Hagen - Poiseuille equation is considered to relate the flow velocity with the square of the pore radius. Changes to the micropore/macropore volume due to hydration of inter-layer clay surfaces, which results in alterations of the pore radius, is not accounted in the theoretical model. The applicability of the statistical model by considering constant pore radii during wetting is, therefore, questionable. The hydration effects in bentonites due to the presence of electrochemical forces are significant, but are ignored in the flow equations. Some past studies (Fredlund et al., 1994; Meerdink et al., 1996; Garnier et al., 1997; Chiu and Shackelford, 1998; Rahimi et al., 2015) reveal that the statistical models underestimated the hydraulic conductivity functions of clays from the SWCC data and such models are not applicable for soils with saturated hydraulic conductivity, $k_s \leq 10^{-7}$ m/s.

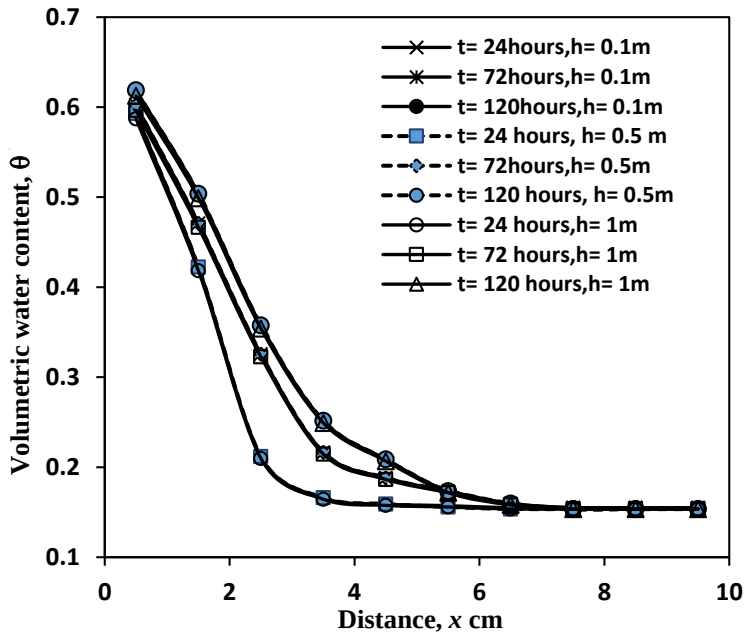

Fig. 8.24 Influence of hydraulic head on flow behaviour of B3 bentonite compacted at dry density, ρ_d= 1.4 g/cm^3

The water migration mechanism in compacted bentonites, therefore, requires a wide attention (Chao et al., 2014) and a detailed study due to various design applications in foundations, nuclear waste repositories, and landfills. A hydraulic conductivity function for compacted bentonites in restrained conditions is required to be developed similar to the recently developed model for unrestrained conditions (Zhang et al., 2016). The electrochemical forces are required to be included for understanding the wetting mechanism in compacted clays.

8.7 Concluding Remarks

The transient moisture distribution data of various bentonites compacted at different densities showed that the bentonite plasticity is not important for restricting the water movement in various applications. Low quality bentonite (B1) compacted at higher density (ρ_d = 1.8 g/cm^3) is able to restrict the water movement as efficiently as the high quality bentonite (B4) compacted at the same density. However, the mechanical stresses generated in the specimen due to water hydration are also important, other than the water movement, in the design of HLNWRs. In such applications, the bentonite plasticity may be equally important to the compaction density.

The widely used Richards' model was validated on the experimental measurements using independently estimated hydraulic properties of the compacted bentonites. The hydraulic model severely underpredicted the water migration, which was found to be diffusion dominant due to low hydraulic conductivities of the compacted bentonites. Further, the assumption of constant pore radius during wetting by the commonly used statistical models for hydraulic conductivity function limit the application for compacted bentonites as the changes in the micro and macro void volumes during the hydration are not accounted. The influence of water density approximations on the transient moisture profile estimation in terms of volumetric water content and theoretical prediction was not

significant for the studied conditions albeit the $SWCC_{SR}$ was severely affected. The approximation of ρ_w = 1 g/cm^3 can be used for the water movement studies.

Chapter 9
General Conclusions

9.1 General

The major conclusions drawn from the analysis in previous contributing chapters were summarized in this chapter. The conclusions from this study were given separately for each chapter. The future scope of this work based on the gaps in the present work was also provided at the end of this chapter.

9.2 Drying SWCC data in unrestrained condition

- Clod technique using non- polar liquids for volume measurement is advantageous for establishing VSC characteristics over other studied techniques. The estimated $SWCC_{SR}$ by combining the measured $SWCC_w$ and clod-VSC data were accurate due to the virtues of the clod technique.

9.3 Wetting SWCC of Bentonites in Volume Restrained Condition

- The vapor sorption behavior of powdered and compacted bentonite specimens during wetting process was different due to the difference in the wetting mechanisms such as monolayer and bilayer hydration of surface cations.
- The sorption rate and equilibrium water content (w_{eq}) were influenced by the bentonite plasticity, compaction density and relative humidity.
- The proposed linearization approach using rectangular hyperbola technique accurately predicted the equilibrium water content of the compacted bentonites based on the initial trend of sorption kinetic data.

9.4 Hysteretic Water Retention Behaviour of Bentonites

- A theoretical method based on Pham et al. (2003) model can be advantageously used for predicting the main wetting data from the easily available initial drying data of various bentonites.

9.5 Wetting hydraulic functions

- The SWCC $_{\theta}$ representation showed a crisscross trend at different suction values as the effect of density is prominent at lower suctions and pore-size effects at higher suction range.
- The effect of compaction density observed in predicted HCF data using vG-Mualem statistical model depicted a crisscross behavior, similar to the unsaturated permeability behavior of texturally dissimilar soils. However, HCF is not influenced by quality of bentonites and compaction density, $\rho_d > 1.6$ g/cm^3.

9.6 Infiltration characteristics of compacted bentonites

- The quality of bentonite does not influence the water movement/ distribution in compacted bentonites, compacted at $\rho_d \geq 1.6$ g/cm^3. However, the developed mechanical stresses at higher density might significantly influence the buffer/ backfill design in HLNW repositories.
- The widely used Richards' equation for unsaturated flow behavior under-predicted the water movement through compacted bentonites as it ignores the hydration induced volume changes and altering electrochemical interactions.
- The effect of water density was not significant on moisture distribution in terms of volumetric water content and theoretical prediction. It was suggested that water density, $\rho_w = 1$ g/cm^3 can be used for flow computations. The water

migration mechanism in compacted bentonites, therefore, requires a wide attention and a detailed study due to various design applications in foundations, nuclear waste repositories, and landfills.

9.7 Scope for future work

1. To develop an experimental program for volume measurement during wetting and drying in unrestrained condition for compacted clays.
2. A hydraulic conductivity function for compacted bentonites in restrained conditions is required to be developed similar to the recently developed model for unrestrained conditions considering changes in the pore-structure during the wetting process.
3. The electrochemical forces are required to be included in Richards' equation for understanding the wetting mechanism in compacted clays.
4. The influence of water density on the hydraulic characteristics of bentonites need to be studied in detail.

References

1. Agus, S. S., & Schanz, T. (2005). Comparison of four methods for measuring total suction. Vadose Zone Journal, 4(4), 1087-1095.
2. Akin, I. D., & Likos, W. J. (2016). Single-Point and Multi-Point Water-Sorption Methods for Specific Surface Areas of Clay.
3. Al-Mahbashi, A. M., Elkady, T. Y., & Al-Shamrani, M. A. (2016). Hysteresis soil-water characteristic curves of highly expansive clay. European Journal of Environmental and Civil Engineering, 1-19.
4. Al-Tarhouni, M., Simms, P., & Sivathayalan, S. (2011). Cyclic behaviour of reconstituted and desiccated–rewet thickened gold tailings in simple shear. Canadian Geotechnical Journal, 48(7), 1044-1060.
5. Ashraf, S. (2008). Clay mineral quantification using gravemetric analysis (Doctoral dissertation, The University of Texas at Arlington).
6. ASTM (2008). ASTM D4943-08: Standard Test Method for Shrinkage Factors of Soils by the Wax Method. West Conshohocken, PA, USA: ASTM International.
7. ASTM (2003). ASTM D5084-03: Standard Test Methods for Measurement of Hydraulic Conductivity of Saturated Porous Materials Using a Flexible Wall Permeameter. West Conshohocken, PA, USA: ASTM International.
8. ASTM (2002). ASTM C493-98: Standard TestMethod for Bulk Density and Porosity of Granular Refractory Materials by Mercury Displacement (Withdrawn 2002). ASTM International, West Conshohocken, PA, USA.
9. ASTM (2010). ASTM D2216-10: Standard Test Methods for Laboratory Determination of Water (Moisture) Content of Soil and Rock by Mass. ASTM International, West Conshohocken, PA.
10. ASTM (2007). ASTM D422-63: Standard Test Method for Particle-size Analysis of Soils. ASTM International, West Conshohocken, PA, USA.
11. ASTM (1998). ASTM D427-04: TestMethod for Shrinkage Factors of Soils by the Mercury Method. ASTM International, West Conshohocken, PA, USA.
12. ASTM (2010). ASTM D4318: Standard Test Methods for Liquid Limit, Plastic Limit, and Plasticity Index of Soils. ASTM International, West Conshohocken, PA, USA.

13. ASTM (2008). ASTM D4943-08: Standard Test Method for Shrinkage Factors of Soils by the Wax Method. ASTM International, West Conshohocken, PA.
14. ASTM (2009). ASTM D7263: Standard Test Methods for Laboratory Determination of Density (Unit Weight) of Soil Specimens. ASTM International, West Conshohocken, PA.
15. ASTM (1994). ASTM D854-92: Standard Test Method for Specific Gravity of Soils. ASTM International, West Conshohocken, PA, USA.
16. ASTM (2012). ASTM E104-02: Standard practice for maintaining constant relative humidity by means of aqueous solutions. West Conshohocken, PA, USA: ASTM International.
17. Azad, F. M., El-Zein, A., Rowe, R. K., & Airey, D. W. (2012). Modelling of thermally induced desiccation of geosynthetic clay liners in double composite liner systems. Geotextiles and Geomembranes, 34, 28-38.
18. Baille, W., Tripathy, S., & Schanz, T. (2014). Effective stress in clays of various mineralogy. Vadose Zone Journal, 13(5).
19. Bardanis, M. E., & Kavvadas, M. J. (2006). Prediction of the limiting void ratio of clayey soils after drying. In Unsaturated Soils 2006 (pp. 1085-1096).
20. Bashir, R., Sharma, J., & Stefaniak, H. (2015). Effect of hysteresis of soil-water characteristic curves on infiltration under different climatic conditions. Canadian Geotechnical Journal, 53(2), 273-284.
21. Bensallam, S., Bahi, L., Ejjaaouani, H., & Shakhirev, V. (2012). Shrinkage curve: experimental study and modelling. International Journal of Engineering, 25(3), 203-210.
22. Bharat, T. V., & Sridharan, A. (2015). Prediction of compressibility data for highly plastic clays using diffuse double-layer theory. Clays and Clay Minerals, 63(1), 30-42.
23. Bharat, T. V., Sivapullaiah, P. V., & Allam, M. M. (2009). Swarm intelligence-based solver for parameter estimation of laboratory through-diffusion transport of contaminants. Computers and Geotechnics, 36(6), 984-992.
24. Bharat, T. V., Sivapullaiah, P. V., & Allam, M. M. (2012). Robust solver based on modified particle swarm optimization for improved solution of diffusion transport through containment facilities. Expert Systems with Applications, 39(12), 10812-10820.

25. Bharat, T. V., Sivapullaiah, P. V., & Allam, M. M. (2013). Novel procedure for the estimation of swelling pressures of compacted bentonites based on diffuse double layer theory. Environmental earth sciences, 70(1), 303-314.
26. Bhattacharjee, S., & Mallick, R. B. (2002). An alternative approach for the determination of bulk specific gravity and permeability of hot mix asphalt (HMA). International Journal of Pavement Engineering, 3(3), 143-152.
27. Bohn, H. L., Myer, R. A., & O'Connor, G. A. (2002). *Soil chemistry*. John Wiley & Sons.
28. Braudeau, E., Costantini, J. M., Bellier, G., & Colleuille, H. (1999). New device and method for soil shrinkage curve measurement and characterization. Soil Science Society of America Journal, 63(3), 525-535.
29. Brooks, R. H, & Corey, A.T. (1964). Hydraulic properties of porous media. Hydrology Paper 3. Colorado State University.
30. BS 1377: Part2, 1990. Methods of Test for Soils for Civil Engineering Purposes.
31. Bulut, R., & Leong, E. C. (2008). Indirect measurement of suction. Geotechnical and Geological Engineering, 26(6), 633.
32. Burdine, N. (1953). Relative permeability calculations from pore size distribution data. Journal of Petroleum Technology, 5(03), 71-78.
33. Burton, G. J., Pineda, J. A., Sheng, D., & Airey, D. (2015). Microstructural changes of an undisturbed, reconstituted and compacted high plasticity clay subjected to wetting and drying. Engineering Geology, 193, 363-373.
34. Cassel, D. K., Warrick, A. W., Nielsen, D. R., & Biggar, J. W. (1968). Soil-water diffusivity values based upon time dependent soil-water content distributions. Soil Science Society of America Journal, 32(6), 774-777.
35. Cerato, A. B., & Lutenegger, A. J. (2002). Determination of surface area of fine-grained soils by the ethylene glycol monoethyl ether (EGME) method.
36. Chao, K. C., Kang, J. B., & Nelson, J. D. (2014). Challenges in water migration modeling for expansive soils. In Soil Behavior and Geomechanics (pp. 204-213).
37. Chapman, H. D. (1965). Cation-exchange capacity. Methods of soil analysis. Part 2. Chemical and microbiological properties, (methodsofsoilanb), 891-901.
38. Chen, L. & Young, M. H. (2006). Green-Ampt infiltration model for sloping surfaces. Water resources research, 42(7), 1-9.
39. Chertkov, V. Y. (2003). Modelling the shrinkage curve of soil clay pastes. Geoderma, 112(1), 71-95.

40. Childs, E. C., & Collis-George, N. (1950, April). The permeability of porous materials. In Proceedings of the Royal Society of London A: Mathematical, Physical and Engineering Sciences (Vol. 201, No. 1066, pp. 392-405). The Royal Society.
41. Chittoori, B. C. S. (2008). Clay mineralogy effects on long-term performance of chemically treated expansive clays (Doctoral dissertation, The University of Texas at Arlington).
42. Chiu, T. F., & Shackelford, C. D. (1998). Unsaturated hydraulic conductivity of compacted sand-kaolin mixtures. Journal of Geotechnical and Geoenvironmental Engineering, 124(2), 160-170.
43. Cho, W. J., Lee, J. O., & Chun, K. S. (1999). The temperature effects on hydraulic conductivity of compacted bentonite. Applied clay science, 14(1), 47-58.
44. Cleall, P. J., Singh, R. M., & Thomas, H. R. (2013). Vapour transfer in unsaturated compacted bentonite. Geotechnique: international journal of soil mechanics, 63(11), 957-964.
45. Cornelis, W. M., Corluy, J., Medina, H., Hartmann, R., Van Meirvenne, M., & Ruiz, M. E. (2006a). A simplified parametric model to describe the magnitude and geometry of soil shrinkage. European journal of soil science, 57(2), 258-268.
46. Cornelis, W. M., Corluy, J., Medina, H., Diaz, J., Hartmann, R., Van Meirvenne, M., & Ruiz, M. E. (2006b). Measuring and modelling the soil shrinkage characteristic curve. Geoderma, 137(1), 179-191.
47. Crescimanno, G., & Provenzano, G. (1999). Soil shrinkage characteristic curve in clay soils: Measurement and prediction. Soil Science Society of America Journal, 63(1), 25-32.
48. Cripps, J. C., & Parmar, K. K. (2015). Investigations into the Self-Healing of Desiccation Cracks in Compacted Clays. In Engineering Geology for Society and Territory-Volume 5 (pp. 1327-1331). Springer, Cham.
49. Dakshanamurthy, V. (1978). A Hyperbolic Equation. Geotechnical engineering, 9, 29.
50. Daniel, D. E. (1984). Predicting hydraulic conductivity of clay liners. Journal of Geotechnical Engineering, 110(2), 285-300.

51. de Almeida, B. G., da Silva, A. P., Raine, S. R., & Figueiredo, G. C. (2009). Evaluation of automotive varnish as a coating for density measurements of soil clods. Soil Science Society of America Journal, 73(2), 449-452.
52. Delage, P., & Cui, Y. J. (2008). An evaluation of the osmotic method of controlling suction∗. Geomechanics and Geoengineering: An International Journal, 3(1), 1-11.
53. Delage, P., Howat, M. D., & Cui, Y. J. (1998). The relationship between suction and swelling properties in a heavily compacted unsaturated clay. Engineering geology, 50(1), 31-48.
54. Dixon, D. A., Graham, J., & Gray, M. N. (1999). Hydraulic conductivity of clays in confined tests under low hydraulic gradients. Canadian Geotechnical Journal, 36(5), 815-825.
55. Döll, P. (1997). Desiccation of mineral liners below landfills with heat generation. Journal of Geotechnical and Geoenvironmental Engineering, 123(11), 1001-1009.
56. Ebrahimi-Birang, N., Fredlund, D. G., & Samarasekera, L. (2007). Hysteresis of the soil-water characteristic curve in the high suction range. In Proc. OttawaGeo Conf (pp. 1061-1068).
57. ENRESA. (2000) FEBEX Project. Full- scale engineered barriers experiments for a deep geological respiratory for high level radioactive waste in crystalline host rock. Final report, Publicación Técnical ENRESA, 354.
58. Feng, M., & Fredlund, D. G. (1999, October). Hysteretic influence associated with thermal conductivity sensor measurements. In Proceedings of the 52nd Canadian Geotechnical Conference, Regina, Sask (pp. 24-27).
59. Fleureau, J. M., Kheirbek-Saoud, S., Soemitro, R., & Taibi, S. (1993). Behavior of clayey soils on drying–wetting paths. *Canadian geotechnical journal*, *30*(2), 287-296.
60. Fleureau, J. M., Verbrugge, J. C., Huergo, P. J., Correia, A. G., & Kheirbek-Saoud, S. (2002). Aspects of the behaviour of compacted clayey soils on drying and wetting paths. Canadian geotechnical journal, 39(6), 1341-1357.
61. Fredlund, D. G. (2006). Unsaturated soil mechanics in engineering practice. Journal of geotechnical and geoenvironmental engineering, 132(3), 286-321.
62. Fredlund, D. G. (2002). Use of soil-water characteristic curves in the implementation of unsaturated soil mechanics. In Proceedings of the 3rd

International Conference on Unsaturated Soils, Recife, Brazil (Vol. 3, pp. 887-902).

63. Fredlund, D. G., Barbour, S. L., & Pham, Q. H. (2003). Evaluation of hysteresis models for predicting the boundary wetting curve. In Proceedings of the 2nd Asian Conference on Unsaturated Soils, Osaka, Japan (pp. 15-17).
64. Fredlund, D. G., & Rahardjo, H. (1993). Soil mechanics for unsaturated soils. John Wiley & Sons.
65. Fredlund, D. G., & Houston, S. L. (2013, January). Interpretation of soil-water characteristic curves when volume change occurs as soil suction is changed. In Proceedings, 1st Pan-American conference on unsaturated soils. Cartagena de Indias, Colombia (Vol. 1, pp. 15-31).
66. Fredlund, D. G., Sheng, D., & Zhao, J. (2011). Estimation of soil suction from the soil-water characteristic curve. Canadian geotechnical journal, 48(2), 186-198.
67. Fredlund, D. G., & Xing, A. (1994). Equations for the soil-water characteristic curve. Canadian geotechnical journal, 31(4), 521-532.
68. Fredlund, D. G., Xing, A., & Huang, S. (1994). Predicting the permeability function for unsaturated soils using the soil-water characteristic curve. Canadian Geotechnical Journal, 31(4), 533-546.
69. Fredlund, M. D., Wilson, G. W., & Fredlund, D. G. (2002). Use of the grain-size distribution for estimation of the soil-water characteristic curve. Canadian Geotechnical Journal, 39(5), 1103-1117.
70. Fredlund, M. D., Wilson, G. W., & Fredlund, D. G. (2002, March). Representation and estimation of the shrinkage curve. In Proceedings of the 3rd International Conference on Unsaturated Soils, UNSAT (pp. 145-150).
71. Fujita, T., Hara, K., Yusa, Y., & Sasaki, N. (1990). Application of elasto-plastic model to mechanical and hydraulic behavior of buffer material under water uptake in a repository. MRS Online Proceedings Library Archive, 212.
72. Fujita, T., Kobayashi, A., and Börgesson, L. 1996. Experimental investigation and mathematical simulation of coupled THM processes of the engineered buffer materials, the TC3 problem. Developments in geotechnical engineering, 79: 369-392.
73. Gallipoli, D. (2012). A hysteretic soil-water retention model accounting for cyclic variations of suction and void ratio. Geotechnique, 62(7), 605.

74. Gallipoli, D., Bruno, A. W., D'Onza, F., & Mancuso, C. (2015). A bounding surface hysteretic water retention model for deformable soils. Géotechnique, 65(10), 793-804.
75. Gallipoli, D., Wheeler, S. J., & Karstunen, M. (2003). Modelling the variation of degree of saturation in a deformable unsaturated soil. Géotechnique., 53(1), 105-112.
76. Gardner, W. R. (1958). Some steady-state solutions of the unsaturated moisture flow equation with application to evaporation from a water table. Soil science, 85(4), 228-232.
77. Garnier, P., Perrier, E., Jaramillo, R. A., & Baveye, P. (1997). Numerical model of 3-Dimensional anisotropic deformation and 1- Dimensional water flow in swelling soils. Soil Science, 162(6), 410-420.
78. Gould, S. J., Kodikara, J., Rajeev, P., Zhao, X. L., & Burn, S. (2011). A void ratio–water content–net stress model for environmentally stabilized expansive soils. Canadian Geotechnical Journal, 48(6), 867-877.
79. Green, W. H., & Ampt, G. A. (1911). Studies on Soil Phyics. The Journal of Agricultural Science, 4(1), 1-24.
80. Grim, R. E. (1968). Clay mineralogy. International series in the earth and planetary sciences. McGraw-Hill, New York.
81. Groenevelt, P. H., & Grant, C. D. (2002). Curvature of shrinkage lines in relation to the consistency and structure of a Norwegian clay soil. Geoderma, 106(3), 235-245.
82. Guerrini, I. A., & Swartzendruber, D. (1992). Soil water diffusivity as explicitly dependent on both time and water content. Soil Science Society of America Journal, 56(2), 335-340.
83. Harnas, F. R., Rahardjo, H., Leong, E. C., & Wang, J. Y. (2014). Experimental study on dual capillary barrier using recycled asphalt pavement materials. Canadian Geotechnical Journal, 51(10), 1165-1177.
84. Haverkamp, R., Vauclin, M., Touma, J., Wierenga, P. J., & Vachaud, G. (1977). A comparison of numerical simulation models for one-dimensional infiltration. Soil Science Society of America Journal, 41(2), 285-294.
85. Hillel, D. (1980). Fundamentals of Soil Physics Academic. San Diego, CA.

86. Hong, W. T., Jung, Y. S., Kang, S., & Lee, J. S. (2016). Estimation of Soil-Water Characteristic Curves in Multiple-Cycles Using Membrane and TDR System. Materials, 9(12), 1019.
87. Hosseini, S. M. M. M., Ganjian, N., & Pisheh, Y. P. (2011). Estimation of the water retention curve for unsaturated clay. Canadian Journal of Soil Science, 91(4), 543-549.
88. Huang, M., Barbour, S. L., Elshorbagy, A., Zettl, J. D., & Cheng Si, B. (2011). Infiltration and drainage processes in multi-layered coarse soils. Canadian Journal of Soil Science, 91(2), 169-183.
89. Huang, L., Zhang, P., Hu, Y., & Zhao, Y. (2015). Vegetation succession and soil infiltration characteristics under different aged refuse dumps at the Heidaigou opencast coal mine. Global Ecology and Conservation, 4, 255-263.
90. Hueckel, T. A. (1992). Water–mineral interaction in hygromechanics of clays exposed to environmental loads: a mixture-theory approach. Canadian Geotechnical Journal, 29(6), 1071-1086.
91. IAEA. (2001). The use of scientific and technical results from underground research laboratory investigations for the geological disposal of radioactive waste. A technical position paper, International Atomic Energy Agency IAEA-TECDOC-1243, ISSN 1011–4289.
92. Ippisch, O., Vogel, H. J., & Bastian, P. (2006). Validity limits for the van Genuchten–Mualem model and implications for parameter estimation and numerical simulation. Advances in water resources, 29(12), 1780-1789.
93. IS (1986). IS 2720: Part XVII: Methods of test for soils: Laboratory determination of permeability. New Delhi, India: Indian Standards Institute, 8-12.
94. IS (1972). IS 2720: Part 6: Methods of Test for Soils: Determination of Shrinkage Factors.
95. Ishikawa, H., Amemiya, K., Yusa, Y., & Sasaki, N. (1990). Comparison of fundamental properties of Japanese bentonites as buffer material for waste disposal. Sciences Geologiques. Memoire, 107-115.
96. Jacinto, A. C., Ledesma, A., & Demagistri, A. (2016). Effect of the clay–water interaction in the hydration of compacted bentonite used in engineered barriers. Geomechanics for Energy and the Environment, 8, 52-61.
97. Jacinto, A. C., Villar, M. V., & Ledesma, A. (2012). Influence of water density on the water-retention curve of expansive clays. Geotechnique, 62(8), 657.

98. Jayanth, S., Iyer, K., & Singh, D. N. (2012). Influence of drying and wetting cycles on SWCCs of fine-grained soils. Journal of Testing and Evaluation, 40(3), 376-386.
99. Jaynes, D. B. (1984). Comparison of soil-water hysteresis models. Journal of Hydrology, 75(1-4), 287-299.
100. Kargas, G., & Kerkides, P. (2011). A contribution to the study of the phenomenon of horizontal infiltration. Water resources management, 25(4), 1131-1141.
101. Karnland, O. (2010). Chemical and mineralogical characterization of the bentonite buffer for the acceptance control procedure in a KBS-3 repository (No. SKB-TR--10-60). Swedish Nuclear Fuel and Waste Management Co.
102. Khorshidi, M., & Lu, N. (2017). Determination of cation exchange capacity from soil water retention curve. Journal of Engineering Mechanics, 143(6), 04017023.
103. Khorshidi, M., & Lu, N. (2016). Intrinsic relation between soil water retention and cation exchange capacity. Journal of Geotechnical and Geoenvironmental Engineering, 143(4), 04016119.
104. Khorshidi, M., Lu, N., Akin, I. D., & Likos, W. J. (2016). Intrinsic relationship between specific surface area and soil water retention. Journal of Geotechnical and Geoenvironmental Engineering, 143(1), 04016078.
105. Kim, C. S. 2017. Evaluation of coupled hydro-mechanical (h-m) behaviour of in situ shaft sealing components for used nuclear fuel. Ph.D. thesis, University of Manitoba.
106. Kim, D. J., Vereecken, H., Feyen, J., Boels, D., & Bronswijk, J. J. B. (1992). On the characterization of properties of an unripe marine clay soil: I. Shrinkage processes of an unripe marine clay soil in relation to physical ripening. Soil Science, 153(6), 471-481.
107. Klute, A. and Dirksen, C. 1986. Hydraulic conductivity and diffusivity: laboratory methods. Methods of Soil Analysis, Part1. Physical and Mineralogical Methods. Soil Science Society of America, Monograph No. 9, Madison, WI, 687–734.
108. Knidiri, J., Bussière, B., Hakkou, R., Bossé, B., Maqsoud, A., & Benzaazoua, M. (2016). Hydrogeological behaviour of an inclined store-and-release cover experimental cell made with phosphate mine wastes. Canadian Geotechnical Journal, 54(1), 102-116.

109. Kodandaramaswamy, K., & Rao, S. N. (1980). The prediction of settlements and heave in clays. Canadian Geotechnical Journal, 17(4), 623-631.
110. Kondner, R. L. (1963). Hyperbolic stress-strain response: cohesive soils. Journal of the Soil Mechanics and Foundations Division, 89(1), 115-144.
111. Krosley, L., Lu, N., & Likos, W.J. (2003). Alternative encasement materials for clod test. Geotechnical. Testing Journal. 26, 1–3.
112. Lagerwerff, J. V., Ogata, G., & Eagle, H. E. (1961). Control of osmotic pressure of culture solutions with polyethylene glycol. Science, 133(3463), 1486-1487.
113. Lambe, T. W. (1951). Soil testing for engineers. John Wiley and Sons, Inc, London.
114. Lauritzen, C. W., & Stewart, A. J. (1942). Soil-Volume Changes and Accompanying Moisture and Pore-Space Relationships 1. Soil Science Society of America Journal, 6(C), 113-116.
115. Lee, J. O., Cho, W. J., & Kwon, S. (2011). Suction and water uptake in unsaturated compacted bentonite. Annals of Nuclear Energy, 38(2), 520-526.
116. Lee, J. O., Cho, W. J., & Kwon, S. K. (2011). Thermal-hydro-mechanical properties of reference bentonite buffer for a Korean HLW repository. Tunnel and Underground Space, 21(4), 264-273.
117. Leong, E. C., & Rahardjo, H. (2002). Soil-water characteristic curves of compacted residual soils. In Unsaturated soils. Proceedings of the 3rd international conference on unsaturated soils (UNSAT 2002), Recife, Brazil (Vol. 1, pp. 271-276).
118. Leong, E. C., Tripathy, S., & Rahardjo, H. (2003). Total suction measurement of unsaturated soils with a device using the chilled-mirror dew-point technique. Geotechnique, 53(2), 173-182.
119. Liebig, T. (2001). U.S. Patent No. 20020018867A1. Washington, DC: U.S. Patent and Trademark Office.
120. Lin, B., & Cerato, A. B. (2012). Hysteretic water retention behavior of two highly clayey expansive soils. In GeoCongress 2012: State of the Art and Practice in Geotechnical Engineering (pp. 1205-1212).
121. Liu, Y., Parlange, J., Steenhuis, T. S., & Haverkamp, R. (1995). A soil water hysteresis model for fingered flow data. Water Resources Research, 31(9), 2263-2266.

122. Lloret Morancho, A., Villar, M. V., Sanchez, M., Gens Solé, A., Pintado Llurba, X., & Alonso Pérez de Agreda, E. (2003). Mechanical behaviour of heavily compacted bentonite under high suction changes.
123. Lu, N., Godt, J. W., & Wu, D. T. (2010). A closed-form equation for effective stress in unsaturated soil. Water Resources Research, 46(5).
124. Lu, N., & Khorshidi, M. (2015). Mechanisms for soil-water retention and hysteresis at high suction range. Journal of Geotechnical and Geoenvironmental Engineering, 141(8), 04015032.
125. Lu, N., & Likos, W. J. (2006). Suction stress characteristic curve for unsaturated soil. Journal of geotechnical and geoenvironmental engineering, 132(2), 131-142.
126. Lu, N., & Likos, W. J. (2004). Unsaturated soil mechanics. Wiley.
127. Lutenegger, A. J., & Cerato, A.B. (2001). Surface area and engineering properties of fine-grained soils. In Proceedings of the International Conference on Soil Mechanics and Geotechnical Engineering, 1, 603-606.
128. Ma, Y., Feng, S., Su, D., Gao, G., & Huo, Z. (2010). Modeling water infiltration in a large layered soil column with a modified Green–Ampt model and HYDRUS-1D. Computers and Electronics in Agriculture, 71, S40-S47.
129. Marinho, F. A. (2005). Nature of soil–water characteristic curve for plastic soils. Journal of Geotechnical and Geoenvironmental Engineering, 131(5), 654-661.
130. Martin, R. T. (1960). Adsorbed water on clay: a review. In Clays and clay minerals. Proceedings of the Ninth National Conference on Clays and Clay Minerals (Vol. 9)
131. Mbonimpa, M., Aubertin, M., Maqsoud, A., & Bussière, B. (2006). Predictive model for the water retention curve of deformable clayey soils. Journal of Geotechnical and Geoenvironmental Engineering, 132(9), 1121-1132.
132. McGarry, D., & Malafant, K. W. J. (1987). The analysis of volume change in unconfined units of soil. Soil Science Society of America Journal, 51(2), 290-297.
133. Meerdink, J. S., Benson, C. H., & Khire, M. V. (1996). Unsaturated hydraulic conductivity of two compacted barrier soils. Journal of geotechnical engineering, 122(7), 565-576.
134. Mijares, R. G., & Khire, M. V. (2010). Soil water characteristic curves of compacted clay subjected to multiple wetting and drying cycles. In GeoFlorida 2010: Advances in Analysis, Modeling & Design (pp. 400-409).

135. Montes-H, G., & Geraud, Y. (2004). Sorption kinetic of water vapour of MX80 bentonite submitted to different physical–chemical and mechanical conditions. Colloids and Surfaces A: Physicochemical and Engineering Aspects, 235(1-3), 17-23.
136. Montes-H, G., Marty, N., Fritz, B., Clement, A., & Michau, N. (2005). Modelling of long-term diffusion–reaction in a bentonite barrier for radioactive waste confinement. Applied Clay Science, 30(3-4), 181-198.
137. Mosser-Ruck, R., Devineau, K., Charpentier, D., & Cathelineau, M. (2005). Effects of ethylene glycol saturation protocols on XRD patterns: a critical review and discussion. Clays and Clay Minerals, 53(6), 631-638.
138. Mualem, Y. (1973). Modified approach to capillary hysteresis based on a similarity hypothesis. Water Resources Research, 9(5), 1324-1331.
139. Mualem, Y. (1976). A new model for predicting the hydraulic conductivity of unsaturated porous media. Water resources research, 12(3), 513-522.
140. Muurinen, A. (2011). Measurements on cation exchange capacity of bentonite in the long-term test of buffer material (LOT) (No. POSIVA-WR--11-10). Posiva Oy.
141. Nam, S., Gutierrez, M., Diplas, P., Petrie, J., Wayllace, A., Lu, N., & Muñoz, J. J. (2010). Comparison of testing techniques and models for establishing the SWCC of riverbank soils. Engineering Geology, 110(1), 1-10.
142. Néel, L. (1942). Théories des lois d'aimantation de Lord Rayleigh. Cahiers de physique, 12, 1-20.
143. Nelson, J. D., Chao, K. C., Overton, D. D., & Nelson, E. J. (2015). Foundation engineering for expansive soils. John Wiley & Sons.
144. Nelson, J., & Miller, D. J. (1997). Expansive soils: problems and practice in foundation and pavement engineering. John Wiley & Sons.
145. Ng, C. W. W., & Leung, A. K. (2011). Measurements of drying and wetting permeability functions using a new stress-controllable soil column. Journal of Geotechnical and Geoenvironmental Engineering, 138(1), 58-68.
146. Nielsen, D. R., Biggar, J. W., & Davidson, J. M. (1962). Experimental Consideration of Diffusion Analysis in Unsaturated Flow Problems 1. Soil Science Society of America Journal, 26(2), 107-111.
147. Nimmo, J. R. (1992). Semiempirical model of soil water hysteresis. Soil Science Society of America Journal, 56(6), 1723-1730.

148. Ogata, H., Goto, S., Sato, K., Fujibuchi, W., Bono, H., & Kanehisa, M. (1999). KEGG: Kyoto encyclopedia of genes and genomes. Nucleic acids research, 27(1), 29-34.
149. Oh, W. T., Vanapalli, S. K., Qi, S., & Han, Z. (2016). Estimation of the variation of matric suction with respect to depth in a vertical unsaturated soil trench associated with rainfall infiltration. In E3S Web of Conferences (Vol. 9, p. 15003). EDP Sciences.
150. Olsson, S. (1991). Geochemistry, mineralogy and pore water composition in uplifted, Late Weichselian-Early Holocene clays from southern Sweden. Lundqua Thesis 28. Lund University, Department of Quaternary Geology. 89 p.
151. Or, D., Lehmann, P., Shahraeeni, E., & Shokri, N. (2013). Advances in soil evaporation physics—A review. Vadose Zone Journal, 12(4).
152. Pachepsky, Y., Timlin, D., & Rawls, W. (2003). Generalized Richards' equation to simulate water transport in unsaturated soils. Journal of Hydrology, 272(1), 3-13.
153. Pan, H., Qing, Y., & Pei-yong, L. (2010). Direct and indirect measurement of soil suction in the laboratory. Electronic Journal of Geotechnical Engineering, 15(3), 1-14.
154. Peng, X., & Horn, R. (2005). Modeling soil shrinkage curve across a wide range of soil types. Soil Science Society of America Journal, 69(3), 584-592.
155. Péron, H., Hueckel, T., Laloui, L., & Hu, L. (2009). Fundamentals of desiccation cracking of fine-grained soils: experimental characterisation and mechanisms identification. Canadian Geotechnical Journal, 46(10), 1177-1201.
156. Pham, H.Q. (2001). "An engineering model of hysteresis for soil-water characteristic curves." MSc thesis, University of Saskatchewan, Canada
157. Pham, H. Q., & Fredlund, D. G. (2011). Volume–mass unsaturated soil constitutive model for drying–wetting under isotropic loading–unloading conditions. Canadian Geotechnical Journal, 48(2), 280-313.
158. Pham, H. Q., Fredlund, D. G., & Barbour, S. L. (2003). A practical hysteresis model for the soil-water characteristic curve for soils with negligible volume change. Geotechnique, 53(2), 293-298.
159. Pham, H. Q., Fredlund, D. G., & Barbour, S. L. (2005). A study of hysteresis models for soil-water characteristic curves. Canadian Geotechnical Journal, 42(6), 1548-1568.

160. Philip, J. R. 1957. The theory of infiltration: 1. The infiltration equation and its solution. Soil science, 83(5), 345-358.
161. Philip, J. R. (1964). Similarity hypothesis for capillary hysteresis in porous materials. Journal of geophysical research, 69(8), 1553-1562.
162. Por, S., Likitlersuang, S., & Nishimura, S. (2015). Investigation of Shrinkage and Swelling Behaviour of Expansive/Non-Expansive Clay Mixtures. Geotech. Eng. J. SEAGS & AGSSEA, 46, 117-127.
163. Poulovassilis, A. (1962). Hysteresis of pore water – an application of the concept of independent domains. Soil Science, 93(6), 405-412.
164. Poulovassilis, A., & Childs, E. C. (1971). The hysteresis of pore water: the non-independence of domains. Soil Science, 112(5), 301-312.
165. Prakash, K., Sridharan, A., & Sudheendra, S. (2014). Hygroscopic moisture content: determination and correlations. Environmental Geotechnics, 3(5), 293-301.
166. Puppala, A. J., Katha, B., & Hoyos, L. R. (2004). Volumetric shrinkage strain measurements in expansive soils using digital imaging technology.
167. Pusch, R. (1982). Mineral–water interactions and their influence on the physical behavior of highly compacted Na bentonite. Canadian Geotechnical Journal, 19(3), 381-387.
168. Pusch, R. (1992). Use of bentonite for isolation of radioactive waste products. Clay Miner, 27(3), 353-361.
169. Pusch, R. (2006). The performance of clay barriers in repositories for high-level radioactive waste. Nuclear Engineering and Technology, 38(6), 483-488.
170. Pusch, R., Nilsson, J., & Ramqvist, G. (1985). Final report of the buffer mass test. Volume I: Scope, preparative field work, and test arrangement (No. NAGRA-NTB--85-58). Nationale Genossenschaft fuer die Lagerung Radioaktiver Abfaelle (NAGRA).
171. Pusch, R., & Yong, R. N. (2006). Microstructure of smectite clays and engineering performance. CRC Press.
172. Pusch, R., Kasbohm, J., Knutsson, S., Yang, T., & Nguyen-Thanh, L. (2015). The role of smectite clay barriers for isolating high-level radioactive waste (HLW) in shallow and deep repositories. Procedia Earth and Planetary Science, 15, 680-687.

173. Qian, X., Koerner, R.M. & Gray, D.H. (2002). Geotechnical aspects of landfill design and construction, Prentice Hall, New Jersey.
174. Qi, S., & Vanapalli, S. K. (2015). Hydro-mechanical coupling effect on surficial layer stability of unsaturated expansive soil slopes. Computers and Geotechnics, 70, 68-82.
175. Rahimi, A., Rahardjo, H., & Leong, E. C. (2015). Effects of soil–water characteristic curve and relative permeability equations on estimation of unsaturated permeability function. Soils and Foundations, 55(6), 1400-1411.
176. Rao, S. N., & Mathew, P. K. (1995). Effects of exchangeable cations on hydraulic conductivity of a marine clay. Clays and clay minerals, 43(4), 433-437.
177. Rayhani, M. H. T., Yanful, E. K., & Fakher, A. (2008). Physical modeling of desiccation cracking in plastic soils. Engineering Geology, 97(1-2), 25-31.
178. Richards, L. A. (1931). Capillary conduction of liquids through porous mediums. Physics, 1(5), 318-333.
179. Romero, E., & Vaunat, J. (2000). Retention curves of deformable clays. Experimental evidence and theoretical approaches in unsaturated soils, 91-106.
180. Ross, D. S., & Ketterings, Q. (1995). Recommended methods for determining soil cation exchange capacity. Recommended soil testing procedures for the northeastern United States, 2, 62-70.
181. Rowe, R. K., Quigley, R. M., & Booker, J. R. (1995). barrier systems for waste disposal facilities, Chapman & Hall, London.
182. Sahu, R. K. (2016). Prediction of compressibility data at high consolidation pressure and preconsolidation pressure of clays of different plasticity. M. Tech Thesis, Indian Institute of Technology, Guwahati, India.
183. Saiyouri, N., Hicher, P. Y., & Tessier, D. (2000). Microstructural approach and transfer water modelling in highly compacted unsaturated swelling clays. Mechanics of Cohesive-Frictional Materials, 5(1), 41-60.
184. Saleh-Mbemba, F., Aubertin, M., & Mbonimpa, M. (2010). Desiccation and shrinkage of low plasticity tailings: testing and preliminary modeling. In Proceedings of the 63rd Canadian Geotechnical Conference and 6th Canadian Permafrost Conference Geo2010, Calgary, Alta.
185. Saleh-Mbemba, F., Aubertin, M., Mbonimpa, M., & Li, L. (2016). Experimental Characterization of the Shrinkage and Water Retention Behaviour of Tailings

from Hard Rock Mines. Geotechnical and Geological Engineering, 34(1), 251-266.

186. Schindler, U., Durner, W., Von Unold, G., Mueller, L., & Wieland, R. (2010). The evaporation method: Extending the measurement range of soil hydraulic properties using the air-entry pressure of the ceramic cup. Journal of Plant Nutrition and Soil Science, 173(4), 563-572.
187. Seiphoori, A., Ferrari, A., & Laloui, L. (2014). Water retention behaviour and microstructural evolution of MX-80 bentonite during wetting and drying cycles. Géotechnique, 64(9), 721-734.
188. Sharma, R. S. (1998). Mechanical behaviour of unsaturated highly expansive clays (Doctoral dissertation, University of Oxford).
189. Siemens, G.A., & Blatz, J.A. (2008). Numerical modelling of shallow foundations on swelling clay soil using the swelling equilibrium limit. 1st European Conference on Unsaturated Soils (E816 UNSAT), Durham, United Kingdom, 2-5 July 2008, 855-860.
190. Siemens, G., Take, W. A., Rowe, R. K., & Brachman, R. W. I. (2012). Numerical investigation of transient hydration of unsaturated geosynthetic clay liners. Geosynthetics International, 19(3), 232-251.
191. Šimůnek, J., & Genuchten, M. V. (1996). Estimating unsaturated soil hydraulic properties from tension disc infiltrometer data by numerical inversion. Water Resources Research, 32(9), 2683-2696.
192. Šimůnek, J., Šejna, M., Saito, H., Sakai, M., & Van Genuchten, M. T. (2008). The HYDRUS-1D software package for simulating the movement of water, heat, and multiple solutes in variably saturated media, version 4.0: HYDRUS Software Series 3. Department of Environmental Sciences, University of California Riverside, Riverside, California, USA, 315.
193. Šimůnek, J., van Genuchten, M. T., & Wendroth, O. (1998). Parameter estimation analysis of the evaporation method for determining soil hydraulic properties. Soil Science Society of America Journal, 62(4), 894-905.
194. Southen, J. M., & Rowe, R. K. (2005). Laboratory investigation of geosynthetic clay liner desiccation in a composite liner subjected to thermal gradients. Journal of Geotechnical and Geoenvironmental Engineering, 131(7), 925-935.

195. Southen, J. M., & Rowe, R. K. (2005). Modelling of thermally induced desiccation of geosynthetic clay liners. Geotextiles and Geomembranes, 23(5), 425-442.
196. Sposito, G., & Prost, R. (1982). Structure of water adsorbed on smectites. Chemical Reviews, 82(6), 553-573.
197. Sridharan, A., Murthy, N. S., & Prakash, K. (1987). Rectangular hyperbola method of consolidation analysis. Geotechnique, 37(3), 355-368.
198. Sridharan, A., & Rao, A. S. (1981). Rectangular hyperbola fitting method for one dimensional consolidation. Geotechnical Testing Journal, 4(4), 161-168.
199. Sridharan, A., Rao, S. M., & Murthy, N. S. (1986). Compressibility behaviour of homoionized bentonites. Geotechnique, 36(4), 551-564.
200. Stewart, R. D., Abou Najm, M. R., Rupp, D. E., & Selker, J. S. (2012). An image-based method for determining bulk density and the soil shrinkage curve. Soil Science Society of America Journal, 76(4), 1217-1221.
201. Sun, W., Sun, D. A., Fang, L., & Liu, S. (2014). Soil-water characteristics of Gaomiaozi bentonite by vapour equilibrium technique. Journal of Rock Mechanics and Geotechnical Engineering, 6(1), 48-54.
202. Tadza, M. Y. M. (2011). Soil-water characteristic curves and shrinkage behaviour of highly plastic clays: an experimental investigation. Cardiff University (United Kingdom)
203. Take, W. A., & Bolton, M. D. (2003). Tensiometer saturation and the reliable measurement of soil suction. Géotechnique, 53(2), 159-172.
204. Tang, A. M., & Cui, Y. J. (2005). Controlling suction by the vapour equilibrium technique at different temperatures and its application in determining the water retention properties of MX80 clay. Canadian Geotechnical Journal, 42(1), 287-296.
205. Tang, A. M., Cui, Y. J., & Barnel, N. (2007). A new isotropic cell for studying the thermo-mechanical behavior of unsaturated expansive clays.
206. Tang, C. S., Shi, B., Liu, C., Suo, W. B., & Gao, L. (2011). Experimental characterization of shrinkage and desiccation cracking in thin clay layer. Applied Clay Science, 52(1), 69-77
207. Tariq, A.U.R., & Durnford, D.S. (1993a). Soil volumetric shrinkage measurements: A Simple Method. Soil Science, 155, 325–330.

208. Tariq, A.U.R., & Durnford, D.S. (1993b). Analytical volume change model for swelling clay soils. Soil Science Society of America Journal. 57, 1183–1187.
209. Tay, Y. Y., Stewart, D. I., & Cousens, T. W. (2001). Shrinkage and desiccation cracking in bentonite–sand landfill liners. Engineering Geology, 60(1), 263-274.
210. Thu, T. M., Rahardjo, H., & Leong, E. C. (2007). Soil-water characteristic curve and consolidation behavior for a compacted silt. Canadian Geotechnical Journal, 44(3), 266-275.
211. Tinjum, J. M., Benson, C. H., & Blotz, L. R. (1997). Soil-water characteristic curves for compacted clays. Journal of geotechnical and geoenvironmental engineering, 123(11), 1060-1069.
212. Tripathy, S., Al-Khyat, S., Cleall, P. J., Baille, W., & Schanz, T. (2016). Soil suction measurement of unsaturated soils with a sensor using fixed-matrix porous ceramic discs. Indian Geotechnical Journal, 46(3), 252-260.
213. Tripathy, S., Bag, R., & Thomas, H. R. (2014). Effects of post-compaction residual lateral stress and electrolyte concentration on swelling pressures of a compacted bentonite. Geotechnical and Geological Engineering, 32(4), 749-763.
214. Tripathy, S., Rao, K. S., & Fredlund, D. G. (2002). Water content-void ratio swell-shrink paths of compacted expansive soils. Canadian geotechnical journal, 39(4), 938-959.
215. Tripathy, S., Tadza, M. Y. M., & Thomas, H. R. (2014). Soil-water characteristic curves of clays. Canadian Geotechnical Journal, 51(8), 869-883.
216. Tripathy, S., Tadza, M., Yuhyi, M., & Thomas, H. R. (2011). On the intrusion of polyethylene glycol during osmotic tests. Géotechnique Letters, 1(3), 47-51.
217. Ukrainczyk, N., Kurajica, S., & Šipušić, J. (2010). Thermophysical comparison of five commercial paraffin waxes as latent heat storage materials. Chemical and biochemical engineering quarterly, 24(2), 129-137.
218. Vanapalli, S. K., Fredlund, D. G., & Pufahl, D. E. (1999). The influence of soil structure and stress history on the soil–water characteristics of a compacted till. Géotechnique, 49(2), 143-159.
219. Van Genuchten, M. T. (1980). A closed-form equation for predicting the hydraulic conductivity of unsaturated soils. Soil science society of America journal, 44(5), 892-898
220. Van Genuchten, M. T., & Nielsen, D. R. (1985). On describing and predicting the hydraulic properties. In Annales Geophysicae (Vol. 3, No. 5, pp. 615-628).

221. Vardon, P. J., Nijssen, T., Yao, Y., & Van Tol, A. F. (2014). Numerical simulation of fine oil sand tailings drying in test cells. In IOSTC 2014: Proceedings of the 4th International Oil Sands Tailings Conference, Lake Louise, Canada, 7-10 December 2014. University of Alberta.
222. Vereecken, H., Maes, J., Feyen, J., & Darius, P. (1989). Estimating the soil moisture retention characteristic from texture, bulk density, and carbon content. Soil science, 148(6), 389-403.
223. Villar, M. V., & Lloret, A. (2008). Influence of dry density and water content on the swelling of a compacted bentonite. Applied Clay Science, 39(1), 38-49.
224. Villar, M. V., & Lloret, A. (2004). Influence of temperature on the hydro-mechanical behaviour of a compacted bentonite. Applied Clay Science, 26(1), 337-350.
225. Vogel, T., Van Genuchten, M. T., & Cislerova, M. (2001). Effect of the shape of the soil hydraulic functions near saturation on variably-saturated flow predictions. Advances in Water Resources, 24(2), 133-144.
226. Wheeler, S. J., Sharma, R. S., & Buisson, M. S. R. (2003). Coupling of hydraulic hysteresis and stress–strain behaviour in unsaturated soils. Géotechnique, 53(1), 41-54.
227. Wijaya, M., Leong, E. C., & Rahardjo, H. (2015). Effect of shrinkage on air-entry value of soils. Soils and Foundations, 55(1), 166-180.
228. Williams, J., & Shaykewich, C. F. (1969). An evaluation of polyethylene glycol (PEG) 6000 and PEG 20,000 in the osmotic control of soil water matric potential. Canadian Journal of Soil Science, 49(3), 397-401.
229. Yaldo, K. (1999). Impact of soil type and compaction conditions on soil-water characteristic curves. Ph. D. Thesis, Department of Civil Engineering, Wayne Stata University, Detroit, Michigan.
230. Yanful, E. K., Mousavi, S. M., & Yang, M. (2003). Modeling and measurement of evaporation in moisture-retaining soil covers. Advances in Environmental Research, 7(4), 783-801.
231. Yang, H., Rahardjo, H., Leong, E. C., & Fredlund, D. G. (2004). Factors affecting drying and wetting soil-water characteristic curves of sandy soils. Canadian Geotechnical Journal, 41(5), 908-920.

232. Ye, W. M., Cui, Y. J., Qian, L. X., & Chen, B. (2009). An experimental study of the water transfer through confined compacted GMZ bentonite. Engineering Geology, 108(3), 169-176.
233. Ye, W. M., Xin, Q., Chen, B., Chen, Y. G. & Cui, Y. J. (2016). Investigation on hydraulic properties of compacted GMZ bentonite used as buffer/backfill material. *3rd Eur. Conf. Unsat. Soils – "E-UNSAT*. **9**, 18003.
234. Yong, R. N., Mohamed, A. M. O., Shooshpasha, I., & Onofrei, C. (1997). Hydro-thermal performance of unsaturated bentonite-sand buffer material. Engineering Geology, 47(4), 351-365.
235. Zettl, J. D., Barbour, S. L., Huang, M., Si, B. C., & Leskiw, L. A. (2011). Influence of textural layering on field capacity of coarse soils. Canadian Journal of Soil Science, 91(2), 133-147.
236. Zhang, F., Fredlund, D. G., and Wilson, G. W. 2015. Hydraulic properties for soils that undergo volume change as soil suction is increased. In Unsaturated Soil Mechanics-from Theory to Practice: Proceedings of the 6th Asia Pacific Conference on Unsaturated Soils (Guilin, China, 23-26 October 2015) (p. 383). CRC Press.
237. Zhang, M., Zhang, H., Zhou, L., Wang, B., & Wang, S. (2014). Hydro-mechanical analysis of GMZ bentonite–sand mixtures in the water infiltration process as the buffer/backfill mixture in an engineered nuclear barrier. Applied Clay Science, 97, 115-124.
238. Zhang, Z., Thiéry, M., & Baroghel-Bouny, V. (2014). A review and statistical study of existing hysteresis models for cementitious materials. Cement and concrete research, 57, 44-60.
239. Zheng, L., Samper, J., & Montenegro, L. (2011). A coupled THC model of the FEBEX in situ test with bentonite swelling and chemical and thermal osmosis. Journal of contaminant hydrology, 126(1-2), 45-60.
240. Zhou, J., & Jian-Lin, Y. U. (2005). Influences affecting the soil-water characteristic curve. Journal of Zhejiang University-Science, 6(8), 797-804.
241. Zornberg, J. G., Bouazza, A., & McCartney, J. S. (2010). Geosynthetic capillary barriers: current state of knowledge. Geosynthetics International, 17(5), 273-300.
242. Zur, B. (1966). Osmotic control of the matric soil-water potential: I. Soil-water system. Soil Sci. 102 (6), 394-398.

List of publications from this research work

Journals

1. Gapak, Y., Das, G., Yerramshetty, U. and Bharat, T.V. (2017). "Laboratory determination of volumetric shrinkage behavior of bentonites: A critical appraisal", *Applied Clay Science*, Elsevier, 135, 554-566.
2. Gapak, Y. and Bharat, T.V. (2018) "Hysteretic water retention behaviour of bentonites", *Journal of Hazardous, Toxic and Radioactive Waste*, 22(3), 04018008.
3. Bharat, T.V. and Gapak, Y. (2018) "Hydration kinetics of bentonite buffer material: Influence of vapour pressure, bentonite plasticity, and compaction density", *Applied Clay Science*, 157, 41- 50.
4. Gapak, Y. and Bharat, T.V. (...) "Wetting soil water characteristic curve and hydraulic conductivities of bentonites in volume restrained conditions." *Geotechnique*, ICE (manuscript communicated).
5. Gapak, Y., and Bharat, T.V. (…) "Applicability of Richard's equation for water infiltration through compacted bentonite", *Canadian Geotechnical Journal* (manuscript communicated).

National and International Conferences

1. Gapak, Y., Yerramshetty, U. and Bharat, T.V. (2015). "Laboratory determination of volumetric shrinkage behavior of plastic clay". *Indian Geotechnical Conference*: IGC 2015, Pune, India, 1-8.
2. Gapak, Y. and Bharat, T.V. (2016). "Water Flow through Unsaturated Compacted Clays", *International conference on soil and environment*, IISC Bangalore
3. Solanki, B., Gapak, Y. and Bharat, T.V. (2016). "Capillary Barrier Effects in Unsaturated Layered Soils", *International conference on soil and environment*, IISC Bangalore
4. Gapak, Y and Bharat, T.V. (2017). "Hysteresis in soil water characteristic of a highly plastic clay", *Indian Geotechnical Conference*: IGC 2017, IIT Guwahati.
5. Gapak, Y and Bharat, T.V. (2018). "Wetting and drying water retention curve of Indian bentonite." *International Conference on Advances in Concrete, Structural, and Geotechnical Engineering*", BITS Pilani, 1-6.